Contribution to the study of a lower power electric arc

Kheira Hameurlaine

UNIVERSITÉ D'ORLÉANS

ÉCOLE DOCTORALE MATHÉMATIQUES, INFORMATIQUES, PHYSIQUE THÉORIQUES ET INGÉNIERIE DES SYSTÈMES

LABORATOIRE : GREMI

THÈSE présentée par :

Kheira HAMEURLAINE

Soutenue le **: 18 décembre 2012**

pour obtenir le grade de : **Docteur de l'université d'Orléans**

Discipline/ Spécialité : Physique

CONTRIBUTION A L'ÉTUDE D'UN ARC ÉLECTRIQUE DE FAIBLE PUISSANCE

THÈSE dirigée par :

Jean-Marc BAUCHIRE	Maitre de conférences	Université d'Orléans

RAPPORTEURS :

Jean-François COUDERT	Professeur des Universités	Université de Limoges
Pierre FRETON	Maitre de conférences	Université Paul Sabatier

JURY :

Stéphane PASQUIERS	Directeur de Recherche	CNRS, LPGP, Orsay
Jean-François COUDERT	Professeur des Universités	Université de Limoges
Jean-Marc BAUCHIRE	Maître de conférences	Université d'Orléans
Pierre FRETON	Maître de conférences	Université Paul Sabatier
Chantal LEBORGNE	Professeur des Universités	Université d'Orléans

Remerciements

A la mémoire de mon petit cœur

Mon fils ADAM

Une thèse n'est pas une fin en soi, mais c'est un moment particulier dans la vie d'un chercheur : il y aura un avant qui ne sera plus, et il y aura un après à construire. Aussi, au moment de franchir cette limite, je ne peux pas ne pas penser à tous ceux qui, de pré ou de loin, auront contribué à ce grand effort car, si l'épreuve est individuelle, ses implications sont sociales, académiques, familiales,, et humaines tout simplement.

Le travail présenté dans ce mémoire a été effectué au laboratoire Groupe de Recherche sur l'Energétique des milieux ionisés (GREMI).

J'aimerais adresser un remerciement particulier à Monsieur Yann Vaills, Directeur de l'école Doctorale de l'Université d'Orléans, pour son aide et soutien tout au long de ces années. Je remercie également Monsieur Laifa Boufendi, pour sa sympathie, sa disponibilité, ses conseils, ainsi que pour son aide précieuse de tous les jours. Je remercie Charles De Izzara qui m'a aidé pour la partie expérimentale.

Je tiens à remercier Chantal Leborgne directrice de laboratoire GREMI, pour son soutien et ses encouragements et ses précieux conseils au cours de cette année.

J'adresse aussi tous mes remerciements au Professeur Emile Pfender et Joachim Heberlein de l'Université de Minnesota (USA) avec qui j'ai eu la chance de partager deux mois d'expériences unique.

Je tiens à remercier Monsieur Jean-François Coudert, Professeur à l'Université de Limoges, et Monsieur, Pierre Freton, Maitre de conférences à l'Université de Paul Sabatier, d'avoir accepté d'être les rapporteurs de ce manuscrit. Leurs remarques et suggestions lors de la lecture de mon rapport m'ont permis d'apporter des améliorations à la qualité de ce dernier.

Je remercie Monsieur Stéphane Pasquiers, Directeur de Recherches au LPGP, d'avoir accepté de participer à ce jury.

J'ai pu travailler dans un laboratoire avec des personnes particulièrement agréable, à Gregoire, toujours souriant et toujours disponible (alors seul face à la nature! Ou face à la thèse !),à Ibra (courage pour la thèse !), à notre rayon de soleil Fatou et El Hadj (fini les bon plats sénégalais !), à David (working with you is a pleasure) et venkat (I bike well now), à Ahmed Khacef, Nadjib Semmar, Jack Matthias, Guy Coudrat, Bernard Dumax, Dunpin Hong.

Je remercie Titaina Gibert (les trèfles et la coccinelle m'ont apportés bonheur), à Mireille (quelle pureté, reste comme tu es !), à Laurent Schwaederle, Hagop Tawidan, Melhem Amer, Lardoue Julien, Hervé Hidalgo, Elianne et Gaettan, à Hamid Acid,à Romain, à mes amies Hayet et miriam (mizmiza et les corrections ! hadi taliya), Majda, Aicha, Fatzou.

Merci à tous pour votre bonne humeur, pour toutes leurs encouragements et soutien.
Un immense merci à mes amis, qui m'auront soutenu dès le début et m'auront aidé dans les périodes de doute.

Mes dernières pensées iront vers ma famille, et surtout mes parents Mohamed et Saada, qui m'auront permis de poursuivre mes études jusqu'à aujourd'hui.
Tous mes remerciements à mon mari Badro bien aimé, sans lequel cette thèse n'aurait jamais vu le jour, pour l'amour, la patience qu'il m'a démontré pendant cette thèse.
Je remercie mes beau parents pour leurs soutien Lila et El hadj Salah Said, à mes beau frères Tarik et Morad, à mes belles sœurs Nadjet, Hakima.
Je remercie ma sœur Ahlem et ses enfants (J'aurais maintenant le temps pour commenter ton joli blog !), mes frères Nassim et Nasro.

Table of contents

List of figures

List of tables

INTRODUCTION GENERALE

Introduction Générale

Un plasma est en général un mélange de particules neutres, d'électrons et d'ions. Il est souvent désigné comme le quatrième état de la matière. Il y a un certain nombre de caractéristiques évidentes qui distinguent un plasma d'un gaz ordinaire :

1) Le plasma est un gaz électriquement conducteur ;

2) Les constituants et les interactions d'un plasma sont plus compliqués que celles d'un gaz ordinaire.

Le caractère énergétique d'un plasma thermique a conduit à un certain nombre d'applications comme le soudage et le découpage, en métallurgie, dans les appareils de coupure électrique **[Boul-1]**, pour le traitement des déchets **[Blai-1, Air-1]**…. De plus les plasmas thermiques sont des émetteurs de rayonnement important. Ils sont à ce titre largement utilisés dans l'industrie de l'éclairage **[Charr-1]**. Un certain nombre de caractéristiques exceptionnelles rendent un plasma utile pour des applications potentielles dans le domaine de la chimie à haute température et le traitement des matériaux, et il semble y avoir un intérêt croissant pour ces nouveaux développements.

Dans les plasmas thermiques, les collisions sont suffisantes pour assurer l'équipartition de l'énergie entre les différentes espèces du système. Ils se caractérisent par une température élevée ($T > 10000K$) et sont souvent générés, à pression atmosphérique ($P > 0.1$ atm) **[Vac-1]**, sous forme d'arcs électriques que nous avons étudiés tout au long de ce travail.

Plus précisément, un arc électrique peut être défini comme une décharge à fort courant traversant un gaz entre deux électrodes **[Vac-1].** Il se caractérise par le fait qu'il génère des écoulements gazeux de fortes importances (de l'ordre de la centaine de mètres par seconde) par combinaison du courant qui le traverse et du champ magnétique auto-induit. Il existe principalement trois types de génération d'arcs électriques et de plasmas thermiques : les arcs libres **[Gonz-1, Hsu-1],** les arcs soufflés et les décharges RF **[Ye-1]**. Les arcs libres sont généralement créés entre une cathode pointue et une anode plate. Aucun mécanisme extérieur ne vient stabiliser la décharge : l'écoulement stabilisateur étant généré par effet Maecker. Les arcs soufflés sont basés sur le même principe que les arcs libres. La seule différence est l'injection d'un gaz qui stabilise la colonne de plasma. Cette injection se fait le plus souvent au proche voisinage de la cathode et peut s'effectuer axialement. Enfin, les décharges RF sont,

quant à elles, maintenues par un système extérieur de type capacitif ou inductif, qui par leur champ électromagnétique ont un effet stabilisateur sur la décharge. Suivant les applications ou les dispositifs précédemment cités, différents gaz plasmagènes sont utilisés : pour le soudage ou le découpage, l'argon est le plus souvent employé car il n'est pas réactif avec le métal à traiter. Son utilisation est généralement complétée par d'autres gaz comme l'azote, l'oxygène ou l'hélium.

Nous allons nous intéresser dans le cadre de ce travail de thèse à une décharge de type arc libre dans l'argon.

L'obtention d'une utilisation efficace et d'une bonne exploitation du plasma nécessite une compréhension approfondie de ses propriétés du plasma et de ses processus physiques. En dépit des efforts considérables théoriques et technologiques, la compréhension du comportement de l'arc reste encore incomplète. Ce manque de compréhension peut être principalement dû à la forte interaction des effets électriques, magnétiques, thermiques et convectifs. En plus de cela, des effets dus aux électrodes sont souvent impossible à contrôler ou à diagnostiquer. Un changement mineur des paramètres de l'arc tels que (la géométrie des électrodes, les impuretés de la surface des électrodes, les impuretés du gaz, etc) entraine des changements importants dans le comportement et l'apparence de l'arc.

Deux approches sont envisageables pour mieux étudier et caractériser un plasma d'arc : l'une par le biais expérimental, et l'autre par la modélisation. L'approche expérimentale repose notamment sur des mesures macroscopiques comme la tension, l'intensité ou des bilans calorimétriques. D'autres techniques de diagnostic ont été mises au point, tels que la spectroscopie d'émission, d'absorption **[Vac-1],** l'interférométrie laser… **[Sny-1].** Ces méthodes permettent d'obtenir diverses grandeurs caractérisant le plasma comme la température locale, les densités électroniques ou les vitesses.

Parallèlement aux études expérimentales, l'utilisation de l'outil informatique a permis le développement de modèles de plasma. Tous les exemples cités concernant les applications industrielles des arcs électriques présentent des géométries souvent extrêmement complexes où l'arc ne possède plus forcément un axe de symétrie naturel. Avec l'amélioration des capacités de calcul des ordinateurs, les modèles et les simulations ont permis de meilleures

connaissances au niveau macroscopique et microscopique des décharges. Les premiers codes de calcul étaient unidimensionnels (1D). Moyennant certaines hypothèses et la résolution de l'équation d'Elenbaas-Heller, ils permettaient, via l'obtention du profil de la température, de caractériser et d'étudier de nombreuses situations et paramètres. Avec l'amélioration des puissances de calcul, sont arrivés ensuite les codes bidimensionnels (2D) où la symétrie de révolution de l'arc était supposée. Ces outils 2D sont encore très utilisés de nos jours, et interviennent dans des cas où la symétrie de l'arc est conservée, notamment dans la modélisation de la colonne d'un arc libre. Ces développements commencent à être bien maîtrisés et sont souvent couplés avec des modules plus complexes en vue de se rapprocher des problématiques.

Ce travail de thèse s'inscrit comme une étape dans une étude plus générale portant sur l'allumage de la combustion. La mise en place d'une simulation numérique de l'allumage passe par la mise au point d'un modèle de la phase d'arc. Les conditions générales d'une telle décharge (courant transitoire, faibles dimensions…) étant difficiles, le développement du modèle se fait par une première étape pour laquelle la décharge est supposée stationnaire et de plus grandes dimensions, du type arc libre. Le choix de cette décharge résulte des possibilités de validation qu'elle offre en raison des nombreux travaux, tant expérimentaux que théorique, pour lesquels elle a servi de support. Le travail de cette thèse porte donc sur la mise en place d'une modélisation auto-cohérente de la colonne positive de l'arc, complété par une approche expérimentale permettant de valider les résultats numériques obtenus. Cette décharge peut être décrite, dans le cadre de l'hypothèse de l'équilibre thermodynamique local (ETL) **[Mos-1] [Zhao-1].** Dans ce cas la seule connaissance du profil de température conduira à une connaissance de l'état du plasma. Il nous a donc paru opportun de développer un modèle « fluide » basé sur les équations hydrodynamiques du plasma destiné à l'étude du comportement de la décharge en utilisant le logiciel commercial Ansys Fluent®, le but étant de réaliser une étape essentielle vers un modèle plus sophistiqué et complet, prenant en compte plus de phénomènes physiques comme par exemple les écarts à l'équilibre thermodynamique **[Tan-1], [Trel-1].**

La présentation de cette étude s'articule autour de quatre chapitres.

Introduction Générale

Le chapitre 1 présente les principales théories et concepts fondamentaux que l'on peut trouver dans la littérature sur les plasmas thermiques, leurs applications, et les arcs électriques libre. Une synthèse des modèles existants pour la description générale de ces arcs libres en prenant en compte les différentes zones, et plus précisément la colonne de plasma, est proposée. L'objectif de ce chapitre n'est pas de faire une liste exhaustive des modèles existants et de leurs variantes mais d'avoir une vue d'ensemble des principaux modèles pour la description d'arc et leurs évolution. Une famille de modèles est présentée, celle à l'équilibre thermodynamique, majoritairement à deux dimensions. Sa spécificité est décrite de façon globale. Les propriétés thermodynamiques et les coefficients de transport du gaz plasmagène indispensables pour la modélisation sont aussi présentés dans ce chapitre. De cette étude découle les bases de notre modèle de colonne de plasma présenté dans le chapitre suivant.

Le chapitre 2 est consacré à la description mathématique des arcs électriques à deux dimensions. Nous décrirons l'arc électrique par les équations de la magnétohydrodynamique. Ce système d'équations aux dérivées partielles étant non linéaire, on a choisi une méthode numérique adapté à ce type d'équations. Nous utilisons le logiciel commercial Fluent 12.0 basé sur la résolution des équations de Navier-Stokes auxquelles les équations de l'électromagnétique ont été couplées.

Pour valider notre méthode, une modélisation d'un arc libre dans l'argon à 100 A avec une distance inter-électrodes de 1 cm est proposée dans la première partie du chapitre 3. Une géométrie et des résultats connus tant expérimentaux que théoriques permettent une confrontation de nos résultats de simulation avec ceux issus de la littérature. Dans une deuxième partie, nous proposerons l'analyse et l'interprétation de ses résultats. Dans la dernière partie nous présenterons l'analyse de l'influence de la nature du gaz et du courant électrique sur les grandeurs caractéristiques du plasma.

Le quatrième chapitre porte sur l'étude expérimentale. Nous présenterons dans la première partie, les bases de la spectroscopie d'émission, le choix et la motivation de la méthode. Dans la deuxième partie, nous présentons des mesures de températures à partir des profils du coefficient d'émission d'une seule raie sur les régions anodique et cathodique. Dans la dernière partie de ce chapitre les résultats expérimentaux sont comparés aux résultats issus de notre modèle et des travaux expérimentaux trouvés dans la littérature.

Bibliography

[Air-1] www.airliquide.ca
« Procédés plasma et TIG. Applications de soudage automatique » 1-800-817-7697

[Blai-1] Blais A, Proulx P, Boulos M I. "Three-dimensional numerical modeling of a magnetically deflected dc transferred arc in argon », J. Phys. D:Apply. Phys. 36, 488-496 (2003).

[Boul-1] Boulos M I, Fauchais P, Pfender E, "Thermal Plasmas, Fundamentals and applications" Vol 1 (New York: Plentum) (1994).

[Charr-1] Charrada K, Zissis G, Aubes M. J. Phys. D: Appl. Phys. 29 2432 (1996).

[Hsu-1] Hsu K.C, and Pfender E. : J.Appl. Phys, 54, pp. 256, (1983).

[Gonz-1] Gonzalez J J, Gleizes A, Proulx P, Boulos M, J. Appl. Phys. 74 3065 (1993).

[Mos-1] Mostaghimi J, Boulos M I " Two-Dimensional electromagnetic field effects in induction plasma modeling" Plasma Chem. Plasma Process. 9 25-44 (1989).

[Trel-1] Trelles J P, Heberlein J V R, Pfender E "Non-equilibrium modelling of arc plasma torches". J. Phys. D: Appl. Phys. 40 5937-5952 (2007).

[Sny-1] Snyder S C, Bentley R E, "A measurement of axial velocity and temperature in free-burning arc using Thomson Scattering ", J.Phys.D, (29), 12, pp 3045-3049 (1996).

[Tan-1] Tanaka Y, J. Phys. D : Appl. Phys. 37 1190-1205 (2003).

[Ye-1] Ye R, Proulx P, Boulos M, J. Phys. D : Appl. Phys 33 2154 (2000).

[Zhao-1] Zhao G Y, Mostaghimi J, Boulos M I "The induction plasma chemical reactor : Part 1". Equilibrium model Plasma Chem. Plasma Process. 10 133-50 (1990).

Introduction Générale

Chapter 1: General Features of Electric Arc Modeling

RESUME DU CHAPITRE 1

Les arcs électriques sont des plasmas thermiques étudiés depuis longtemps en recherche fondamentale et utilisés dans de nombreuses applications industrielles.

La création d'un arc en laboratoire dès le 19esiècle, indique que les décharges électriques à pression atmosphérique sont relativement faciles à obtenir. Leur compréhension et leur modélisation est donc une question d'intérêt autant scientifique qu'industriel. Le développement du matériel informatique et des logiciels facilitent la compréhension du comportement global de la décharge.

Dans ce chapitre, nous présentons une brève étude historique sur la modélisation des arcs électriques. On s'est intéressé plus précisément aux arcs libres car leur géométrie est relativement simple en comparaison à d'autres configurations.

Dans cette étude bibliographique, nous présentons les caractéristiques générales de l'arc libre. Ce dernier peut être divisé en deux parties en fonction de la distribution de potentiel électrique : la colonne d'arc et les régions de gaines proches des électrodes. La colonne d'arc, avec un gradient de potentiel relativement faible, représente le corps principal de l'arc. Une brève description de la colonne en utilisant des équations de conservation est donnée ainsi que les propriétés thermodynamiques et les coefficients de transport, ces deniers étant indispensable pour la modélisation.

1.1 Introduction

High intensity electric arcs are common and relative simple thermal plasmas. They have been used for a long time for fundamental research as well as for many industrial applications. During the long history of commercial applications, progress was mostly based on the empirical approach of trial and error. However, due to the complexity and the vast number of possible parameter combinations, the development strongly relies upon the practical experience of the individual developer and not directly on the general existing knowledge of this discharge.

The first observation of the arcing phenomenon stems from the nineteenth century which indicates that atmospheric pressure gas discharge are relative easy to obtain. The understanding and modeling is a thus a matter of scientific interest which during the last decades is largely facilitated since modern computing hardware and advanced software provides the means and opportunities to compute the overall discharge behavior in a quantitative way.

This work is dedicated to contribute to the understanding of the overall discharge properties by using commercial software. This objective is reached by the development and validation of existing modeling software. The investigations are applicable to thermal plasmas, which are distinguished from other types of plasmas by several characteristics which will be discussed in the next section.

1.2 Thermal Characterization of plasma

Atmospheric pressure plasmas, generated by driving a relative large DC electric current through a gas, are classified as thermal plasmas and are usually considered to be in or close to Local Thermodynamic Equilibrium (LTE). This implies thermal and chemical equilibrium. The first one means that the temperature of electrons and heavy particles are the same; the second one that the degree of ionization and dissociation and the occupation of internal states are ruled by the laws of equilibrium statistical mechanics. One of the reasons for the presence of (near) LTE is that the high density of active species makes the plasma collision dominated. The frequent interactions of the particles facilitate the distribution of energy over the various particles and internal states.

As shown in figure 1.1 when the pressure approaches atmospheric values, the large density of particles and therefore the large amount of collisions guarantee one of the fundamental requirement for Local Thermal Equilibrium (LTE), that is $T_e = T_h$.

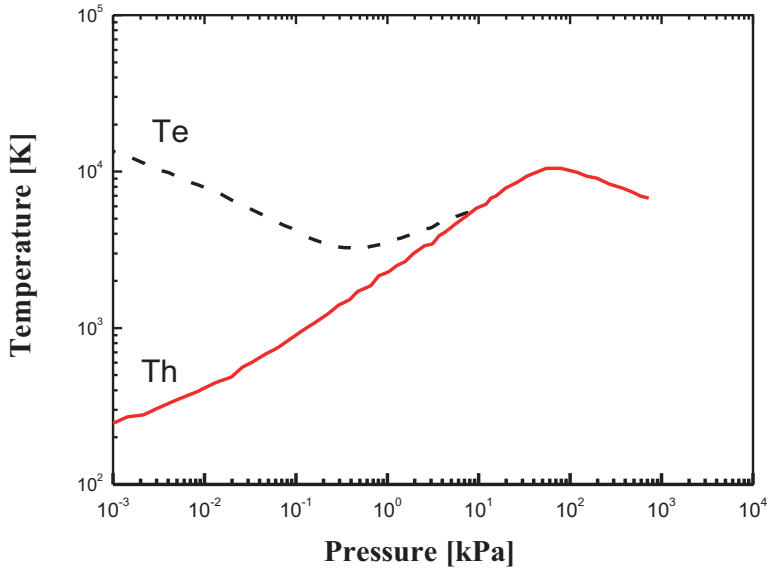

Figure 1. 1: Behavior of electrons (Te) and heavy particles (Th) temperature in an arc plasma as function of pressure [Boul-1].

1.3 Fields of model applications

Heat transfer processes generated by arc plasmas are important for several applications. In numerous applications the arc heat is used directly for the process (transferred arc process).

As demonstrated in figure 1.2, discharge powers range from a few W to several MW and discharge pressures are atmospheric in most cases. Some examples of high intensity arc applications are listed below:

- Arc lamps **[Charr-1]**, at low frequency alternating current (AC) or direct current (DC), these are mainly optimized for the following aspects:
  - Electrode geometry and erosion reduction,
  - Performance of an optimal global energy balance,
  - Favorable radiative properties.
- Welding arcs **[Ush-1]**

Optimized arc configurations will permit higher processing quality and performance,

The impact of new gas mixtures and electrode materials can be determined in advance.

- Arcs furnaces **[Drou-1]**
  - For steel and high melting point materials synthesis,
  - Optimized high power torches will allow replacing conventional carbon electrodes.
- Plasma torches for enhanced or even new applications such as:
  - Waste destruction **[Fauc-1]**,
  - Gas heating for re-entry simulation and space propulsion,
  - Plasma chemistry and materials deposition (plasma spraying) or removal (plasma etching).
- Circuit breakers **[Sch-1]**

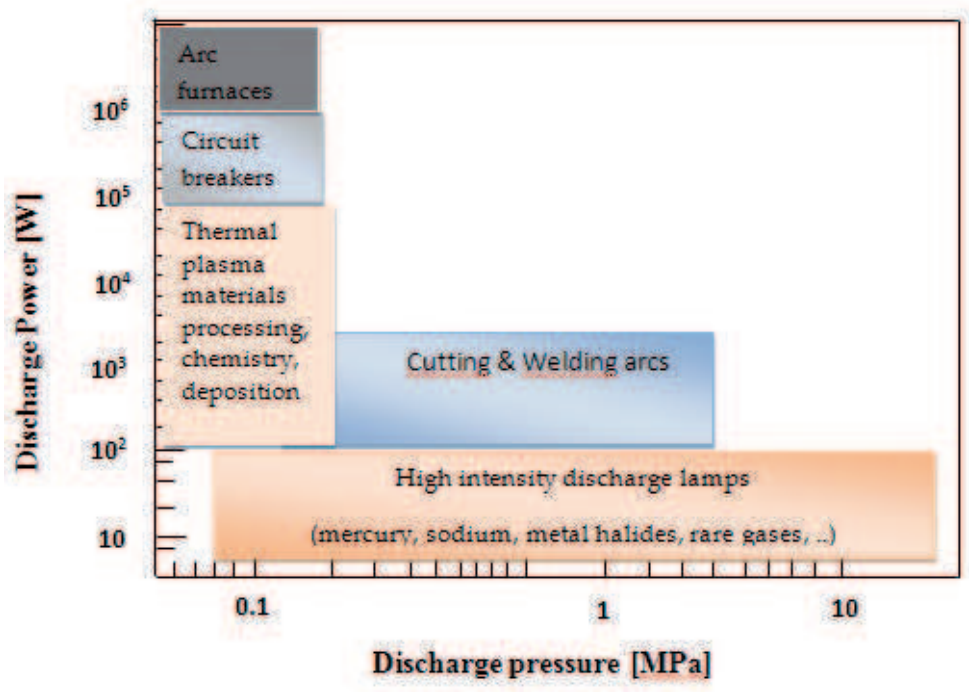

Figure 1. 2: Applications of high intensity arc gas discharge.

In these applications electric arcs are used because they offer the ability to combine high heat fluxes with high energy and radical densities in a controlled environment or process medium.

While the number of important applications would warrant extensive efforts in arc plasma modeling, the difficulties associated with the construction of such models have limited their performance usefulness. Heat transfer under plasma conditions requires consideration of several special effects **[Pfe-1]**:

1. Plasmas are reacting gases with dissociation, ionization, and recombination reactions influencing the energy transport, and the presence of multiple species determining the values of the transport coefficients.
2. Arc plasmas have very high temperatures and energy densities, and are consequently surrounded by very steep gradients in temperatures and densities. This leads to non-equilibrium kinetics and compositions which obscure the description of the energy transport. In particular in the electrode regions, the gradients can be so steep (in the order of 10^8K/m) or several hundred degrees per mean free path (mfp)) that the continuum concept may break down and discontinuities in properties may be encountered.
3. Heat transfer to the electrodes is intimately tied to the current transfer and the heat generation, so that a change of either one of these phenomena will affect the other.
4. Arc plasmas display instabilities, and for many applications, transient descriptions of the plasma have to be offered.

These factors lead to situations that are unique for arc plasmas which make it difficult to transfer technical solution derived for other research fields, such as combustion.

1.4 Historical background and Review of arc discharge modeling in LTE

Investigations for the understanding and modeling of electric arcs started with the first observations of arc phenomena, in the beginning of 19th century. After that the technology of

electric arc was mainly based on theoretical understanding and the prediction of experimental situations.

1.4.1 Aims of the models

In order to improve the performance of scientific and technological plasma sources presented in the previous section, a thorough understanding of such devices is necessary. Generally, this objective has been achieved by carrying out experiments and modeling. Numerical simulation has become an indispensable addition to plasma diagnostics, especially in situations where experimental tests are costly or difficult to implement. These complications may be due to the limited accessibility to the plasma, due to time scales or simply because the quantities of interest are difficult to measure directly.

The aim of modeling is to give a self-consistent description of the plasma as function of external control parameters such as the geometry, the nature and mass flow rate of the plasma gas, the used materials, the current density and the boundary conditions. However, in reality, the development of thermal plasma modeling does not allow a complete self-consistent description, because of the lack of understanding of phenomena such as radiation, turbulence, plasma-electrode interactions... These limitations in our knowledge impose simplifications and assumptions on the models.

Researchers and engineers have two possible ways of treating a problem:

- ✓ Developing their own “home-made” code ;
- ✓ Or using commercial software.

Home-made codes have very often been used to study specific physical aspects, to make parameter studies or to evaluate the influence of one or a few parameters on a simplified geometry. In recent years, self-consistent three-dimensional numerical codes have started to appear, at least for some plasma regimes. The current available computers have the capability to tackle the plasma complexity. Moreover the codes are often constructed in such a way that it—or parts of it—can be re-used for other applications than the one for which it had been developed originally.

Examples of codes that have been developed along these lines are the hybrid plasma equipment model (HPEM) of Kushner and co-workers **[kus-1]**, **[Mar-1]** and the PLASIMO modeling framework that is being developed at Eindhoven University of Technology by Van der Mullen and his group **[Van-1], [Pla-1]**.

On the other hand several commercial software packages are used by the thermal plasma community: to mention FLUENT, OpenFoam, and PHOENICS.

These commercial software packages have been sufficiently well developed and validated to describe hydrodynamics flows, and many equations can be implemented, in theory. However, these codes were initially developed for the description of fluid mechanics and combustion problems and as such they were not primarily suited for thermal plasma processes. Moreover we have experienced that the source codes of these software packages have several black box features.

1.4.2 Historical review arc modeling discharge

Table 1.1 represents a small collection of milestones in the 200 years history of arcing phenomenon.

Year	Contributor	Contribution
1878	Siemens	Arc melting
1890	Moissant, Heroult	Arc furnaces
1901	Marconi	Arc radio transmitter
1902	Aytron	Monograph The electric arc
1935	Elenbaas	High pressure mercury lamp
1950	Maecker	Segmented arc for fundamental research
1983	Hsu	1st attemp of a 2-D LTE model for the arc column arc synthesis of fullerenses
1989	Tsai, Kou	Column model with boundary fitted coordinates
1990	Delalondre	Integrated 2-D column-cathode model
1995	Kaddani	3D modeling of unsteady high pressure arcs in argon
1997	Lowke	2D arc welding
2000	Freton	2D/3D free burning arc
2004	Blais	3-D column model
2006	Lago	2D/3D column and anode model
2009	Murphy	2D model of TIG with different shielding gas mixtures

Table 1. 1: Short history of arc discharge modeling.

This table shows that concerning arc modeling, every thirty years or so, a qualitative advance has been made in the overall development. The first work attempt of two-dimensional LTE arc model is elaborate by **[Hsu-1].** The use of commercial software starts since 2000. Our work is a contribution in modeling by using software Fluent **[Flue-1].**

.

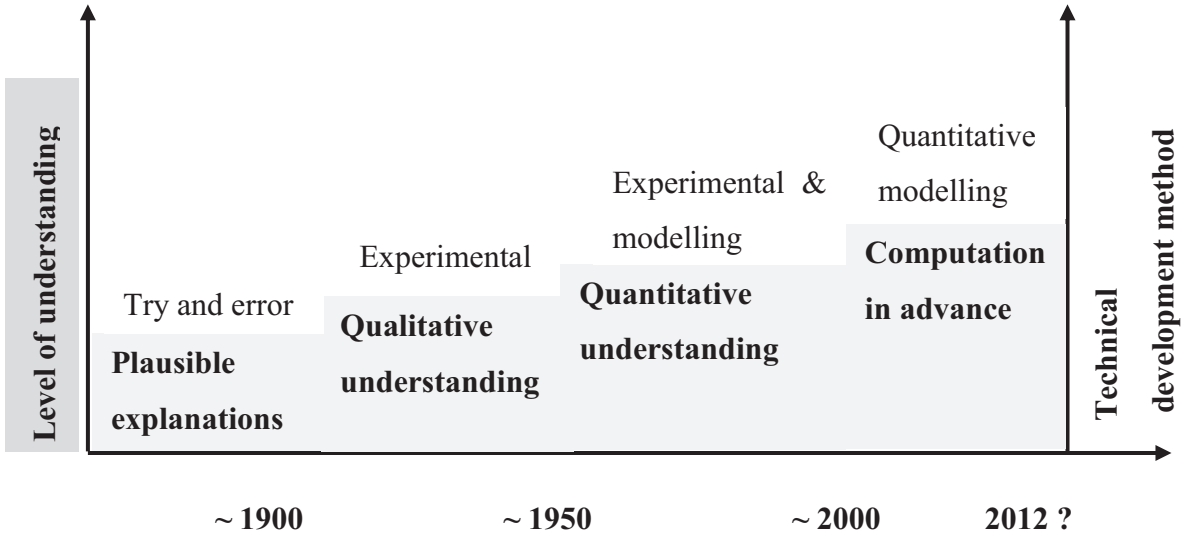

Figure 1. 3: Development of high intensity discharge science and technology.

The first important work that considered heat transfer and fluid flow coupled to electromagnetic forces was done by **[Hsu-1].** In that work, a steady, 2-dimensional model of a`10 mm long free-burning arc was considered. It was continued by **[Mck-1],** who made a refined representation of the heat and current flux density at the electrode surface. Both studies dealt with tungsten electrodes, a known current density and water-cooled anode surfaces.

Over time, various two-dimensional numerical models of increased sophistication have emerged such as the work of **[Cho-1], [Lee-1]** and **[Goo-1].** Lowke et al **[Low-1]** have developed numerical models with improved capabilities. These included a more accurate prediction of the electrode temperature distribution by **[Cho-1],** the introduction of various aspects of electrode geometry in the calculation domain by **[Lee-1], [Goo-1]**, and different shielding gas (mixture of argon and hydrogen) **[Low-1]** and **[Mur-1],** effect of an axial magnetic field on a DC argon arc using CFD **[Lin-1]**, and the turbulence models on highly constricted plasma cutting arc by **[Qianh-1]**. Schnick et al **[Schn-1]** presents a model that takes into account metal vapor and that is able to predict the local central minimum in the radial distributions of temperature and electric current density. The influence of the different values for the net radiative emission coefficient of iron vapor formation mechanism in arc welding was dealt with by Tashiro et al **[Tash-1].**

The majority of these studies considered the case of axisymmetric flows and the investigations were mainly concentrated on the interaction between the arc and the electrodes.

The results confirmed that the boundary conditions on the electrodes have a profound effect on the arc discharge.

However, some physical aspects of the arc problem, like the influence of a non-uniform gas injection and the geometrical asymmetry cannot be considered by two-dimensional models. For a proper description a complete three-dimensional model is then required.

Recently, a number of three-dimensional models have been reported in literature. The first of these models were still constrained by some symmetry assumption. For example, Delalondre et al **[Delan-1]** studied a symmetric transferred arc with an argon shielding gas. Also the arc fluctuations were considered, but due to the symmetry assumptions these fluctuations were constrained to two horizontal planes (corresponding to the cathode and the anode surfaces). Further development of the model was concentrated on relaxing the symmetry constraint, considering a 3D unsteady model of the free burning arc by Kaddani et al **[Kadd-1].** No symmetry assumption was set. But due to computational reasons the complete geometry was simplified to two parallel planes, including the cathode and the anode (represented by two predefined conducting circular regions). The results were compared with the work of Hsu et al **[Hsu-1].** The comparison was done only along the axis of symmetry and significant differences were reported.

The study of a free burning arc by Freton et al **[Fre-1]** presented a more detailed 3D geometry. First, a 2D configuration was presented and compared with the case studied by Hsu et al **[Hsu-1]** in order to validate the model. Then, the results of the 2D free-burning arc calculation were compared with a complete 3D calculation done using the same boundary conditions. As expected, the results showed no significant difference, and it was concluded that a 2D model can still be an efficient and accurate representation for an axisymmetric problem.

Development of two and three dimensional model in, 10 mm, 200 A by Blais et al **[Blais-1]** and **David et al [David-1]** in pure argon for the deflection of dc transferred arcs using an external magnetic field were also done. The arc is deflected by the use of a conductor aligned parallel to the arc axis through which flows an electric current. The values of velocity and temperature obtained between two-dimensional and three-dimensional cases are different for two reasons: first, the 3D arc is not free-burning but transferred, and the second, the insulation (boundary condition through cathode) is slightly different between two-dimensional

and three-dimensional grids, this work indicate that the electrical insulation at the tip of the cathode has a major effect on the temperature and velocity fields. This same geometry of free-burning arc is proposed by Lago et al **[Lago-1]** to describe the arc and its interaction with a composite material in an anodic configuration. This model in two-dimensions is used to quantify the degradation level of the material versus the pulse duration and the current density value, then in this same work, a three-dimensional model is developed and used to evaluate the degradation of the composite material. The results indicate that the Joule effect has a significant influence in this type of materials: damages caused by the Joule effect term dominate **[Avr-1].** The material degradation predicted by the 2D model not taking the lateral convective force into account is underestimated compared with the 3D models results.

1.5 Fundamental arc physics

An electric arc distinguishes itself from other discharge modes by a relatively high current density ($J > 10^6$ A/m^2), low cathode fall (<10 V) and high luminosity. According to its potential distribution, the arc may be divided into two parts: the arc column and the electrode regions. The arc column with a relatively small potential gradient represents the main body of the arc while the electrode regions (cathode and anode) contain the electrode surface and the transition zone towards the arc column. The arc column represents a true plasma in which quasi-neutrality is present and the pressure is (almost) uniform. Some exceptions on pressure uniformity can be found at high current values (*I>5000A).*

In such arcs the interaction of the current with the self-induced magnetic field produces a pressure gradient in the radial direction (pinch effect) so that the pressure becomes elevated in the axis of the arc column.

To operate a steady arc requires some kind of stabilizing mechanism to keep the arc column in a certain position; for example a limitation of the current flow area to maintain high temperatures. Those stabilizing methods may be either provided externally by walls, vortices or magnetic fields or by the arc itself; this is known as self-stabilization. The combination of self generated electromagnetic field and current density provides, via $\vec{J} \times \vec{B}$ the main self-stabilization mechanism that can be expected for high intensity free-burning arcs.

The strong cathode jet induced by the electromagnetic force stabilizes the column of free-burning arcs. These induced plasma jets occurring as soon as the arc cross section varies,

are an important phenomena of high intensity arcs. An example of a free-burning arc by Tanaka et al **[Tana-1]** is given in figure 1.4 and 1.5.

Figure 1. 5: Appearance of argon arc plasma [Tana-1].

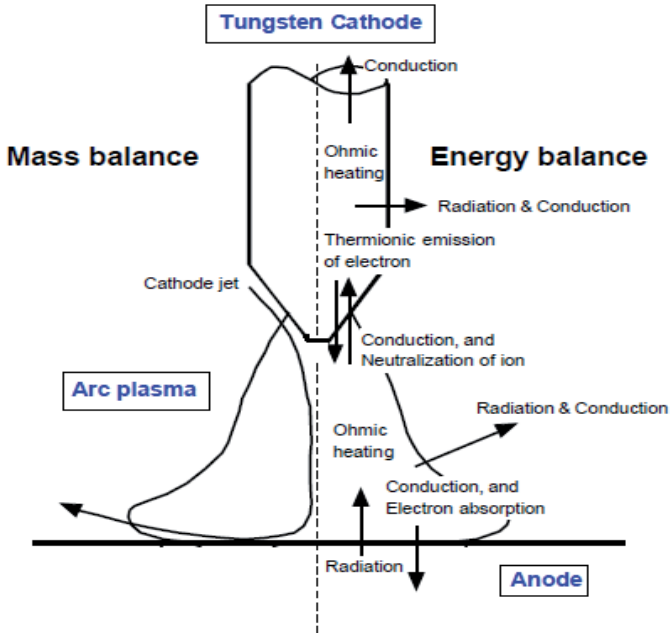

Figure 1. 4: Schematic of free-burning arc [Tana-1] .

Free-burning arcs are of industrial importance in welding, arc furnaces, and switch-gear and arc heaters for chemical processing (see [Low-2]**.**

1.5.1 Description of plasma using conservation equations

Since high-pressure plasma is collision-dominated, it can be viewed as a continuum (a fluid) and described by a relatively small set of conservation equations.

The modeling of the arc behavior requires the simultaneous solution of a set of equations which describes the conservation of:

- ✓ Mass
- ✓ Momentum
- ✓ Energy
- ✓ Current

More details about the conservation equations together with the appropriate boundary conditions will be given in next chapter.

The mathematical difficulties such as solving a system of coupled nonlinear differential equations on structured or unstructured grids, the requirement of complete data

sets of thermo-physical plasma properties (LTE or non-LTE), and the choice of suitable boundary conditions (in 2 or 3 dimension) have been long-standing challenges for modeling the free-burning arc in its totality.

Furthermore, strong gradients in the temperature, particle densities and the potential distribution near the electrodes may cause significant deviations from LTE. These topics are dealt with by **[Pok-1]** and **[Haid-1]** for the region close to cathode, by **[Jenis-1], [Yang-1]** for the anode region and by **[Cram-1]** and **[Snyd-1]** for the arc fringes**.**

1.6 Plasma Properties

The thermodynamic and transport properties required for the arc model represent one of the most important input data-structures. Such a database is needed for any plasma modeling activity. In this section a brief overview of such properties of an argon plasma at atmospheric pressure is presented. In the case of LTE these properties can be expressed as function of temperature.

1.6.1 Equilibrium Properties

Calculations of plasma properties under LTE are rather straightforward, because both electrons and heavy particles have the same temperature while this temperature determines the plasma composition.

1.6.1.1 Plasma composition

The chemical composition of a plasma in thermodynamic equilibrium (or LTE) can be obtained by solving a system of nonlinear equations (the mass action law, the ideal gas law and the condition for charge neutrality) if the partition functions of the various species are known.

In this study we use the Argon plasma composition given by Boulos et al **[Boul-1].** The plasma is primarily composed of argon atoms, ions, and electrons (Ar, Ar^{+}, Ar^{++}, Ar^{+++} and e^{-}).

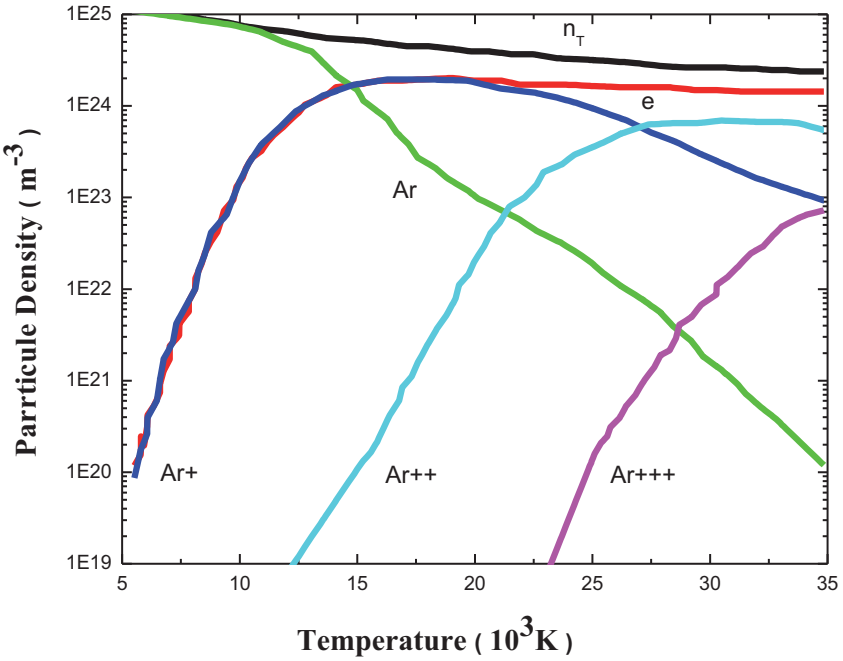

Figure 1. 6: Temperature dependence of the composition (species number densities) of an argon plasma at atmospheric pressure [Boul-1].

Figure 1.6 shows the temperature dependence of the argon plasma composition at chemical equilibrium and at atmospheric pressure. As the temperature increases, the density of atomic Ar decreases monotonically due to the progressive first ionization. From about 15000 K, the number density of Ar^{+} decreases steadily while Ar^{++} is formed. The electron density is not significantly changed over the temperature range from 15000 K up to 25000 K. At 25000 K the number density of Ar^{+++} is still two orders of magnitude less than that of Ar and four orders less than $n(Ar^{+})$ and $n(Ar^{++})$.

1.6.1.2 Thermodynamic and transport properties

The thermo-physical properties of plasmas which are usually subdivided into thermodynamic and transport properties are prerequisite for studies of the arc behavior. Once the plasma composition is known, the thermodynamic properties (mass density, internal energy, enthalpy, entropy and specific heat) can be determined with the calculated plasma composition **[Boul-1].**

For the LTE simulations in this study of a pure argon plasma, we have used the thermodynamic properties calculated by the **[Boul-1]** as a function of temperature at a pressure of 1 atm.

.

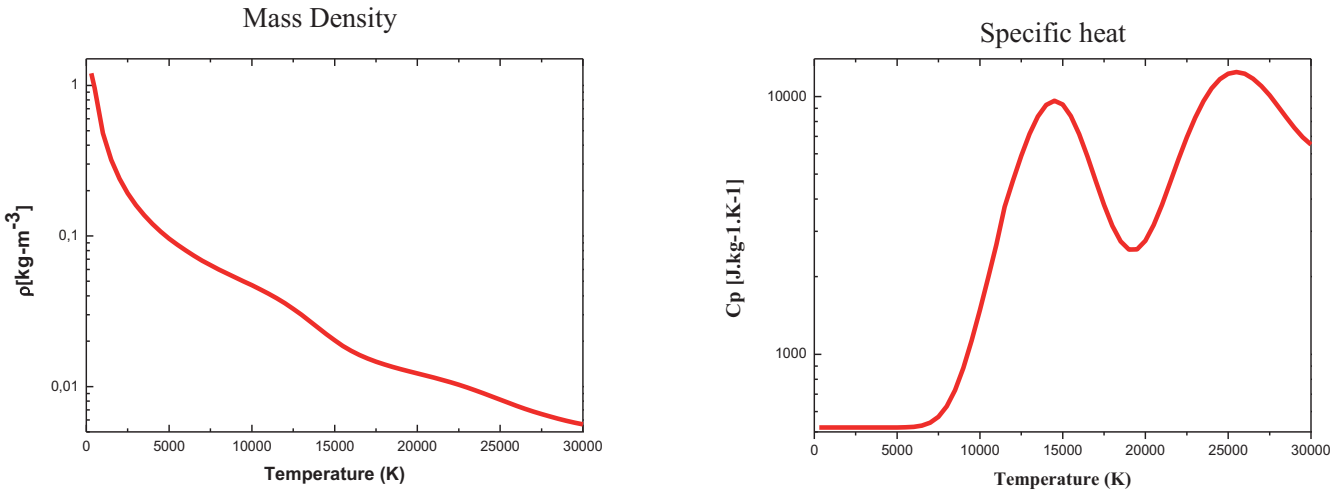

Figure 1. 7: Thermodynamic properties of Argon, thermal plasmas in LTE as function of equilibrium temperature T for p = 1 atm [Boul-1].

These transport properties include viscosity, thermal conductivity, electrical conductivity, which are used to describe the transport phenomena within plasma and its surrounding. Transport properties can be calculated using the Chapman-Enskog approximation theory of the Boltzmann equation (i.e. see **[Boul-1]**) and requires the knowledge of interaction potentials, collision cross sections, or collision integrals.

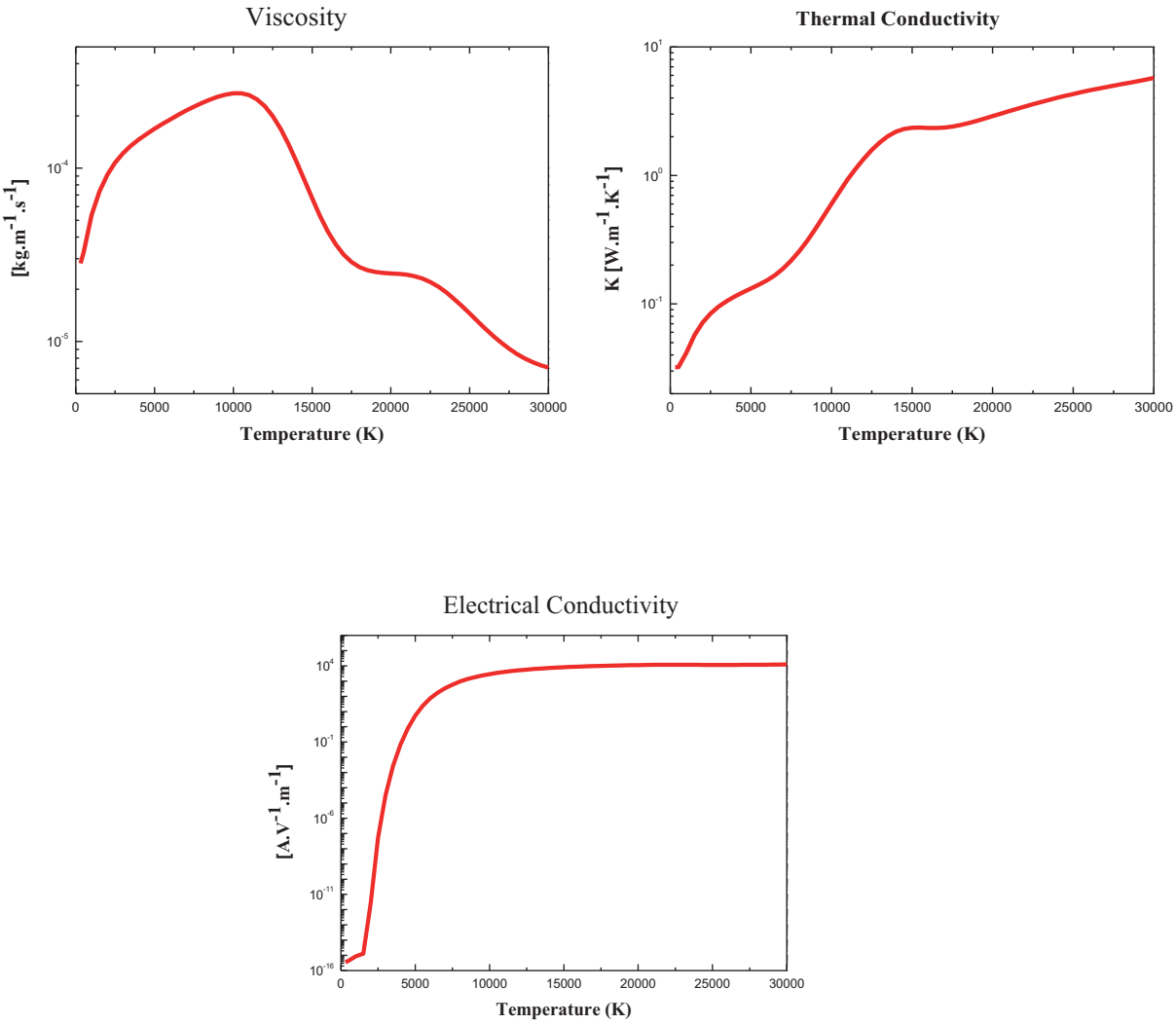

Figure 1. 8: Transport properties of Argon, thermal plasmas in LTE as function of equilibrium temperature T for p = 1 atm [Boul-1].

1.7 Orientation and scope of our work

The understanding of the arc behavior still remains incomplete. This lack of understanding may be primarily due to the strong interaction of electrical, magnetic, thermal and fluid dynamic effects, in addition to the surface effects which are frequently impossible to control. Moreover minor changes of the arc parameters like the electrode geometry, impurities of the electrodes surfaces and the impurities of the working gas may give rise to substantial changes in behavior and appearance of the arc.

The complexity of the electrodes regions demands more investigations to achieve a better understanding, but the hostile environment and the steep gradients of the plasma

parameters in the vicinity of electrodes or walls make diagnostics very difficult. Therefore we will approach the problem by the study of free-burning arc because of its simpler geometry. We have mainly based our study on Hsu's **[Hsu-1]** work which represents the base of most of the studies related to arc modeling.

We propose a study of free-burning arc column modeling. We have used the Fluent® software, based on volume finite method. In chapter 2, we present more details concerning the mathematical model describing the plasma in LTE.

The validation of our model is obtained by comparison the results from literature and experimental measurements.

1.8 Conclusion

In this chapter, we have presented historical background on thermal plasma modeling and theirs applications. All models cited are based on the LTE assumption. We have presented a general characterization of free-burning arc discharge. The next chapter is devoted to present the physical model, configuration and computational domain followed by the basic equations and structures of the model.

Bibliography

[Ayr-1] Ayrton H, The electric arc, The Electrician Printing and Publishing Co., New York, (1902).

[Avr-1] Avrootskij V A, sergievskaya IM and Sobotevskaya E G. "Electrical characteristics of graphite epoxy composite and their lightning protection" 20th Int.Conf.On Lightning Protection (Interlaken) 1-3, (1990).

[Boul-1] Boulos M, Fauchais P, and Pfender E. Book : "Thermal Plasmas, fundamentals and applications", vol. I.Plenum Press, NY.(1994).

[Blais-1] Blais A, Proulx P and Boulos M I. "Three-dimensional numerical modeling of a magnetically deflected dc transferred arc in argon". J.Phys.D:Appl.Phys.36 488-496, (2003).

[Charr-1] Charrada K, Zissis G, Aubes M. J. Phys. D: Appl. Phys. 29 2432 (1996).

[Choo-1] Choo R., Szekely J. and Westhoff R.C. " Modeling the welding arc", Metall. Mater. Trans. B, 23, pp. 357-69, (1992).

[Delan-1] Delalondre C, Douce A, Gonzales M., Gleizes A., and Guillot J.B. Proc. 14th Int. Symp. Plasma Chem. ed M Hrabovsky, Konrad and Kopecky, Vol 1, pp. 321, (1999).

[Delan-2] Delalondre C and Simonin O. " Modeling of high intensity arcs including a non-equilibrium description of the cathode sheath", J. Physique Coll. 51 no. C5, 199-206, (1990).

[David-1] David B, Vittorio C, Emanuele G, Sandro M, and Andrea M. "Three-Dimensional Time-Dependent Modeling of Magnetically Deflected Transferred Arc" IEEE Transactions on Plasmas Science, VOL. 33, NO. 2, (2005).

[Drou-1]Drouet M G, Nadeau F. J. Phys. E :Sci.Instrum 15 268 (1982).

[Fauc-1] Fauchais P, Vaerdelle A. IEEE Trans. Plasma Sci. 25, 1258-80, (1997).

[Fre-1] Freton P, Gonzalez J. J., Gleizes A. "Comparison between a two and a three-dimensional arc plasma configuration", J. Phys. D:Appl Phys. 33, 2442-2452, (2000).

[Flue-1] Fluent.inc, "Fluent 12.1 User's Guide", (2012).

[Jenis-1] Jenista J, Heberlein J V R and Pfender E. "Numerical model of the anode region of high-current electric arcs" IEEE Trans. Plasma Sci. 25 883–90, (1997).

[Hsu-1] Hsu K.C., Etemadi K. and Pfender. E."Study of the free burning high intensity argon arc" J.Appl. Phys, 54, pp. 1293-1301, (1983).

[Haid-1] Haidar J.: "Non-equilibrium modeling of transferred arcs", J. Phys. D: Appl. Phys. 32 263–72, (1999).

[Goo-1] Goodarzi M., Choo R. and Toguri J.M.: " The effect of the cathode tip angle on the GTAW arc and weld pool: I. Mathematical model of the arc". Journal of Physics D:Applied Physics, Vol 30,Number 19, pp. 2744-2756, (1997).

[Kadd-1] Kaddani A., Zahrai S., Delalondore C., Simonin O.: "3D modeling of unsteady high pressure arcs in argon", J. Phys. D:Appl Phys. 28, pp. 1-12, (1995).

[Kus-1] Kushner M J.:" Hybrid modeling of low temperature plasmas for fundamental investigations and equipment design", J. Phys. D: Appl. Phys. 42 194013, (2009).

[Low-2] Lowke J J, "Simple theory of free-burning arcs", J. Phys. D: Appl. Phys., Vol. 12, (1979).

[Lee-1] Lee Y.S. and Na S.J.: "A numerical analysis of a stationary gas tungsten welding arc considering various electrode angles" Suppl.Weld J., pp. 269-79, (1996).

[Low-1] Lowke J., Morrow R., Haidar J. and Murphy A.B.: " Prediction of Gas Tungsten Arc Welding Properties in Mixtures of Argon and Hydrogen". IEEE Trans. Plasma Science, 25, pp. 925-930, (1997).

[Lago-1] Lago F, Gonzalez J J, Freton P, Uhlig F, Lucius N and Piau G P.: "A numerical modeling of an electric arc and its interaction with the anode: part III. Application to the interaction of lightning strike and an aircraft in flight". J.Phys.D: Appl. Phys.39 2294-2310 (2006).

[Lin-1] Li-Lin., Xia Wei-Dong. : "Effect of an axial magnetic field on a DC argon arc". Chin. Phys. Soc. Vol 17 No 2, 1674-1056 (2008).

[Mar-1] see: http://uigelz.eecs.umich.edu/

[Maec-2] Maecker H, Der elektrische Lischtbogen, Ergebnisse der Exakten Naturwissenschatfen 25 293-358, (1951).

[Mck-1] McKellliget J. and Szekely J.: "Heat transfer and fluid flow in the welding arc Metal" .Trans 17A, pp. 1139-1148, (1986).

[Mur-1] Murphy A B, Tanaka M, Tashiro S, Sato T and Lowke J J. "A computational investigation of the effectiveness of different shielding gas mixtures for arc welding". J. Phys. D: Appl. Phys. 42 115205, (2009).

[Pok-1] Pokrzywka B, Musiol K, Pellerin S, Pawelec E and Chapelle J.: " Spectroscopic investigation of the equilibrium state in the electric arc cathode region", J. Phys. D: Appl. Phys. 29 2644–9, (1996).

[Pfe-1].Pfender E,.Heberlein J, " Advances in Heat Transfert", chapter 4 : "Heat Transfer Processes and Modeling of Arc Discharges", Fridman A, Y.I.Cho, Vol 40, ISBN: 978 0 12 373923 0, (2007).

[Pla_1] see: http://plasimo.phys.tue.nl/

[Schn-1] Schnick M, Fuessel U, Hertel M, Haessler M, Spille-Kohoff A and A B Murphy. : "Modeling of gas–metal arc welding taking into account metal vapour", J. Phys. D: Appl. Phys. 43 434008 (11pp), (2010).

[Sch-1] Schlitz L Z, Garimella S V, Chan S H. J. Appl. Phys 85 2540, (1999).

[Tana-1] Tanaka M., Yamamoto K., Tashiro S., K Nakat., E Yamamoto., K Yammazaki, K Suzuki, A B Murphy, J J Lowke,.: "Time-dependent calculations of molten pool formation and thermal plasma with metal vapour in gas tungsten arc welding". J.Phys.D:Appl.Phys, 43-434009 (11pp), (2010).

[Tash-1] Shinichi Tashiro, Tasuku Zeniya, Kentaro Yamamoto, Manabu Tanaka, Kazuhiro Nakata1, Anthony B Murphy, Eri Yamamoto, Kei Yamazaki and Keiichi Suzuki. "Numerical analysis of fume formation mechanism in arc welding". J. Phys. D: Appl. Phys. 43 434012, (2010).

[Qianh-1] Qianhong Zhou, Hui Li, Xu Xu, Feng Liu, Shaofeng Guo, Xijiang Chang, Wenkang Guo and Ping Xu. "Comparative study of turbulence models on highly constricted plasma cutting arc". J. Phys. D: Appl. Phys. 42 015210, (2009).

[Ush-1] Ushio M, Tanaka M, Lowke J J, IEEE Trans.Plasma Sci 32, 108, (2004).

[Van-1] Van Dijk J, Peerenboom K, Jimenez M, Mihailova D and van der Mullen J. " The plasma modeling toolkit plasimo". J. Phys. D: Appl. Phys. 42 194012, (2009).

Chapter 2: LTE-Two Dimensional Arc Column Modeling

RESUME DU CHAPITRE 2

Dans un modèle, les lois qui régissent les phénomènes physiques sont traduites par des équations mathématiques. La résolution, analytique ou numérique, de ces équations permet de déterminer les grandeurs physiques qui caractérisent le système.

L'objectif de la modélisation est de donner une description cohérente de plasma en fonction de paramètres externes tels que, la géométrie, la nature de gaz, la densité de courant et les conditions aux limites. En réalité, la modélisation d'un plasma thermique ne permet pas une complète description auto-cohérente, ceci par notamment par manque de compréhension des phénomènes tels que le rayonnement, la turbulence, ou les interactions du plasma avec les électrodes.
Ces limites imposent des hypothèses simplificatrices sur les modèles. Par ailleurs, la résolution des équations qui régissent ces modèles est généralement difficile ce qui nécessite encore de faire appel à des simplifications.

Les phénomènes (électrique, magnétique, fluide) dans un plasma d'arc peuvent être décrit par un modèle magnétohydrodynamique (MHD) comprenant, les équations de Navier-Stokes, de l'énergie et de l'électromagnétisme.
L'ensemble des équations du modèle MHD est résolu par le logiciel Ansys Fluent, basé sur la méthode des volumes finis.
Ce chapitre décrit brièvement la façon dont est utilisé le solveur de Fluent pour la résolution du modèle MHD d'arc libre dans l'argon.

2.1 Introduction

We have presented in chapter 1 an historical review on thermal plasma modeling, their applications, the aim of models, the difficulties associated with the formulation of such models and the ways of treating these problems. This chapter is dedicated to the base of modeling and the mathematical formulation of the problem.

Since the plasma, in a high intensity and high pressure arc, is collision dominated, the mean free paths for all species are much smaller than the macroscopic characteristic length. Therefore, the plasma can be viewed as a continuum fluid and described by a set of partial differential equations. The goal of thermal plasma model is to provide a self-consistent description of the plasma based on only macroscopic parameters such as the geometry, the nature of gas, the mass flow rate and the current density.

Hence, for more general consideration, each species in the plasma may be regarded as a separate continuum fluid coexisting with the continuum fluids of the other species. In the following, the conservation equations of mass, momentum and energy are obtained. As the electron temperature approaches the heavy particle temperature, the set of two-temperature energy equations (one for the electron temperature, the other for the heavy particle temperature) becomes the global energy equation for LTE assumption.

2.2 Base of LTE thermal plasma modeling

The self-consistent plasma model of entire arc contains typically a combination of the following sub-modules figure 2.1:

• A module for calculating the electromagnetic field in the plasma region and the other regions is needed. This electromagnetic field is governed by the Maxwell equations (dating from the year 1865) **[Max-1].** Regarding the plasma as a single fluid, a module for calculating its characteristics such as velocity $\vec{v}$, mass density ρ and pressure p is required. In general, these are governed by the momentum balance equations; since a plasma is a Newtonian fluid, these reduce to the Navier–Stokes equations (1822) **[Nav-1, Stok-1].**

• The Navier–Stokes equations must be closed by an equation of state, which expresses the relation between the mass density and pressure field. This is usually obtained by combining Dalton's law $P = \sum_i P_i$ (1805) **[Dalt-1]** for the (total) pressure P with the ideal gas law $P_i = nkT_i$ (1834) **[Clap-1]** for the partial pressures P_i of the species i in the plasma. Here k is Boltzmann's constant, n_i and T_i are the particle density and temperature of species i respectively.

• T_i. is obtained by energy equation.

• The calculation of the density n_i of species i is in the plasma composition module, see composition of argon plasma in chapter 1.

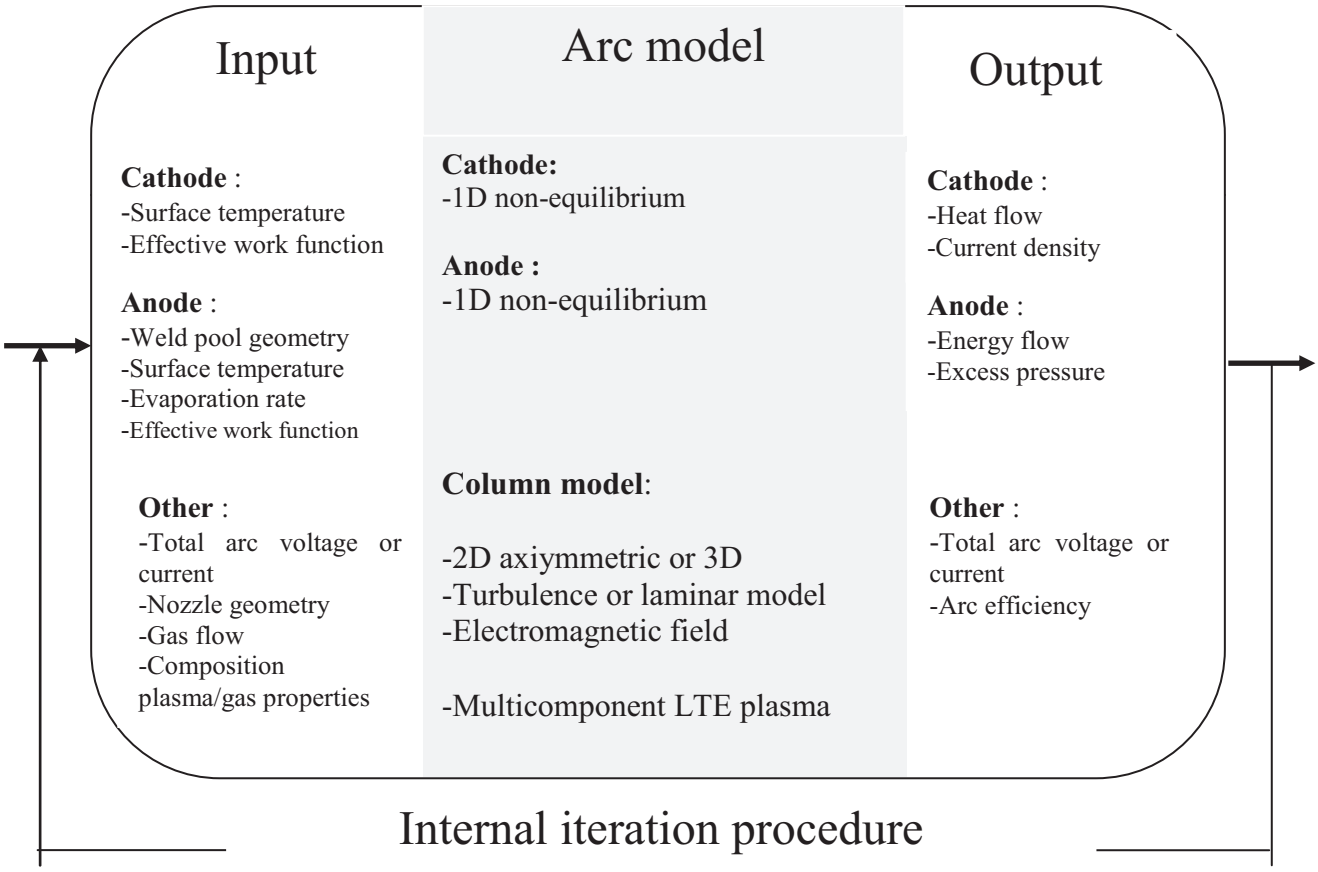

Figure 2. 1: Example of an entire arc modeling module.

Motion of high-density plasma (the degree of ionization is assumed high) induces electric currents, which together with the magnetic field influence the motion of the plasma **[Frid-1].** Such phenomena can be described by the system of magneto-hydrodynamic (MHD) equations including, the Navier-Stokes **[Nav-1, Stok-1]** equation and taking into account the magnetic force on the plasma current.

2.3 Magneto-Hydrodynamics model of plasma

These following assumptions are applied to MHD model, and made in the statement of the mathematical model of arc:

- ✓ The arc is in Local Thermodynamic Equilibrium **[Hsu-1]**, i.e. the electron and heavy-particle temperatures are very similar. This assumption has been shown to be valid through-out most of argon free-burning arc, except for in the fringes of the arc and near the cathode and anode surfaces **[Hsu-2, Hsu-3],**
- ✓ The arc is steady,
- ✓ The arc is rotationally symmetric, and the flow is laminar,
- ✓ Gravity and heat dissipation due to viscosity effects are negligible.

2.3.1 Device of the study

In this work, we study a free burning arc which is usually created in Tungsten Inert Gas (TIG) industrial device. It is the most widely employed type of plasma torch and produces arc plasma between a tungsten cathode and a copper anode using argon shielding gas and for electrodes gap of few mm, as sketched on figure 2.2.

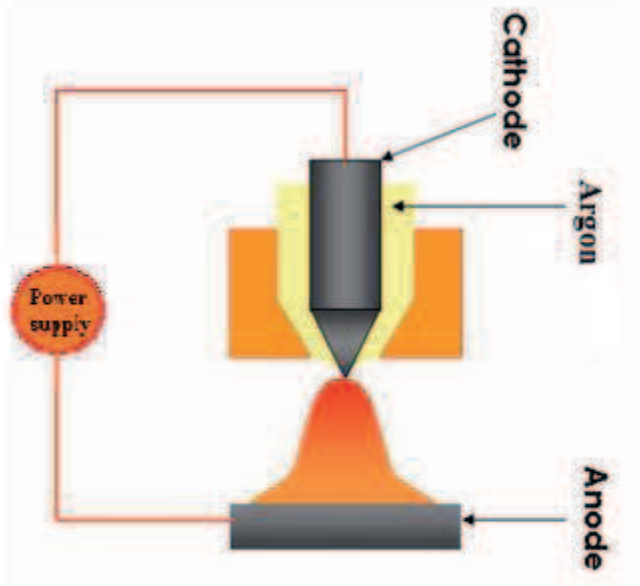

Figure 2. 2: Schematic TIG.

Many of the published studies of free-burning arc plasma consider significantly short arcs of 1 cm, for example, in studies of Hsu [**Hsu-2]** and McKelliget **[Mck-1].** In order to compare our results with those of Hsu, we have chosen the following computational domain figure 2.3.

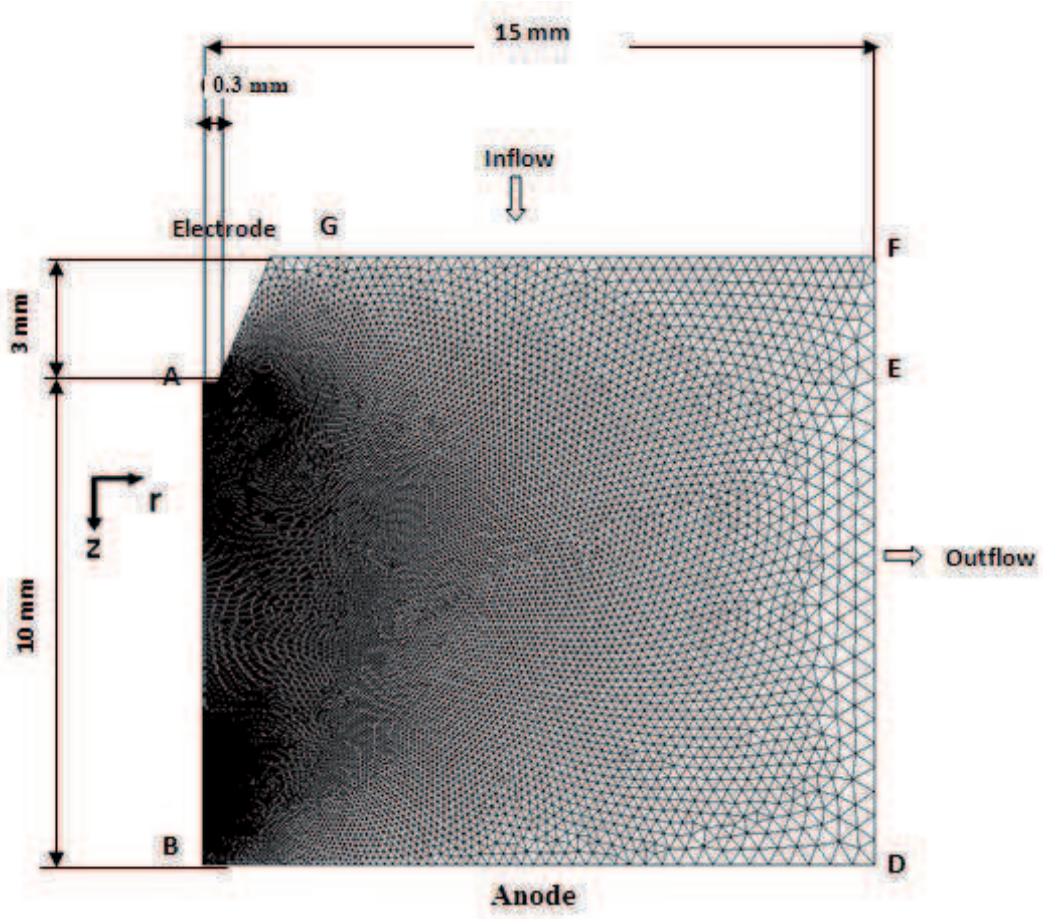

Figure 2. 3: Computational domain.

The argon gas is injected through GF. During the operation mode, the voltage as a result of the applied electric current is going through the ionized argon gas between the tungsten cathode and the anode. The arc column is therefore formed between the cathode-tip and the anode.

2.3.2 Conservation Equations of flow

Based on these previous assumptions, the conservation equations are expressed in terms of cylindrical coordinates (r, z, θ) where r is the radial distance, z is the axial distance, and θ is the azimuthal coordinate.

2.3.2.1. Mass conservation or continuity equation:

Mass conservation equation describes the transport of a conserved quantity. This conserved quantity cannot increase or decrease, it can only move from place to place.

$$\frac{\partial \rho u}{\partial x} + \frac{1}{r}\frac{\partial \rho r v}{\partial r} = 0 \qquad (2.1)$$

Where u and v are the axial and the radial velocity, ρ is the density, the source term of this equation equal to zero.

2.3.2.2. Momentum conservation equation

The conservation of momentum is the application of the principal fundamental of dynamic (Newton law), this law mean or expressed in the following way: the temporal variation in momentum of a fluid particle is equal to the resultant of all forces that influence or action on the fluid particle.

Two types of the forces acting on a fluid particle are distinct:

- Surface forces : - Pressure forces
  -Viscosity forces
- Volume forces: - Gravity forces = 0
  - Electromagnetic forces

Momentum per volume unit is equal to: $\rho \boldsymbol{v}$, then the momentum conservation equation in cylindrical coordinate can be written:

$$\rho \boldsymbol{u}\frac{\partial u}{\partial z} + \rho \boldsymbol{v}\frac{\partial u}{\partial r} = -\frac{\partial P}{\partial z} + 2\frac{\partial}{\partial z}\left(\mu \frac{\partial u}{\partial z}\right) + \frac{1}{r}\frac{\partial}{\partial r}\left(\mu \boldsymbol{r}\frac{\partial u}{\partial r}\right) + \frac{1}{r}\frac{\partial}{\partial r}\left(\mu \boldsymbol{r}\frac{\partial v}{\partial z}\right) + \boldsymbol{j_r B_\theta} \quad (2.2)$$

$$\rho \boldsymbol{u}\frac{\partial v}{\partial z} + \rho \boldsymbol{v}\frac{\partial v}{\partial r} = -\frac{\partial P}{\partial z} + \frac{\partial}{\partial z}\left(\mu \frac{\partial v}{\partial z}\right) + \frac{2}{r}\frac{\partial}{\partial r}\left(\mu \boldsymbol{r}\frac{\partial v}{\partial r}\right) + \frac{\partial}{\partial z}\left(\mu \frac{\partial u}{\partial r}\right) - \frac{\partial \mu v}{r2} - \boldsymbol{j_z B_\theta} \quad (2.3)$$

Where μ is the viscosity, P is the static pressure, j_r is the current density in the radial direction, j_z is the current density in the axial direction, B_θ is the magnetic flux density in the azimuthal direction, the product $j_r B_\theta$ is the axial component of electromagnetic force

produced by the current and the self-induced magnetic flux density in the solution domain, $-j_z B_\theta$ is the radial component of the electromagnetic force.

2.3.2.3. Energy conservation equation

The equation of conservation of energy results from the first thermodynamic law which defines the variation of the total energy of a particle fluid as the sum of the amount heat and work received by the particle fluid under some assumptions.
By convention, the amount of energy received by the system is counted positively and the quantities transferred outside the environment are counted negatively.

In our case of the fluid particle, the total energy of a system is the sum of the kinetic energy e_c, of the potential energy e_P issue from all the internal forces of system and from the internal energy e_{int}. This grandeur e_{int} is an extensive grandeur of state not measurable, only the total variation of energy can be determined. Thus, when the system exchanges heat transfer δ_q and work δ_f with the external environment, its total energy varies as:

$$d(e_c + e_P + e_{int}) = \delta_q + \delta_f \quad \textbf{(2.4)}$$

In our case, we use the enthalpy to define the energy of a system as we work at constant pressure. The enthalpy is written as function of internal energy.

$$H = e_{int} + PV \quad \textbf{(2.5)}$$

The energy conservation equation is therefore written:

$$\underbrace{\rho \boldsymbol{u}\frac{\partial \boldsymbol{h}}{\partial \boldsymbol{z}} + \rho \boldsymbol{v}\frac{\partial \boldsymbol{h}}{\partial \boldsymbol{r}}}_{\text{Convection}} = \underbrace{\frac{\partial}{\partial z}\left(\frac{K}{C_p}\frac{\partial h}{\partial z}\right) + \frac{1}{r}\frac{\partial}{\partial r}\left(\frac{K_r}{C_p}\frac{\partial h}{\partial r}\right)}_{\text{Conduction}} + \underbrace{\frac{j_z^2 + j_r^2}{\sigma}}_{\text{Joule heating}} + \underbrace{\frac{5}{2}\frac{K}{e}\left(\frac{j_z}{C_p}\frac{\partial h}{\partial r} + \frac{j_r}{C_p}\frac{\partial h}{\partial r}\right)}_{\text{Enthalpy flux of electrons}} - \underbrace{\boldsymbol{S_r}}_{\text{Radiative energy}} \quad \textbf{(2.6)}$$

Where h is the enthalpy per mass unity, C_p is the specific heat at the constant pressure, K_r is the thermal conductivity, σ the electrical conductivity, S_r the radiation, K is the Boltzmann constant and e is the electron charge.

The thermal energy Eq. (2.6) consists of the two convection terms, the two diffusion terms, the Joule heating source term and the transport source term of the enthalpy due to the electron drift.

We can develop energy conservation equation (2.6) function of temperature by involving the specific heat as:

$$C_P = \frac{\partial h}{\partial T} \quad \textbf{(2.7)}$$

The calculation of the energy transported by radiation in the arc plasma is very difficult and requires some remarks. The methods the most frequently used for calculating radiation are based on simplifications of the radiative transfer equation, as the average absorption coefficient method and the net emission coefficient method.

- **Average absorption coefficient method**: assumes that the plasma radiates as gray body of the spectrum. Therefore this coefficient does not vary function of frequency. The spectrum is divided into different bands, defined in which the absorption coefficient is considered constant for a given temperature. The most methods used are P1 method and discrete ordinates method.

- **Net emission coefficient method [Low-1]**: this approach based on geometric simplification of the plasma, considers the plasma as an isothermal and homogeneous sphere with radius Rp. In our model, the used database of ε_N is chosen for Rp = 5 mm.

Different works for argon **[Cre-1, Hu_1],** air **[Nag-1]** and SF_6 **[Err-1],** show that the radiation is estimated properly in the hottest regions of arc by the emission net coefficient, while the average absorption coefficient is more accurate in regions of lower temperature.

However, the net emission coefficient method is mainly used in the thermal plasma modeling **[Low-92], [Bau-1], [Fre-1].** In fact, the results of this method have the advantage to be directly integrated into the code as a linear source term.

In our LTE model, we have use a net emission coefficient **[Hu-1]** $\varepsilon r = \varepsilon r(T)$, therefore:

$$Qr = 4\pi\varepsilon_r \quad \textbf{(2.8)}$$

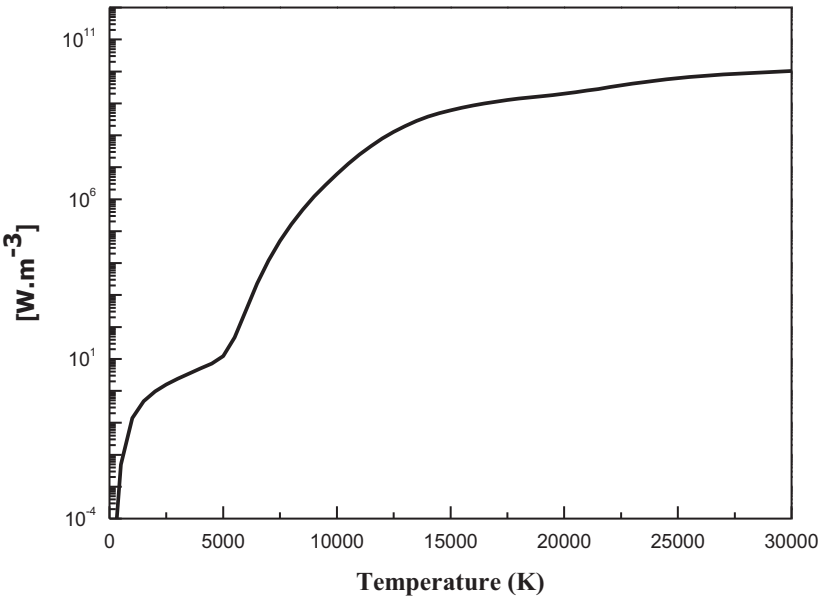

Figure 2. 4: Net emission coefficient in argon plasma.

It can be seen from this figure that the profile of ε_r increases with temperature. At low temperature, the emissions produced by the process of desexcitations of excited atoms are primarily responsible for the radiation losses. The value of net emission coefficient becomes more important at high temperatures when the ionization processes are predominant.

Finally, the last term of the energy equation (2.6) represents the enthalpy of electron due to the electron drift, assuming that the current density is mainly due the contribution of electrons. Delalondre **[Del-1]** show that this term contributes approximately 5% to the rise of temperature in the column of arc. In the anode zone, this mode of energy transfer is dominant and contributes about 60% by raising the temperature in this region, then we can neglect this term in arc column modeling in first approximation.

2.3.3 Electromagnetic Equations for the Arc

The equations for the conservation of axial and radial momentum (2.2)-(2.3) include source terms for the electromagnetic forces. The electromagnetic forces are given by:

$$\vec{F} = \vec{J} \times \vec{B}$$

(2.9)

In two-dimensional axis-symmetric system the radial and the axial component of the source terms in the momentum equations are given by:

$$F_r = -J_z . B_\theta \quad \textbf{(2.10)}$$

$$F_z = J_\mathrm{r} . B_\theta \quad \textbf{(2.11)}$$

Thus, in order to determine these source terms the current density and the azimuthal magnetic flux density have to be calculated.

For a moving conductive fluid, ohm's law takes the following form:

$$\vec{J} = \sigma_e \vec{E} \quad \textbf{(2.12)}$$

Where $\overrightarrow{E}$ represent the electric field.

The plasma is electrically neutral:

$$\vec{\nabla} . \vec{J} = 0 \quad \textbf{(2.13)}$$

The electric potential is given by:

$$\vec{E} = -\vec{\nabla} V \quad \textbf{(2.14)}$$

Combining equations (2.13), (2.12) and (2.14) gives:

$$\vec{\nabla} . (-\sigma_e . \vec{\nabla} V) = \vec{\nabla} . (\sigma_e . \vec{E}) = \vec{\nabla} . (\vec{J}) = 0 \quad \textbf{(2.15)}$$

where V is the electrical potential, $\vec{E}$ is electrical field, $\vec{J}$ is current density and σ_e is electrical conductivity.

The radial and axial current density can be calculated from the electrical potential equation:

$$\mathrm{j_{z=}} - \sigma_\mathrm{e} \frac{\partial \mathrm{V}}{\partial \mathrm{z}} \quad \textbf{(2.16)}$$

$$\mathrm{j_{r=}} - \sigma_\mathrm{e} \frac{\partial \mathrm{V}}{\partial \mathrm{r}} \quad \textbf{(2.17)}$$

2.3.3.1. Calculation of magnetic field

The calculation of electromagnetic forces Eq.(2.10, 2.11), the source term of the axial and radial momentum conservation equations are obtained by the vector product between the current density and magnetic field $\vec{B}$. So we need to know at every moment, or each iteration, the distribution of the magnetic field created by current, conductors and the electric arc. The objective of this part is to study different methods to calculate $\vec{B}$. Therefore, the analysis of

these methods helps us to establish a criterion of choice. To get the local magnetic field $\vec{B}$, we present three different methods: two direct methods (Biot and Savart law, and Ampère theorem) and an indirect method (potential vector A).

2.3.3.2. Direct methods

- **Biot and Savart law [Pur-1]**

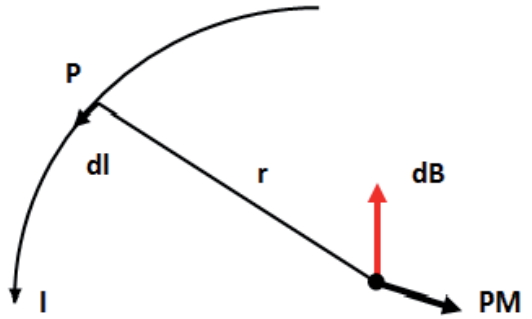

Figure 2.5: Biot and Savart Law.

Consider close of the point **P**, a circuit element **dl** traversed by a current **I**. The **dl** vector is oriented in the direction of current. **r** is the distance between the dl element and the point **M** for which we want to determine the magnetic field.

r is called the unit vector parallel to the **PM** vector. The Biot and Savart law expresses that the magnetic field element **dB** at M point created by the wire element **dl** traversed by the current **I** is written:

$$d\vec{B} = \frac{\mu_0 IdL \times r}{4\pi r^3} \quad \textbf{(2.18)}$$

Using the superposition of magnetic field principle, the total field created by all the circuits contained in the space can be written as:

$$\vec{B} = \iiint \frac{\mu_0 IdL \times r}{4\pi r^3} \quad \textbf{(2.19)}$$

where μ_0 is the permeability of space ($4\pi \times 10^{-7}$ T mA^{-1}).

The inconvenience of this approach in modeling is the computation time occupied by the resolution of this triple integral at each point of domain.

- **Ampere Theorem [Pur-1]**

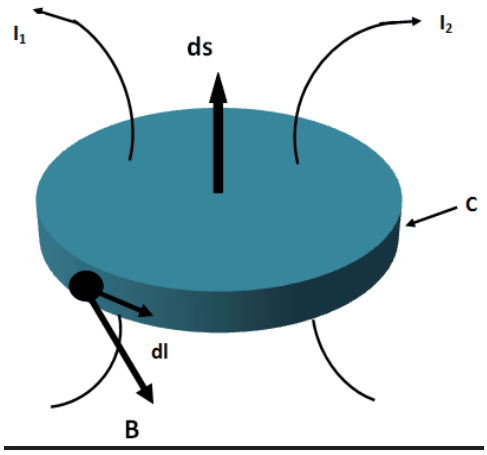

Figure 2. 6: Ampere's Theorem.

The circulation of the axial vector of magnetic field created by the current distribution along any curve but closed C, called Ampere's curve, is equal to the product of μ_0 by the algebraic sum of the current witch traversed C, figure (2.6).
The Ampere's theorem is expressed by the relationship:

$$\oint_C \vec{B}dl = \mu_0 \sum \mathrm{I} = \mu_0 \iint_S \mathrm{J}d\vec{s} \qquad \textbf{(2.20)}$$

Ampere's theorem is used only in the computational domain has a high degree of symmetry.

2.3.3.3. Indirect methods

- **Vector potential**

This approach consists to express the magnetic field as function of the vector potential.

The electromagnetic equations for the magnetic field:

$$\vec{\nabla}.\ \vec{B} = 0 \quad \textbf{(2.21)}$$

$$\vec{\nabla} \times\ \vec{\mathrm{B}} = \mu_0 \vec{\mathrm{j}} \quad \textbf{(2.22)}$$

Equation (2.21) allows representing the magnetic field as the rotational of vector function:

$$\vec{\mathrm{B}} = \vec{\nabla} \times \vec{\mathrm{A}} \quad \textbf{(2.23)}$$

We call $\vec{\mathrm{A}}$ the vector potential satisfies a relationship called Gauge Poisson conditions obtained by substituting equation (2.21) in equation (2.22). This relation is written:

$$\Delta\, \vec{\mathrm{A}} = -\mu_0 \vec{j} \quad \textbf{(2.24)}$$

Equation (2.43) can be projected along the axes:

$$\frac{\partial^2 A_z}{\partial z^2} + \frac{1}{r}\frac{\partial}{\partial r}\left(r\frac{\partial A_z}{\partial r}\right) + \mu_0 j_z = 0 \quad \textbf{(2.25)}$$

$$\frac{\partial^2 A_r}{\partial z^2} + \frac{1}{r}\frac{\partial}{\partial r}\left(r\frac{\partial A_r}{\partial r}\right) - \frac{A_r}{r^2} + \mu_0 j_r = 0 \quad \textbf{(2.26)}$$

Equations (2.25) and (2.26) are two scalar conservation equations for the components of magnetic potential A_z and A_r.

Knowing the magnetic potential, the calculation of the magnetic field is straightforward from (2.23), which for an axis-symmetric bidimensional coordinate system becomes:

$$B_\theta = \frac{\partial A_r}{\partial z} - \frac{\partial A_z}{\partial r} \quad \textbf{(2.27)}$$

This method is used when we know the distribution of current density.

The selection criterion of these methods is based on the distribution of current density. We use the Biot-Savart law in the case the current density is not known, only the total current is provided.

When the current density is given, there is the possibility of using either Ampere's law or the vector potential. The Ampere's law will be applied when simplification related to the symmetry of the domain that allows to solving simple integral. Therefore, the calculation of the field $\vec{\mathrm{B}}$ represents a numerical integration on all cells.

In our modeling we have used the vector potential method.

The validation of vector potential method in 2D was done in different works **[Fre-2, Baud-1]**, by making a comparison between analytically magnetic field results and results of model using Fluent Software.

The equations of MHD are now completely defined. Now we define the boundary conditions.

2.4 Boundary Conditions

In order to solve the transport equations for the calculation domain, boundary conditions need to be specified. There is three types of boundary condition: Dirichlet condition, Neumann conditios and Cauchy condition. A complete listing of boundary conditions for this model are presented in table 1.1.

As the calculation domain for u, v, p, h the area ABDFG, figure 2.3. An unstructured mesh is realized by **Gambit 2.4.6 [Gambi-1]**, total numbers of nodes, cells and faces are 20127, 39813 and 59939 respectively.

The distance between the cathode-tip and the anode surface is kept at 10mm. then the inflow boundary (line EF) is taken 3 mm above the cathode-tip and the outflow boundary (line EC) is 14 mm away from the axis. The boundary conditions are as follow:

	AB (axis)	BD (anode)	FD (outlet)	FG (inlet)	GA (cathode)	EA (cathode-tip)
u	$\frac{\partial u}{\partial r} = 0$	$u = 0$	*Pressure outlet*	$\rho u = 0.002$	$u = 0$	$u = 0$
v	$v = 0$	$v = 0$	*Pressure outlet*	$v = 0$	$v = 0$	$v = 0$
h	$\frac{\partial h}{\partial r} = 0$	$\emptyset = 0$	$T=T_o$ (1000 K)	$T=T_o$ (1000 K)	$T=T_1$ (3000 K)	$T=T_1$ (3000 K)
V	$\frac{\partial V}{\partial r} = 0$	$V = 0$	$\frac{\partial V}{\partial r} = 0$	0	$\frac{\partial V}{\partial r} = 0$	$J = j_{given}$
A_z	$\frac{\partial A_z}{\partial r} = 0$	$\frac{\partial A_z}{\partial z} = 0$	0	0	$\frac{\partial A_z}{\partial n} = 0$	$\frac{\partial A_z}{\partial z} = 0$
A_r	$\frac{\partial A_r}{\partial r} = 0$	$\frac{\partial A_r}{\partial z} = 0$	0	0	$\frac{\partial A_r}{\partial n} = 0$	$\frac{\partial A_z}{\partial z} = 0$

Table 2. 1: Boundary conditions for the LTE model.

Along the centerline AB the symmetry conditions are used. The radial component of velocity is imposed equal to zero and all other variables are governed by the Newman conditions. At the line BD (copper anode), a no slip condition for the velocity is postulated, the electrical potential is assumed to be equal zero, because we choose the anode as reference of electrical potential. We also impose on the anode a null heat flux, a radial and axial velocity equal to zero. As no interaction between the arc column and the electrodes are taken into account, some boundary conditions are difficult to impose. For example, the zero thermal flux to the anode cannot be completely satisfying. A better way would be to impose a experimental temperature profile. But we do not have it for all values of the current intensity studied. We have preferred to keep the same boundary condition to compare all cases, knowing that true isotherms are "attached" to the anode for smaller radius values. In that way, temperatures at the anode are surely overestimated.

At the line FD, the temperature is assumed to be 1000 K, no current flow, atmospheric pressure (Newman conditions). On the cathode surface GA, no slip conditions are used and the temperature is assumed to be 3000K. At the line FG, the temperature is taken as 1000 K. The most critical condition in this modeling is the current density distribution along the line EA.

Since it is very difficult to measure the plasma temperature and the electric field strength near the cathode tip, there are three mathematical model in literature for the boundary conditions on the cathode-tip: exponential model **[Hsu-2][Kov-1][Fre-1],** parabolic model **[Ush-1][Fre-2]** and constant model **[Mck-1], [Choo-1].** According to these studies, a constant profile is chosen:

$$J = \frac{1}{2\pi r_h^2} \qquad \textbf{(2.28)}$$

Where J = 3,54x10^8 A/m^2 for 100 A, r the radius of cathode-tip is assumed to be 0.3 mm. Like the temperature boundary condition on anode, this constant current density leads to overestimate the temperature at the vicinity of the cathode. This work is a first step to a more detailed model. A more interesting approached would be for example to calculate the electric current also in the cathode.

The set of conservation equations, presented previously represents a highly nonlinear system of coupled differential equations which must be solved simultaneously with boundary conditions and thermal properties of plasma. This system has no analytical solution to obtain

the field variables u, v, p, h, V as function of r and z. Therefore a numerical solution is usually sought to solve this system of equations. A numerical tool was developed, based on the commercial CFD software Fluent 12 **[Flue-1]**. This software is based on the finite volume method adapted through dedicated UDF (User Defined Function) to different peculiarity of plasmas, such as the electromagnetic field, the Joule heat generation, the radiation losses, and the thermo-physical properties of the gas. In this part, details on the development of the simulation tool are presented.

2.5 Numerical method of resolution

2.5.1 Conservation Equations written in the Patankar form

The numerical method for solving the fluid flow problem is based on volume finite element scheme developed by Patankar S V (1981) **[Pat-1].** In the following, the technical bases of their method briefly discussed by **[Pat-1]** indicate that the differential equations (conservation laws) have the same common form which may be expressed as:

$$\underbrace{\frac{\partial \rho \phi}{\partial t}}_{\text{Temporel term}} + \underbrace{\nabla.(\alpha \rho \overrightarrow{u_\phi})}_{\text{Convective term}} = \underbrace{\nabla.\Gamma_\Phi \nabla_\phi}_{\text{Diffusive term}} + \underbrace{S_\phi}_{\text{Source term}} \qquad \textbf{(2.29)}$$

Where ϕ is the dependent variable, Γ_ϕ and S_ϕ are the diffusion coefficient and the source term of the variable ϕ, respectively. To cast the conservation differential equation of mass, momentum, energy, electrical potential, radial and axial potential vector into equation (2.29), the associated quantities are:

Conservation equations	Φ	α	Γ_Φ	S_Φ
Mass	1	1	0	0
Axial momentum	u	1	μ	$-\frac{\partial P}{\partial z} + 2\frac{\partial}{\partial z}\left(\mu \frac{\partial u}{\partial z}\right) + \frac{1}{r}\frac{\partial}{\partial r}\left(\mu r \frac{\partial u}{\partial r}\right) + \frac{1}{r}\frac{\partial}{\partial r}\left(\mu r \frac{\partial v}{\partial z}\right) + j_r B_\theta$

Radial momentum	v	1	μ	$-\frac{\partial P}{\partial z}+\frac{\partial}{\partial z}\left(\mu\frac{\partial v}{\partial z}\right)+\frac{2}{r}\frac{\partial}{\partial r}\left(\mu r\frac{\partial v}{\partial r}\right)+\frac{\partial}{\partial z}\left(\mu\frac{\partial u}{\partial r}\right)-\frac{\partial \mu v}{r2}-j_z B_\theta$
Energy	h	1	$\frac{K}{C_P}$	$\frac{j_z^2+j_r^2}{\sigma}+\frac{5}{2}\frac{K}{e}\left(\frac{j_z}{C_p}\frac{\partial h}{\partial z}+\frac{j_r}{C_p}\frac{\partial h}{\partial r}\right)-S_r$
Electric potential	V	0	σ	0
Axial potential vector	A_z	0	1	$\mu_0 j_z$
Radial potential vector	A_r	0	1	$-\frac{A_r}{r^2}+\mu_0 j_r$

Table 2. 2: Two dimentional MHD equations of thermal plasma in LTE.

2.5.2 Implementation of MHD model in Fluent

Fluent software contains the broad physical modeling capabilities needed to model flow, turbulence, heat transfer, and reactions for industrial applications ranging from air flow over an aircraft wing to combustion in a furnace. However, the solver is not designed to study a plasma flow, and in addition, it is contained in a “black box”.

The numerical method for solving the fluid flow problem is based on volume finite element.

To adapt the solver of Fluent to the resolution of a plasma arc using MHD model, we use a code written and compiled in C language, called UDF (User-Defined Function). This code must be developed by the user.

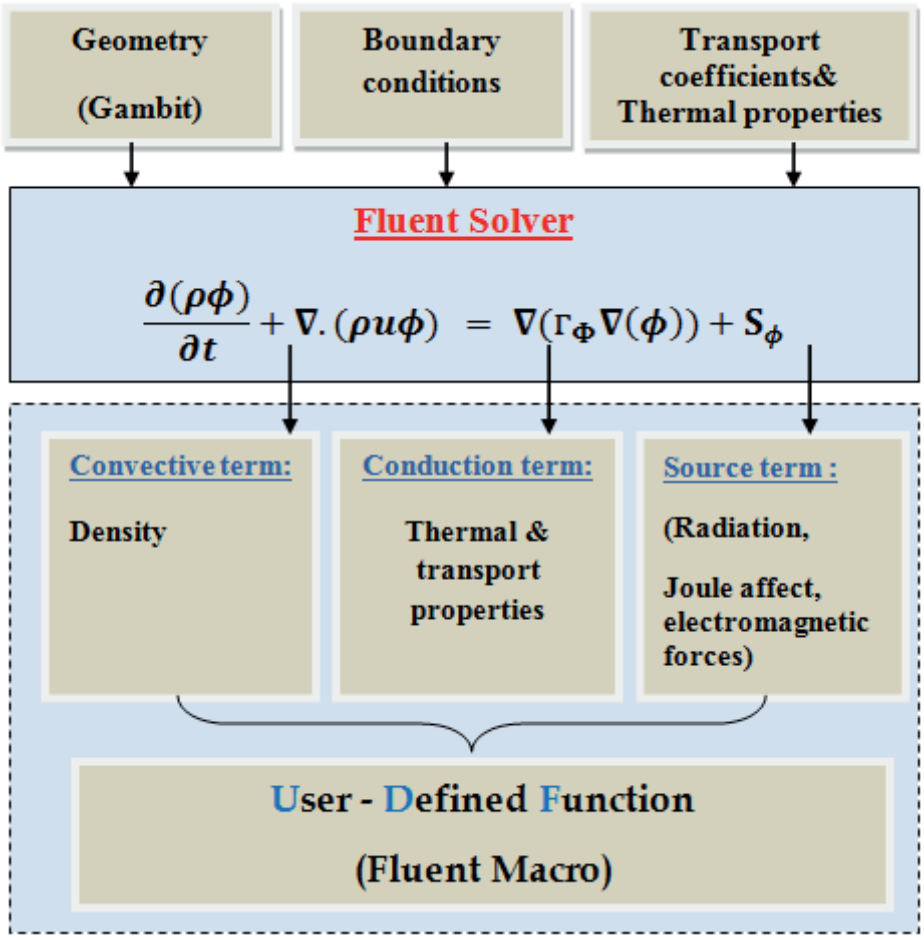

Figure 2.7: Simplified scheme of Fluent solver adapted to arc plasma.

To illustrate scheme, we take an example of variable ϕ= V, the electric potential, r_ϕ equal to electrical conductivity (the diffusion coefficient) and the source term S_ϕ of electrical potential equation equal to zero. In this example, we develop the code that calculate the electrical potential using UDS (User-Defined Scalar), we define a UDS transport equation by setting the parameters for the four terms presented in figure 2.7, temporal term equal to zero because we are in steady case, the source term equal to zero, then we defined only the convection and diffusion terms.

The UDS is written through macro type "DEFINE_DIFFUSIVITY" to describe the diffusion coefficient, and the macro "DEFINE_SOURCE" to describe the term source for each equation.

The same principle was applied to the calculation of axial and radial vectors component. When we want to access face or cell variables that are computed for user-defined scalar transport equation we use this macros table 2.3.

Macro	Argument Types	Returns
F_UDSI(f,t,i)	face_t f, Thread *t, int i Note: i is index of scalar	UDS face variables
C_UDSI(c,t,i)	cell_t c, Thread *t, int i	UDS cell variables

Table 2. 3: Accessing User-Defined Scalar Face/cell Variables

We can use C_UDMI when we want to store cell variables that are computed for user-defined scalar equations, for example, the electric field, current density, magnetic field, electromagnetic forces, joule heating and radiative losses.
Before we can use C_UDMI to store variables in memory, we need first to allocate memory location(s) in the User-Defined Memory panel in Fluent.

Macro	Argument Types	Returns
C_UDMI(c,t,i)	cell_t c, Thread *t, int i	UDM cell variables

Table 2. 4: Accessing User-Defined Memory cell Variables

2.6 Conclusion

We have presented the magneto-hydrodynamic equations assuming continuum, conductor and neutral fluid in Local Thermodynamic Equilibrium. This nonlinear system with partial derivative has no analytical solution. The finite volume seems to be the most appropriate method for this problem, to do this, we use the solver of software Fluent.

From the literature synthesis carried out in chapter 1, we have shown the importance of work on free-burning arc in argon. The works focuses on theoretical and experimental studies. Therefore, in next chapter, the validation of our model is performed on this type of arc for different values of current.

Bibliography

[Bau-1] Bauchire J M. :« Modélisation numérique d'une torche de projection à plasma : influence de la géométrie et de la turbulence sur les propriétés du plasma »,. Thèse de doctorat de l'Université Paul Sabatier, 184P, (1997).

[Baud-1] Baudoin Fulbert. : « Contribution à la modélisation d'un arc électrique dans les appareils de coupure basse tension »,. Thèse de doctorat de l'Université Blaise Pascal-Clermont II, 65P, (2004).

[Boul-1] Boulos M, Fauchais P, and Pfender E. Book : "Thermal Plasmas, fundamentals and applications", vol. I.Plenum Press, NY.(1994).

[Clap-1] Emile Clapeyron. : « Mémoire sur la puissance motrice de la chaleur » J. Ecole polytech. 14 153–90, (1834).

[Cre-1] Cressault Y. : « Propriétés des plasmas thermiques dans des mélanges argon-hydrogène-cuivre », Thèse de doctorat de l'Université Paul Sabatier, 220P, (2001).

[Choo-1] Choo. R. T. C., Szekelt J., Westhoff R C. : "On the calculation of the free surface Temperature of Gaz-Tungsten-Arc Weld Pools from First Principal: Part I. Modeling the Welding Arc", Metal, Trand., Vol 23 B, PP. 357-368, (1992).

[Del-1] Delalondre C. : « Modélisation aérothermodynamique d'arcs électriques à forte intensité avec prise en compte du déséquilibre thermodynamique local du transfert thermique à la cathode »,. Thèse de doctorat de l'Université de Rouen, 160p, (1990).

[Dalt-1] Dalton J.: "On the absorption of gases by water and other liquids" Memoirs and Proc. of the Manchester Literary and Philosophical Society 1 271–86, (1805).

[Err-1] Erraki A .: « Etude du transfert radiatif dans les plasmas thermiques :application au SF6 et au mélange argon-fer », Thèse de doctorat de l'Université Paul Sabatier, 189P, (1999).

[Fre-1] Freton P, Gonzalez J. J., Gleizes A. : "Comparison between a two and a three-dimensional arc plasma configuration", J. Phys. D:Appl Phys. 33, 2442-2452, (2000).

[Fre-2] Freton Pierre. : « Etude d'un arc de découpe par plasma d'oxygène Modélisation-expérience », Thèse de doctorat de l'Université Paul Sabatier, 64P, (2002).

[Fri-1] Fridman A, Lawrence A. Kennedy.: Plasma Physics and Engineering, second edition, ISBN : 978 1 4398 1228 0,.New York, 345P, (2010).

[Flue-1] Fluent Inc, "Fluent 12.1 User's Guide", (2012).

[Gambi-1] Fluent Inc, "Gambit User's Guide".

[Gleiz-1] Gleizes Alain, Moez Bouaziz, Jean-Jacques Gonzalez, and Manitra Razafinimanana. : "Influence of the Anode Material on an Argon Arc", IEEE Transactions on Plasma Science , Vol. 25, No. 5, 891, (1997).

[Hu_1] J. Hu, H.L. Tsai.: Arc welding. Part I: "The arc, International Journal of Heat and Mass Transfer" 50 833–846, Heat and mass transfer in gas metal, (2007).

[Hsu-1] Hsu K.C, and Pfender E. : J.Appl. Phys, 54, pp. 256, (1983).

[Hsu-2] Hsu K.C., Etemadi K. and Pfender. E.: "Study of the free burning high intensity argon arc" J.Appl. Phys, 54, pp. 1293-1301, (1983).

[Hsu-3] Hsu K.C., and Pfender. E.: J.Appl. Phys, 54, pp.4359, (1983).

[Kov-1] Kovitya P., Cram L E A. "Two dimensional Model of Gas-Tungsten Welding Arcs". Welding Journal, PP.34-39, (1986).

[Low-92] Lowke.J.J., Kovitya P, Schmidt H P.: "Theory of free-burning arc columns including the influence of the cathode". J.Phys. D : Appl. Phys., Vol.25, pp1600-1606, (1992).

[Low-1] Lowke J J, J. Quant. Spectrosc. Radiat. Transfer 14 111, (1974).

[Mck-1] McKellliget J. and Szekely J.: "Heat transfer and fluid flow in the welding arc" Metall.Trans 17A, pp. 1139-1148, (1986).

[Max-1] Maxwell J C A.: "Dynamical theory of the electromagnetic field" Phil. Trans. R. Soc. Lond. 155 459–512, (1865).

[Nav-1] Navier C-L. : « Mémoire sur les lois du mouvement des fluides » Mém. Acad. Sci. 6 389, (1822).

[Nag-1] Naghizadeh-Kashani Y. : « Calcul du transfert radiatif dans un plasma d'air », Thèse de doctorat de l'Université Paul Sabatier, 179P, (1999).

[Pur-1] Purcell E M. Berrkeley.: « Cours de Physique, électricité et magnétisme ». Paris : Armand Colin, 460 p, (1993).

[Stok-1] Stokes G G.: "On the theories of the internal friction of fluids in motion" Camb. Trans. 8 287, (1845).

[Ush-1] Ushio M., Matsuda F. : "Mathematical Modelling of Heat Transfer of Welding Arc" (Part 1), JWRI, 1982, Vol 11, n°1, PP. 7-15, (1982).

[Ve-1] Versteeg H.K,. Malalasekera W.: "An introduction to Computational Fluid Dynamics". Longman, Edinburgh, (1995).

Chapter 3: Results and Discussion of LTE Two-Dimensional Model

RESUME DU CHAPITRE 3

Après avoir discuté des détails du modèle d'arc et des hypothèses adoptées, nous allons examiner dans ce chapitre quelques-uns des résultats que nous avons obtenu dans un gaz d'argon à 100, 70, 50 A et avec une distance inter-électrodes de 1 cm:

- ✓ A l'ETL,
- ✓ Deux dimensions,
- ✓ Stationnaire,

et comparer ces résultats avec les résultats expérimentaux et numériques existants dans la littérature.

Dans une deuxième étape, nous utiliserons ce modèle validé pour étudier l'influence de quelques paramètres qui nous ont paru important. Ces paramètres sont de deux types : paramètres électriques et nature de gaz.

Chapter 3: Results and discussion of LTE Two-Dimensional Model

3.1 Introduction

In the previous chapters, a self-consistent physical model of the arc column discharge was developed. The necessary plasma transport coefficients were given (chapter 1), and the basic of the numerical calculation schemes was discussed (chapter 2).
This chapter will first show results predicted for a free-burning arc discharge, the experimental and theoretical validation of the model will also be discussed.
By a variation of the fundamental arc parameters like electrical current and gas nature, the model will prove its ability to produce results in positive column.

3.2 Presentation and analysis of results

3.2.1 Validation of the model

Comparison between our numerical simulation and measured temperature fields and other calculations provide from literature is discussed in this section. The solutions of the conservation equations for the entire free-burning arc are presented, excluding the cathode and anode regions.

3.2.1.1 Comparison Model/Experiment

The plasma temperatures are derived from measured radial intensity distributions with electric current at 100 A in argon gas and a gap of 10 mm between the anode and cathode. These spectroscopic measurements come from the work of **Etemadi** et al (1983) **[Etem-1]** and are shown in Fig.3.1 (left half of these figures). Calculated temperature profiles for 100 A atmospheric pressure argon arc (electrode gap of 10 mm are plotted in Fig 3.1(right half of these figure).

The comparison between the calculated isotherms in argon, with spectroscopic measurements of **Etemadi** et al (1983) **[Etem-1]** comprised between 11 kK and 13 kK, show a good agreement. The difference between calculated and experimental temperature increases as we approach the cathode, with a maximum difference of 3000 K on plotted isotherms.

Since the cathode region sucks gas from its surrounding by the electromagnetic pumping force, the induced flow enters the arc core from the fringes and as it approaches the anode it is forced to turn around in r direction.

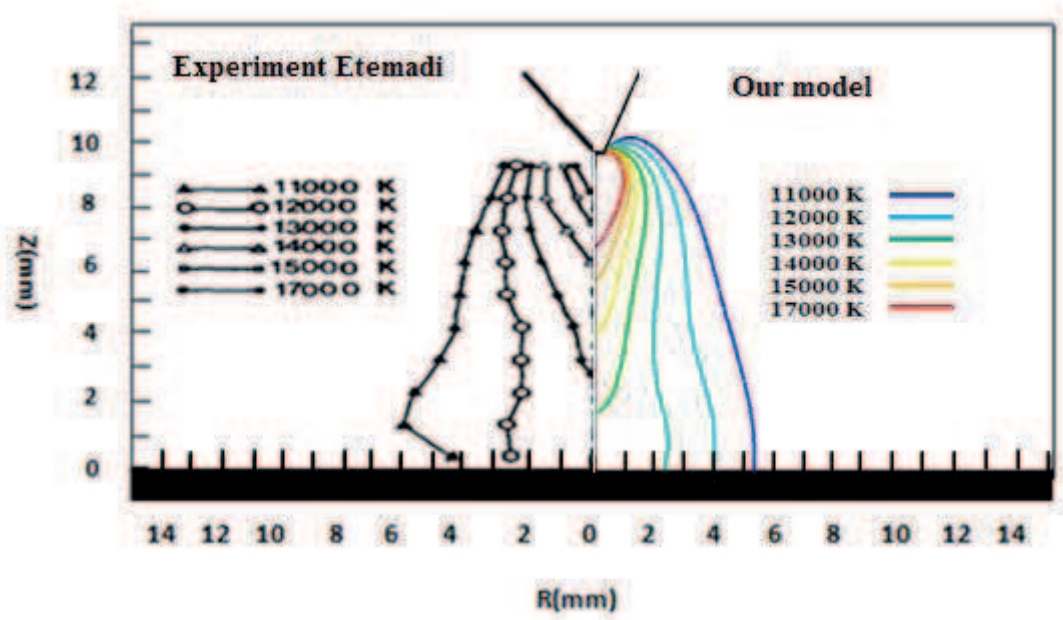

Figure 3. 1: Measured and calculated isotherms of free-burning argon arc, (1= 100 A, d =10mm).

We observe radial spreading of the isotherms towards the anode. The highest of temperature is observed in the hot region (cathode-tip).

The maximum radius of thermal plasma estimated with our calculation is around of 6.2 mm and it agrees with the value of radius deducted from experiment results.

The most significant deviations between calculated and measured data are observed in cathode and anode regions. These differences are mainly due to our boundary conditions which do not match exactly the experimental device.

3.2.1.2 Comparison Model/Model

The plasma temperatures are derived from our model with electric current at 100 A in argon gas and gap of 10 mm between the anode and cathode. They are plotted in Fig 3.2 (right half of these figure) with results from the model of Hsu et al (1983) **[Hsu-1]** shown in Fig 3.2 (left half of these figures).

The comparisons between the calculated isotherms in argon, 100 A, and those of the model of Hsu et al (1983) **[Hsu-1]** comprise between 11 kK and 17 kK shows a good agreements in general.

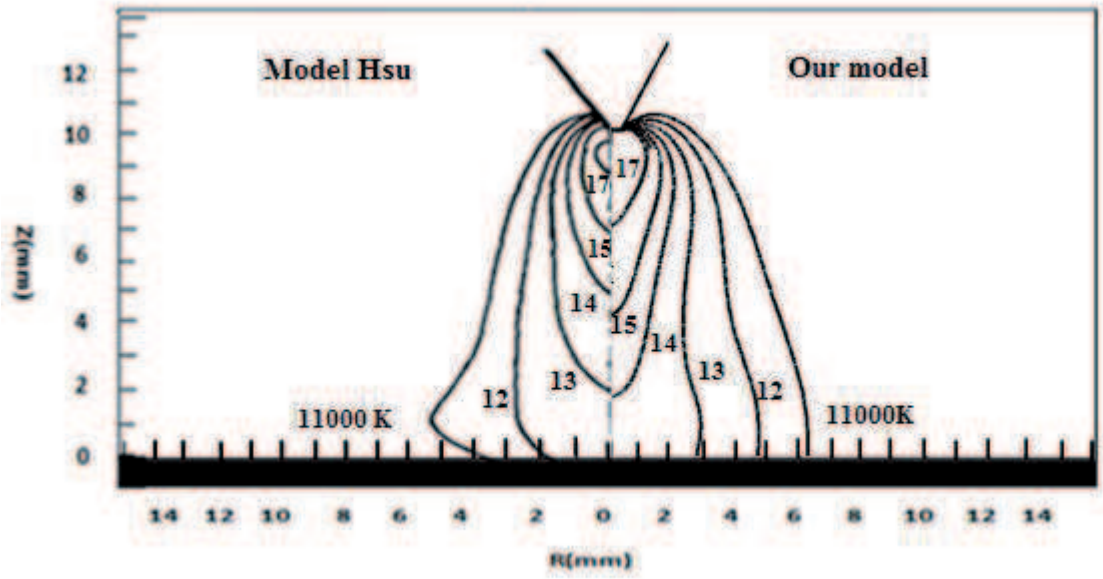

Figure 3. 2:Comparison between our calculated isotherms of free-burning argon arc and Hsu model (1= 100 A, d =10mm).

It can be seen that the temperature decreases from the cathode to the anode. This behavior is explained by the current density which is very high near the cathode-tip, but decreases rapidly with increasing distance from the cathode.

We observe on Figure 3.2 a difference between values of isotherms of our model and those of Hsu **[Hsu-1].** The largest difference is elevated by the isotherms 17 and 15 kK in the hot region and on the anode region by the isotherms 11 and 12 kK.

This difference can be explained by different parameters in modeling like geometry of the cathode truncated or pointed and the different boundary conditions of current density on the cathode-tip and heat flux on the anode.

In our model we use a constant profile of current density (Eq 2.28), but Hsu **[Hsu-1]** use an exponential profile. In literature the most significant difference is observed close to the cathode, the highest temperature at cathode is obtained with constant profile of current density and a minimum temperature is obtained with exponential profile of current density, the difference is about 5 kK with 200 A **[Baud-1].**

On the anode, we impose a null heat flux but Hsu **[Hsu-1]** uses an experimental profile which is a more realistic choice.

3.2.2 Presentation of results

Figure 3.3 shows the temperature along the axis of symmetry AB of our model.

At the cathode, the temperature corresponds to the boundary condition of 3 kK. The temperature increases to a maximum at z = 3 mm, from there, a slight decrease in temperature along the axis AB.

On the same figure, the comparison between temperature profile from the model and from experimental results of Etemadi **[Etemad-1]** shows a good agreement in general.

The comparison is done on the axis**,** because we do not have the values of experimental temperature close to the cathode, we observe that the axial temperature of model is superior to that found experimentally. The model tends to overestimate the temperature, we observe a difference of 1kK at distance of 4 mm, 5 mm and 6 mm, and about 800 K at 9.6 mm.

This can be explained by the boundary condition of temperature imposed on the cathode-tip of value 3kK and this influences the value of temperature along the axis.

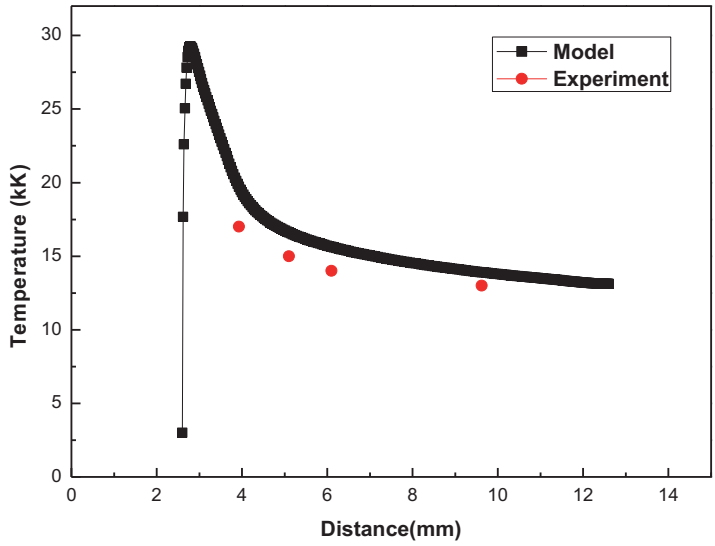

Figure 3. 3:Axial temperature of free-burning argon arc, (I= 100 A).

Figure 3.4 represents the velocity along the axis AB. We note a maximum of 460 $m.s^{-1}$ at z = 3 mm below the cathode-tip. Then, the velocity deceases rapidly to become zero at the anode.

We have not done a comparison of velocity profile with other works, the reason almost of works in free-burning arc in argon is performed with an electrical current of 200 A, and in our model, we are limited with a maximum of current 100 A with this geometry of cathode, beyond this value of current, the temperature exceed 30kK, and our data base of thermodynamic properties is limited to 30 kK.

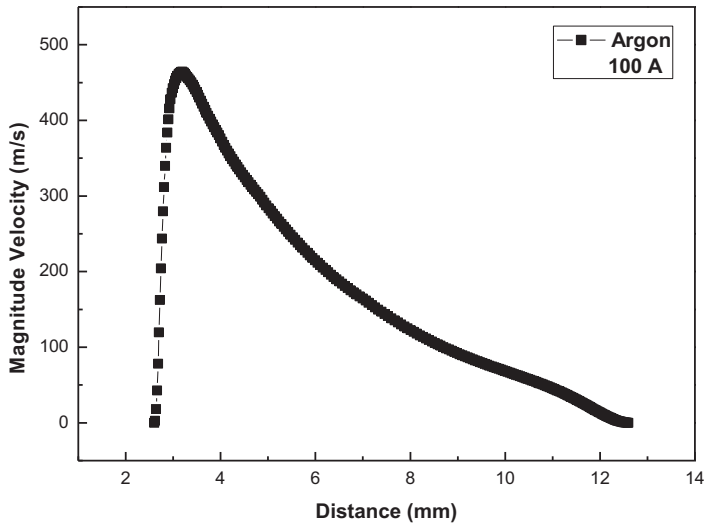

Figure 3. 4:Axial velocity of argon free-burning arc, (I=100 A).

The profile of velocity is largely conditioned by the mathematical model of current density. Indeed, a spatial distribution of the different current density at the cathode-tip changes the value of electromagnetic forces responsible for the magnetic pumping.
This peculiarity is found in the literature, see table 3.1. Thus, the maximum of velocity varies from 260 $m.s^{-1}$ to about 500 $m.s^{-1}$, a difference of over 100 % according to the authors.

Authors	**Mathematical model of current density on the cathode**	**Maximum velocity ($m.s^{-1}$)**
[Fre-1]	exponential	260
[Hsu-1]	exponential	294
[Goo-1]	constant	390
[Low-1]	constant	430
[Zhu1]	constant	500

Table 3. 1: Maximum of velocity in free-burning arc of argon (200 A).

Figure 3.5 represents the current density along the axis AB. At the cathode-tip, the value of current density J_{max} corresponds to the equation (2.28), whether 3.54×10^8 A/m^2.
The current density is very high near the cathode-tip, but decreases rapidly with increasing distance from the cathode. This current density represents the electric current per unit area of

cross section of the arc. Then the arc radius increases as current density decreases so that current intensity remains constant along the arc.

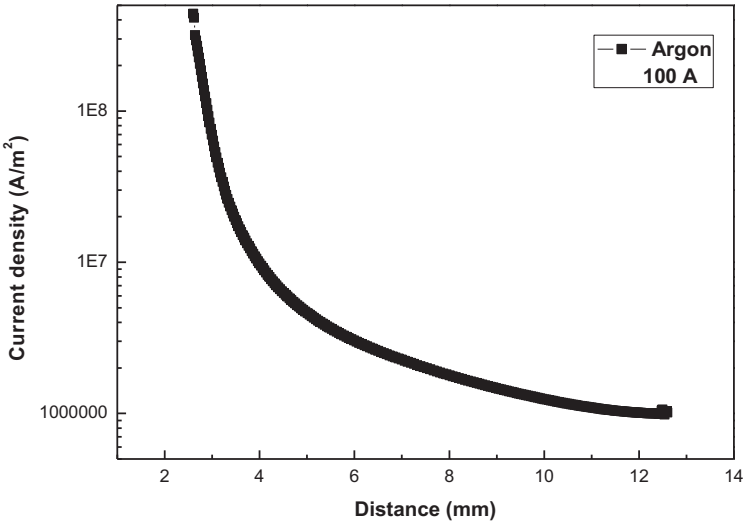

Figure 3. 5:Current density of argon free-burning arc, (I = 100).

Figure 3.6 represents the electric potential along the axis AB. We observe a voltage drop in the column of arc of 11.4 V. This voltage drop is equal to 11.2 V **[Baud-1]** and of 13.3 V in **[Hsu-1]** with 10 mm of distance between electrodes. There is a small difference between these values, since the voltage drop in column depends linearly on the distance between electrodes.

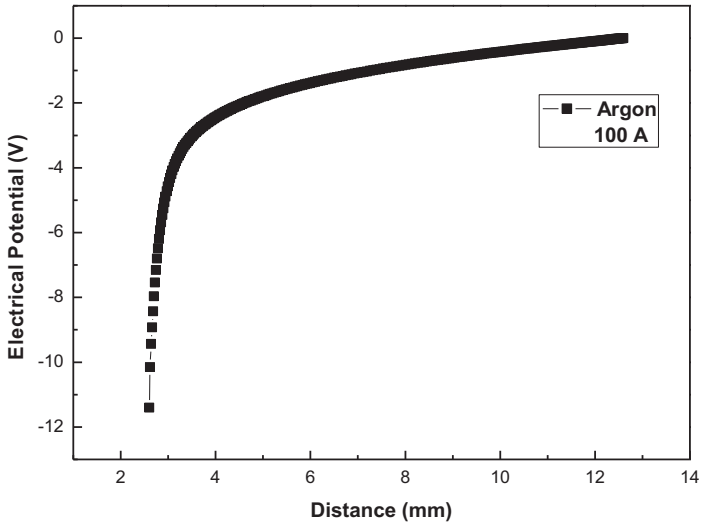

Figure 3. 6: Electric potential of argon free-burning arc, (I= 100 A).

To know the total voltage drop between the two electrodes, it should be add to this value, the voltage drops of anode and cathode, not considered in our model. This value is about 8.7 V in experimental work of Hsu et al **[Hsu-1],** and of 8 V in the work of Freton et al **[Fre-1].**

The centerline temperature, the axial velocity component and the over pressure are shown in figure 3.7. The velocity U increases rapidly near the cathode due to the electromagnetic forces and it drops sharply in front of the anode resulting in a pressure increase.

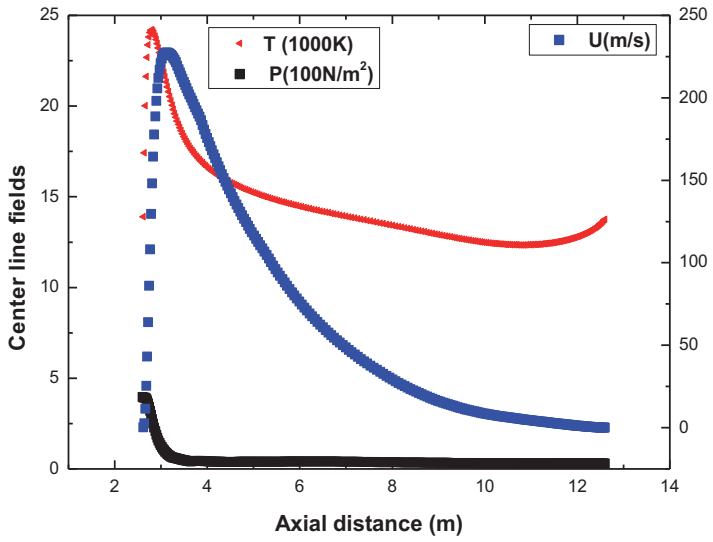

Figure 3. 7: Axial velocity, temperature and over pressure distribution in free burning arc at 1atm, 100 A

Figure 3.8 shows the centerline distribution of the electric field, the current density, and the electrical potential with 100 A current. The current density is very high near the cathode tip but decreases fast away from the cathode. Since the arc core is almost partially ionized. The electrical conductivity at the centerline decrease slightly. Therefore, the curves of the electric field strength and of the current density are similar.

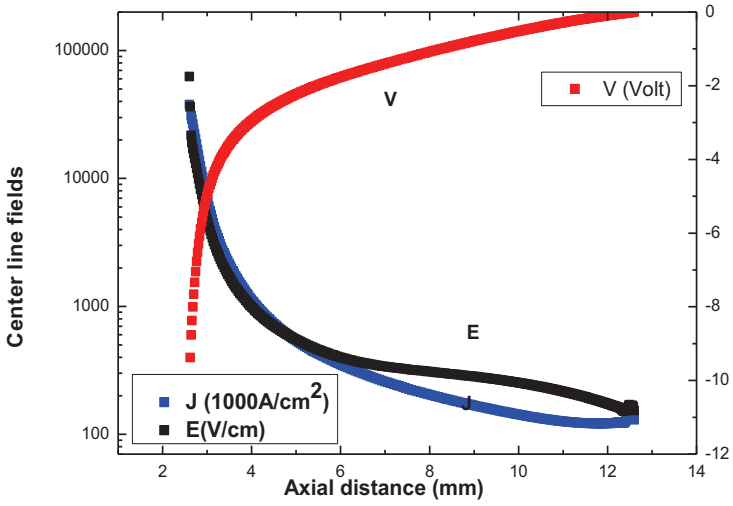

Figure 3. 8: Electric potential, electric field and current density distribution in free burning argon arc at 1atm, 100 A.

3.2.3 Analysis of results

To explain the different phenomena observed previously, figure 3.9 represents the vector of current density near the cathode-tip, there are two components axial and radial of current density. We observe a maximum value of current density on the segment AG1 (cathode-tip) of 3.54 $\times 10^{8}$A/m^{2}, because we have imposed on the cathode-tip this value of current density corresponding to 100 A This explains the very low value of current density on the segment GG1 about 1.92$\times 10^{-12}$ A/m^{2}.

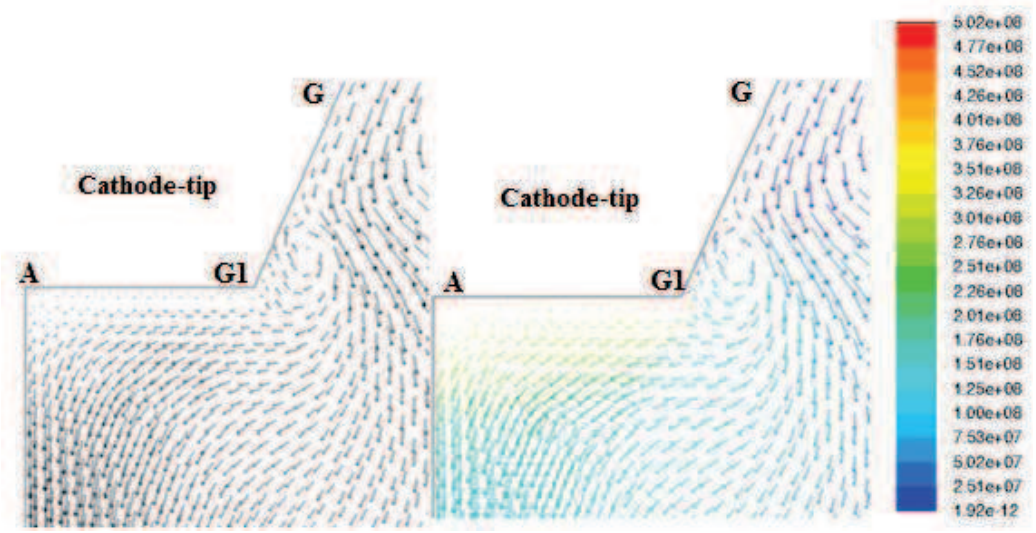

Figure 3. 9: Axial current density vectors on the cathode- tip100 A.

However, the effect of "pinch" observed in figure 3.1 is mainly due to the electromagnetic forces at the cathode-tip. The radial component responsible for the "pinch" of the thermal plasma created by the combination of $\overrightarrow{J_z}$ with $\overrightarrow{B_\theta}$. In contrast, the presence of an axial component to the electromagnetic force is due to the radial component of the current density near the cathode. The combination of $\overrightarrow{J_r}$ with $\overrightarrow{B_\theta}$ produces an axial force directed from the cathode to the anode figure 3.10.

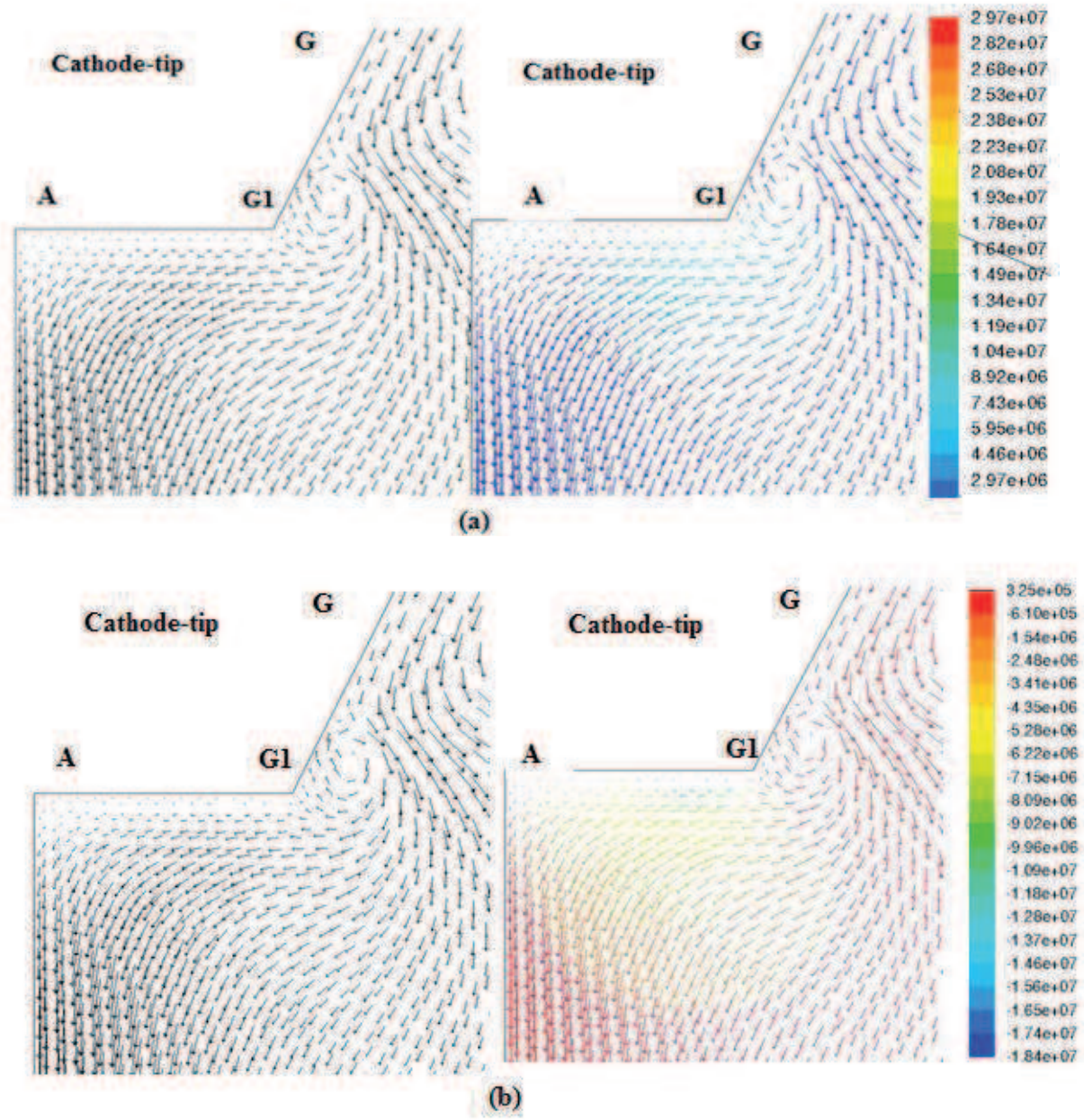

Figure 3. 10: Axial (a) and radial (b) Lorentz forces in free-burning arc of argon in 100 A.

Thus, as it can be seen in this figure 3.11, the radial component of electromagnetic forces tips the velocity vectors at the cathode-tip. The axial component of electromagnetic force induces a flow of plasma from the cathode to the anode.

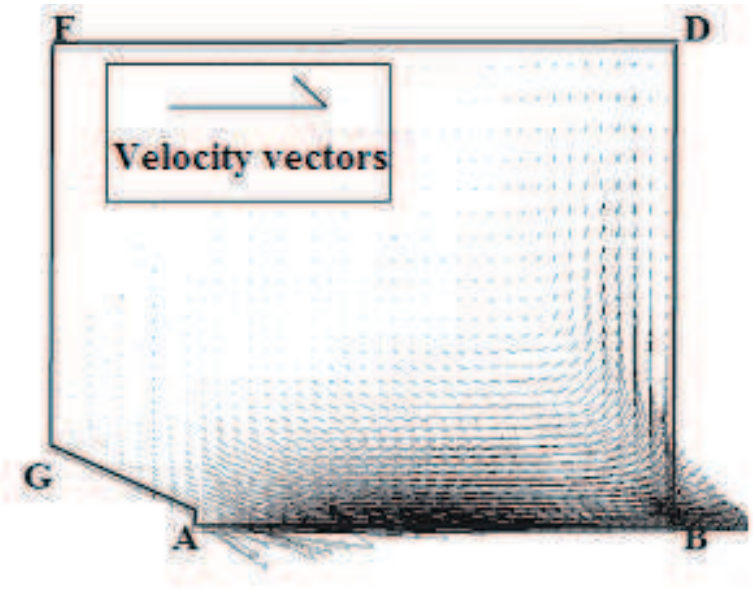

Figure 3. 11: Velocity field in free-burning argon arc.

3.3 Parametric study

We will study the influence on the characteristic of thermal plasma parameters such as: the electric current and the nature of the gas.

3.3.1 Effects of electric current changes

Figure 3.12 shows the temperature profiles with different electric currents. It can be seen that the profile shapes of temperature change little, but the values are obviously different. The highest temperatures are all in the centre of the arc near the cathode (between coordinates 2 and 4 mm). The arc plasma shows a contract state owing to electromagnetic force and temperature decreases along both of the axial and radial direction from the centre of the arc.

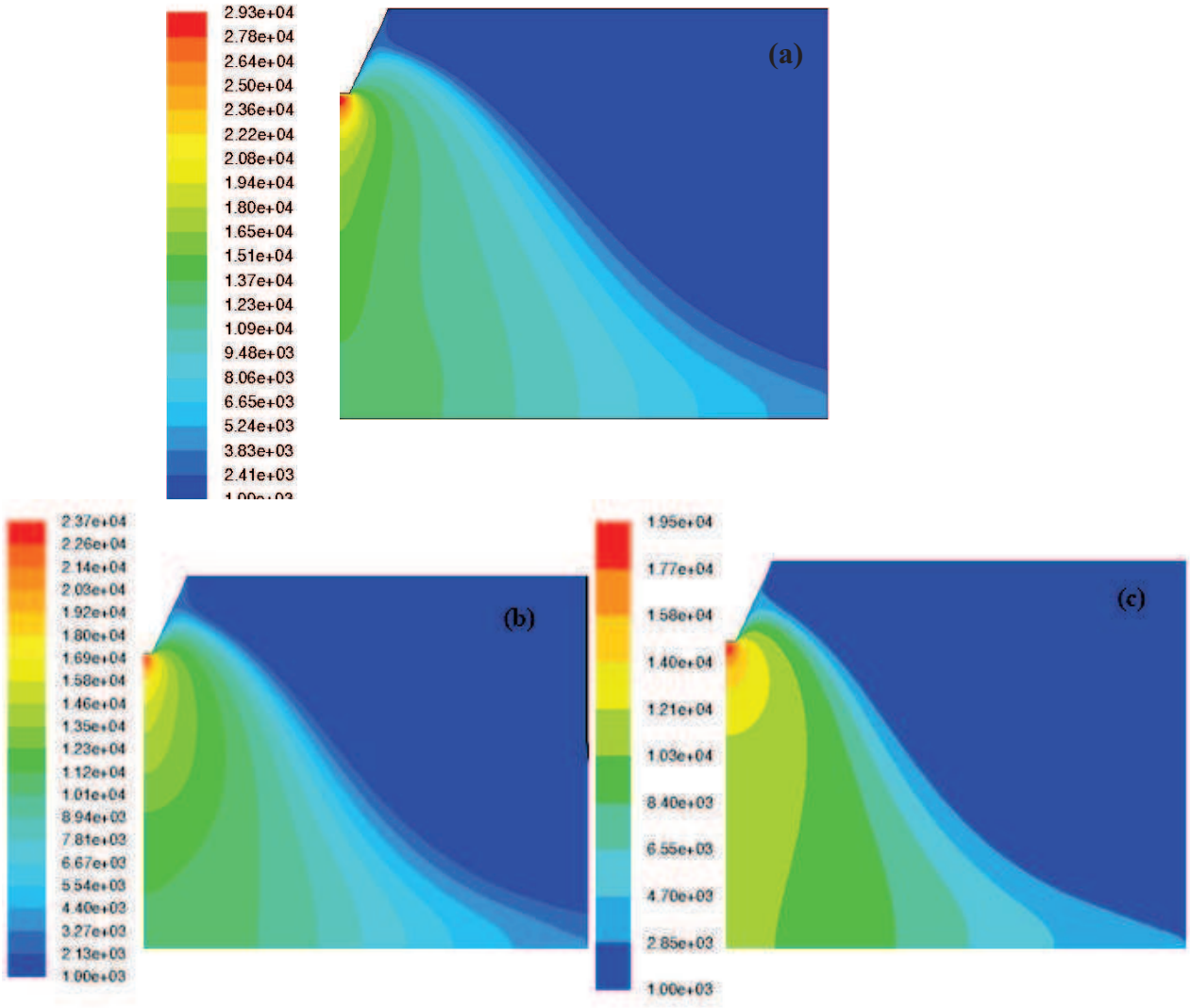

Figure 3. 12: Temperature profile of different current (100 A (a), 70 A (b), 50 A (c))

It is seen that the strong cathode jet on the anode surface forms the typical bell shape in the front of the anode due to stagnation. The highest temperature in figure 3.12 is 29300 K and the lowest temperature plotted is 1000 K.

The temperature changes along the axis are indicated in figure 3.13 The highest temperatures are 2.9×10^4, 2.3×10^4 and 1.9×10^4 K when the current changes from 100 to 70 and 50 A. As it can be seen, with the increase of the electric current (i.e. the input electrical power) the arc temperature rises.

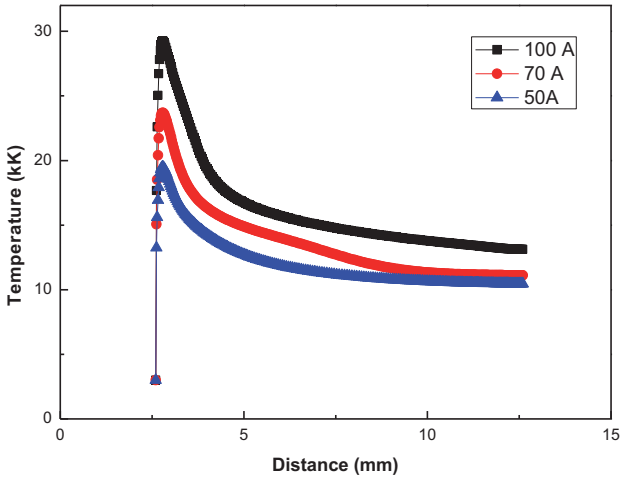

Figure 3. 13: Temperature changes along axis (different currents).

Figure 3.14 shows the potential along the axis. It can be seen that with the increase of the current, the potential of cathode decreases, i.e. the voltage of the arc increases, the potential drop in 100, 70 and 50 A is 11.4 V, 9.7 V and 8.7 V respectively. It can be noticed that all the curves become steeper near the cathode (3 mm), which indicates a sharp cathode potential drop.

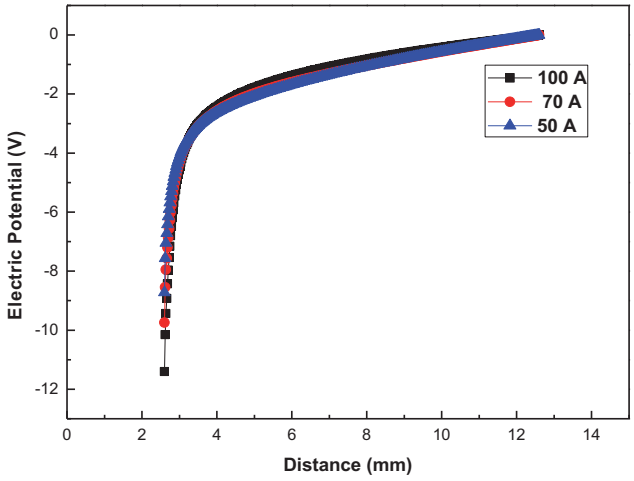

Figure 3. 14: Potential changes along axis (different currents).

Figure 3.15 presents the distribution of the velocity when the current is 100 and 70 A, respectively.

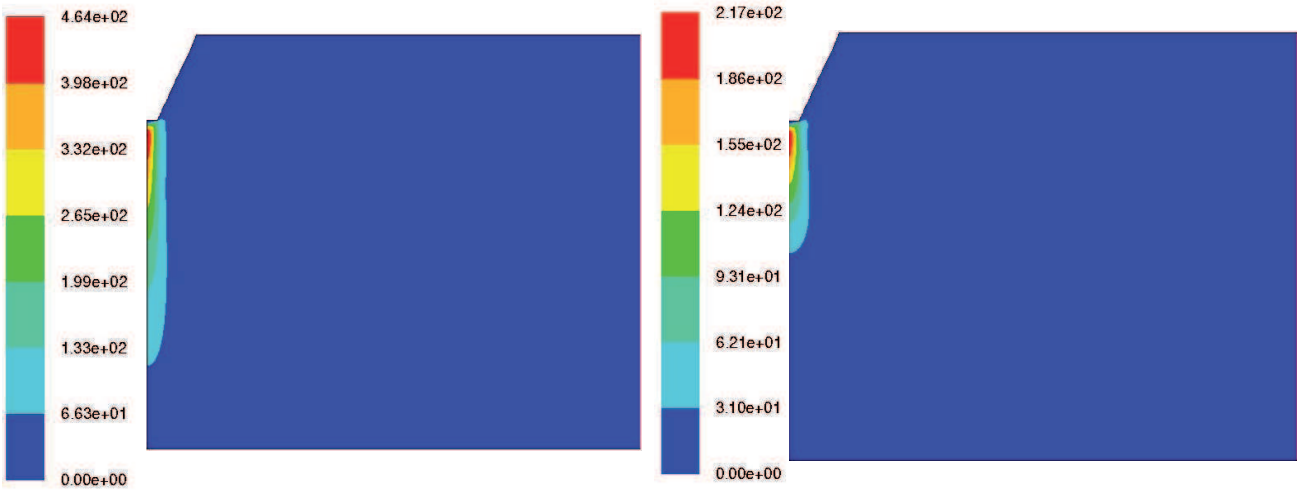

Figure 3. 15: Distribution of velocity vector (right100 A; left, 70A).

The velocities along the axis are shown in figure 3.16, the values of velocity change more significantly. The highest velocities are 464, 217 and 93 m/s when the current decreases from 100 to 70 and 50 A.

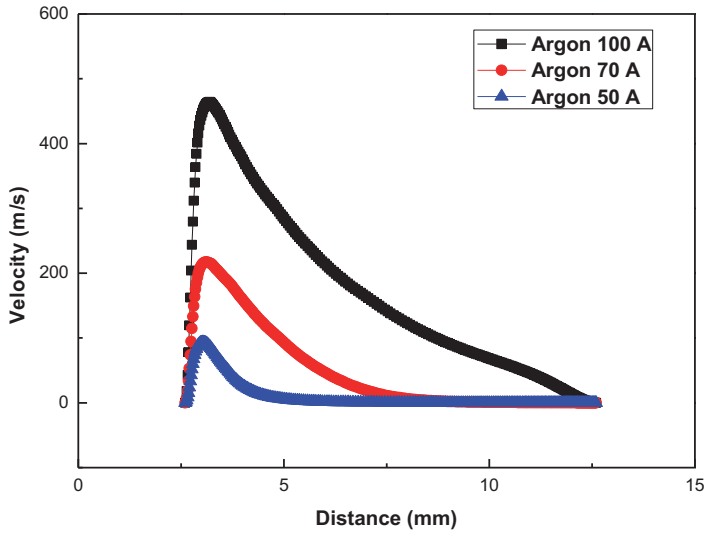

Figure 3. 16: Velocity changes along the axis (different currents).

With the increase of the current, temperature, voltage drop, and both the axial and radial current density also increase, then, the electromagnetic forces increases too. These forces occur exclusively in the momentum conservation equation, yet it is this equation that determines the velocity fields, that explains the flow increase.

The decrease of current brings less energy to the arc (1140, 697 and 435 W for 100, 70 and 50 A respectively.

The key results of these calculations for three parameter combinations are summarized in Table 3.2, while the values in column refer to constant electrode gap (d = 10 mm). Key parameters are maximum temperature T_{max}, maximum axial velocity U_{max}, voltage drop Ø, and axial current density on cathode-tip J_{max}.

	100 A	**70 A**	**50 A**
T_{max}(K)	29000	23000	19000
U_{max}(m/s)	464	217	93
Ø (V)	11,4	9,7	8,7
J_{max}(A/m^2)	$3{,}54\times 10^8$	$2{,}47\times 10^8$	$1{,}7\times 10^8$

Table 3. 2: Summary of the essential result in argon.

3.3.2 Influence of the nature of gas

Figure 3.17 shows the velocity along the axis AB in argon and air free-burning arc with different value of current. We note a maximum of velocity is at z = 3 mm below the cathode-tip, this maximum equal to 217 m.s^{-1} in argon gas and to 282 m.s^{-1} in air gas with 70 A, and equal to 90 m.s^{-1} in argon gas and to 97 m.s^{-1} in air gas with 50 A. Then, the velocity deceases rapidly in both gases to become zero at the anode.

The difference observed between the axial velocity in argon and air may be caused by electromagnetic forces, the $\vec{J} \times \vec{B}$ term present in the momentum conservation equation. The current density related to the electrical conductivity by Ohm's law:

$$\boldsymbol{j = -\sigma grad V} \qquad \textbf{(3.1)}$$

As electrical conductivity in argon is quite similar to the air one (figure 3.18) for a given temperature, the different temperature fields obtained (at 70 A for example) could induce differences of electromagnetic forces, and thus of the source term of momentum conservation

equation, and therefore different axial velocity profiles. We can also think that the different viscosities, between argon and air, have an influence on the calculated velocity fields.

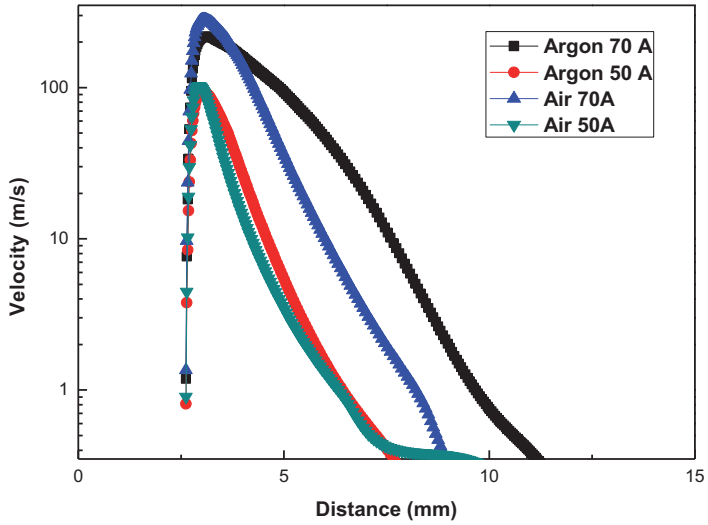

Figure 3. 17: Axial velocity with different current (Air/Argon).

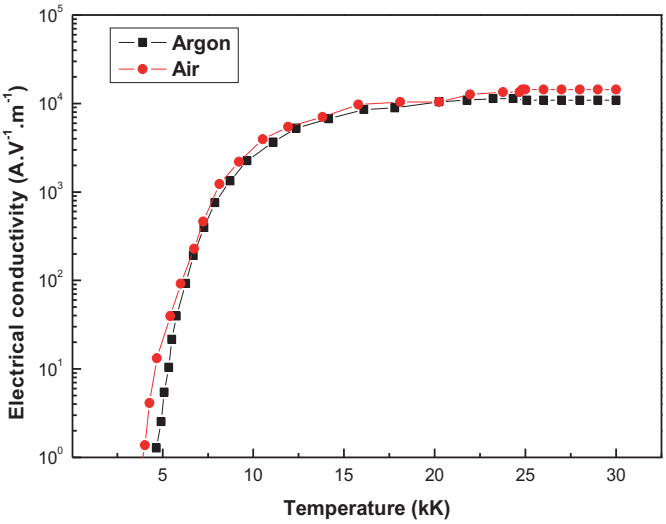

Figure 3. 18: Electrical conductivity (Air/Argon).

Figure 3.19 shows the temperature along the axis AB in argon and air free-burning arcs. In both gases, the maximum of temperature is at z = 3 mm below the cathode-tip, this maximum equal to 23.7 kK with 70 A, the profile of temperature is the same is argon and air gas with 50 A and the maximum of temperature at z = 3 mm equal to 19.6 kK. Then, the temperature decreases in both gas along the axis, and at z = 12 mm near to the anode, the temperature decreases little to become 10 kK at the anode.

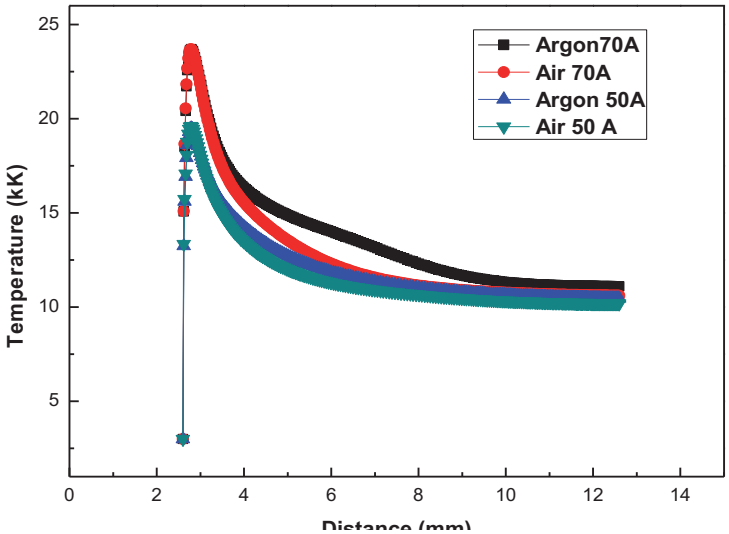

Figure 3. 19: Axial temperature with different current (Air/Argon)

Figure 3.20 shows the isotherms for different electric currents and gases. It can be seen that the results are different according to current values and gas nature.

The highest temperatures, around 23.7 kK, are all in the centre of the arc near the cathode (between coordinates 2 and 4 mm) in 70A with both gases argon and air, and about 19.6 kK with 50A in argon and air. The arc plasma shows a contract state owing to electromagnetic force and temperature decreases along both of the axial and radial directions from the centre of the arc.

The temperature changes along the axis are indicated in figures 3.19 and 3.20. We observe that the temperatures along the axis are higher in argon than in air. To explain this behavior of temperature in both gases, we look to the net emission coefficient figure 3.21.

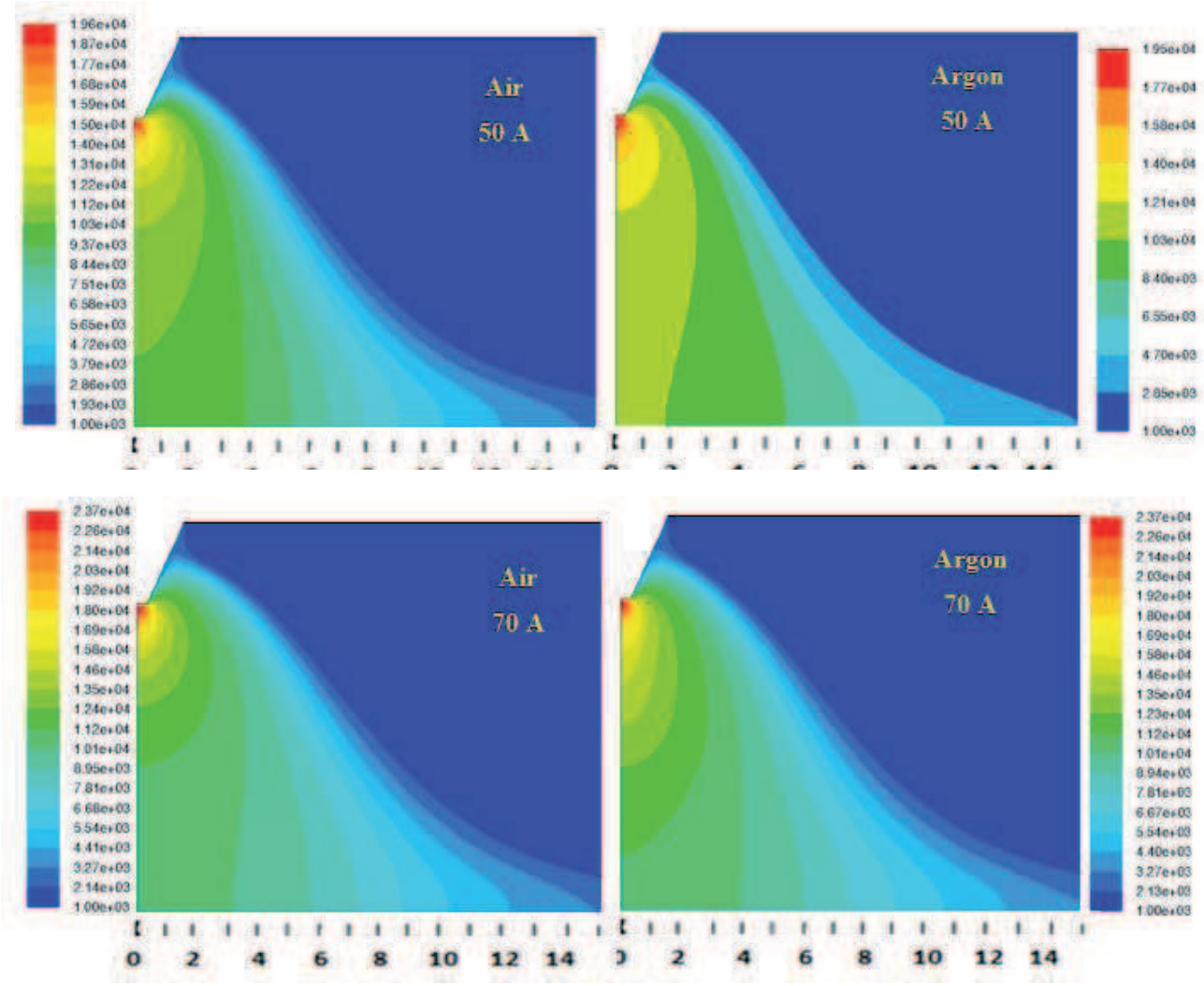

Figure 3. 20: Temperature profile of different currents and gases.

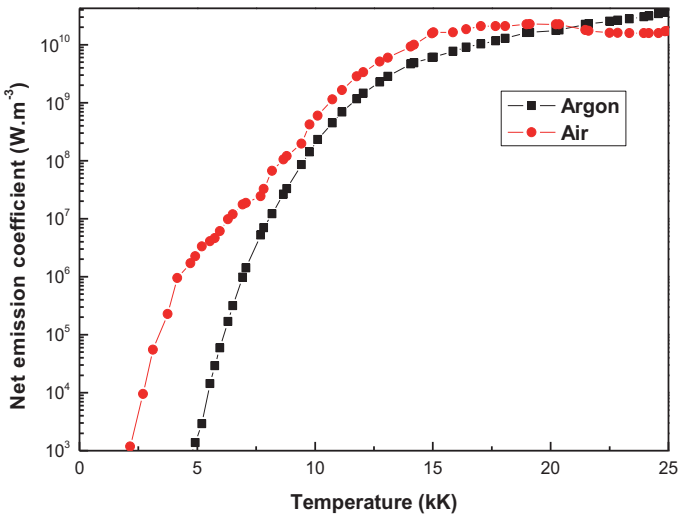

Figure 3. 21: Net emission coefficient (Air/Argon).

This coefficient is directly proportional to the radiation energy dissipated per volume unit by the thermal plasma. We observe that for temperature below 20 kK, the radiative losses are more important in air than in argon. Thus, when the radiative losses increase, the temperature of arc decreases and the expansion of isotherms for both gases considered is smaller.

The cooling of the plasma for air in comparison with argon could also come from the difference observed on thermal conductivities figure 3.22. As thermal conductivity is higher for air, it enhances the cooling of the plasma.

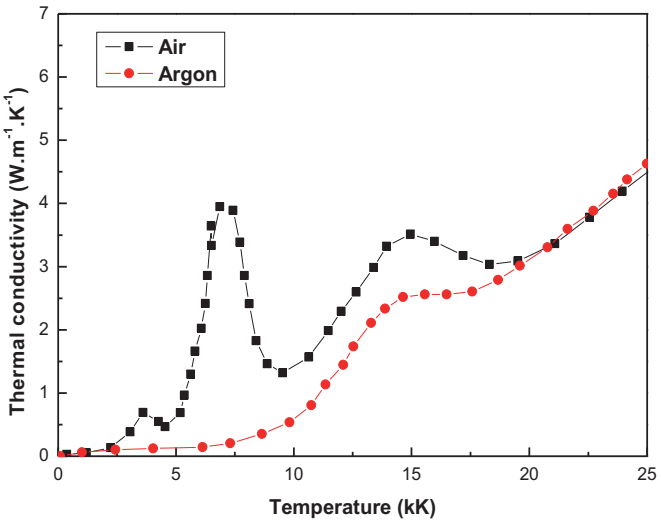

Figure 3. 22: Electrical conductivity (Air/Argon).

Figure 3.23 shows the electrical potential along the axis AB in argon and air free-burning arcs. In both gases we observe a voltage drop in the column of arc of 10.1, 9.7 V respectively in air and argon with 70A and 8.7, 9.4 respectively in argon and air with 50 A.

As previously mentioned, the cooling processes occurring in the plasma are higher in air than in argon. Even if electrical conductivity in air seems to be slightly higher for air, the global losses have to compensate by a higher electrical input power, which explains the higher voltage drop observed when arc is created in air.

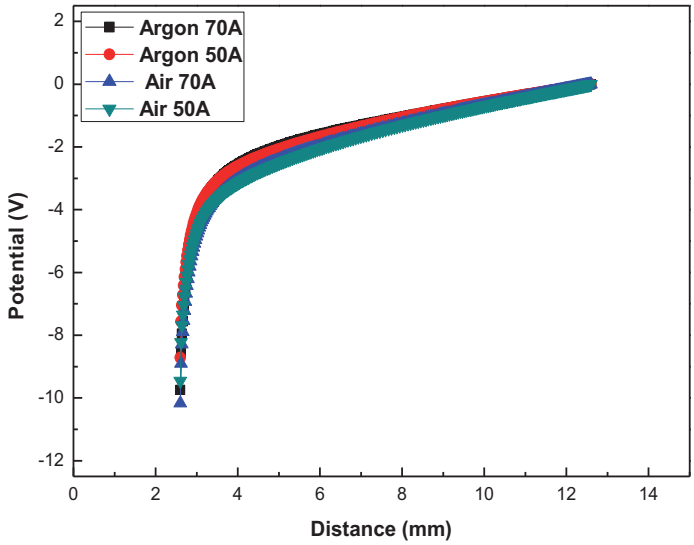

Figure 3. 23: Electrical potential of different current (Air/Argon)

We have to focus that using air in such a device, i.e. TIG, is not realistic as metallic electrodes, especially the cathode, will be rapidly consummated by oxygen. We have done it because this work is a first step to a more detailed modeling on small transient arc discharge in air.

3.4 Conclusion

Initially, we have performed a free-burning arc numerical simulation in argon at 100 A. The objective of this simulation was to compare our results with those obtained by Hsu et al **[Hsu-1],** experimentation and modeling. A detailed analysis of various quantities concluded about the validity of our model. From there we have deepened our study with the analysis and the influence on the characteristic of thermal plasma as the influence of nature of gas and current.

Bibliography

[Baud-1] Baudoin Fulbert: « Contribution à la modélisation d'un arc électrique dans les appareils de coupure basse tension »,. Thèse de doctorat de l'Université Blaise Pascal-Clermont II, 65P, (2004).

[Boul-1] Boulos, M ., Fauchais, P., and Pfender, E.,.Book : "Thermal Plasmas, fundamentals and applications", Vol. I.Plenum Press, NY.(1994).

[Capi-1] Capitelli, M., Colonna, G., Gorse, C., D'angola A.: "Transport properties of high temperature air in local thermodynamic equilibrium". Eur. Phys. J. D, Vol.11, PP 279-289, (2000).

[Dev-1] Deveto R,S.: "Transport coefficients of ionized argon". The Physics of Fluids, Vol. 16, n°5, PP 616-623, (1973).

[Etema-1] Etemadi K. "Investigation of High-Current Arcs by Computer-Controlled Plasma Spectroscopy", Thesis of the University of Minnesota (1982).

[Fre-1] Freton Pierre. : « Etude d'un arc de découpe par plasma d'oxygène Modélisation-expérience », Thèse de doctorat de l'Université Paul Sabatier, 64P, (2002).

[Hsu-1] Hsu K.C., Etemadi K. and Pfender. E.: "Study of the free burning high intensity argon arc". J.Appl. Phys, 54, pp. 1293-1301, (1983).

[Low-1] Lowke J.J., Kovitya P., Schmidt H.P. "Theory of free-burning arc columns including the influence of the cathode". J.Phys.D : Appl. Phys. Vol, 25, PP, 1600-1606, (1992).

[Murp-1] Murphy AB.: "Transport coefficient of air, Argon-Air, Nitrogen-Air, and Oxygen-Air", Plasma Chemistry and Plasma Processing, , Vol.15, n°2, PP 279-307, (1995).

[Murp-2] Murphy AB., Arundell C J.: "Transport coefficient of argon, Nitrogen-Oxygen, and Argon-Oxygen", Plasma Chemistry and Plasma Processing, , Vol.14, n°4, PP 451-489, (1994).

[Zhu-1] Zhu P., Lowke J.J., Morrow R A. "Unified theory of free burning arcs, cathode sheats and cathodes". J.Phys.D : Appl.Phys., Vol, 25, pp.1221-1230, (1992).

Chapter 4: Experimental study

Chapter 4: Experimental study

RESUME DU CHAPITRE 4

Afin de valider le modèle d'arc 2D à l'ETL présenté aux chapitres précédents, nous avons choisi de le confronter à des résultats expérimentaux. De nombreuses méthodes de diagnostic existent, la plupart sont basées sur l'étude de la lumière émise par le plasma (spectroscopie) ou bien sur l'étude d'un faisceau lumineux traversant ce dernier (interférométrie, spectroscopie d'absorption, déflectométrie).

Notre choix s'est porté, par soucis de simplicité, sur la spectroscopie d'émission atomique. Après un bref rappel concernant la composition d'un spectre d'émission, nous présentons différentes techniques de diagnostic. Nous avons choisi la méthode de Fowler-Milne qui permet, moyennant l'hypothèse d'un plasma à l'ETL, d'obtenir la température à partir des profils du coefficient d'émission d'une seule raie.

Le dispositif expérimental est présenté en détail, puis les résultats sont discutés. A cette occasion, on remarque que les mesures à proximité de la cathode sont inexploitable à cause d'un fort déséquilibre thermique du plasma, tandis que les mesures à proximité de l'anode sont perturbés par un effet mirage du à l'échauffement de l'air entourant l'électrode.
Finalement, les résultats expérimentaux sont comparés aux résultats issus de notre modèle et des travaux d'Etemadi et al.

Chapter 4: Experimental study

4.1 Introduction

In order to define completely the state of a plasma and to characterize the discharge, generally, the following must be known at each point within the medium and at each instant of time:

- The population densities of discrete energy levels for each different type of particle;
- The temperature field in the column and in the vicinity of the electrodes;
- The detailed radiation processes.

To access to those quantities, numerous diagnostic methods are available. Due to the high temperature of the plasma column, most of them are non intrusive. They involve analysis wether of the light generated by the arc (emission spectrocopy) or of light beam after its passage throught the plasma (absorbtion spectroscopy, interferometry, shadowgraphy...).

In the plasma column of a TIG (Tungten Inert Gas) device, the typical temperature is around 10000 K. As a consequence, atomic emission spectroscopy is a reliable method to probe it since atoms starts to emit strongly for temperature above 6000 K.

The main goal of this chapter is perform experiments and to validate our model results. First, elementary physical processes and laws involved in atomic emission spectroscopy will be reviewed. Then some measurement methods will be discussed. Finally, the experimental device will be presented and a comparison between experimental and model results will be performed.

4.2 Elementary processes

We will decry here all elementary processes involved in plasma in order to understand the origin of light emission used in spectroscopy.

4.2.1 Radiative excitation and deexcitation

An excited atom on a level m can be desexcited spontaneously to a level n:

$$A(m) \rightarrow A(n) + photon \qquad \textbf{(4.5)}$$

The photon emitted during this process has a wavelength λ. It can be related to the m and n level energy by the relationship:

$$\Delta E_{nm} = \frac{hc}{\lambda} \quad \textbf{(4.2)}$$

Where h is the Planck constant, c the light velocity and λ the photon wavelength. For some kind of excited state, the radiative deexcitation is prohibited by selection rules and the deexcitation is generally produced by collision. Those are called "metastable" state.

The inverse of the deexcitation process is called radiative excitation or photo-excitation. It occurs when an atom catch a photon to change its energetic level, from n to m state.

$$A(n) + photon(\Delta E_{mn}) \rightarrow A(m) \quad \textbf{(4.3)}$$

4.2.2 Collisional excitation and deexcitation

During the collision of an electron or an atom on another atom, an electron of this last can be bring to a superior energy level. It is an inelastic collision: a part of the kinetic energy of the particle is converted into potential energy.

$$A(m) + particle \rightarrow A(n) + particle$$

(4.4)

4.2.3 Three body recombination

If an electron collides with a particle near an ion, and lose just enough energy, it may perform a recombination of the form:

$$\mathrm{A}^+ + e^- + particle \rightarrow A + particle + h\nu \quad \textbf{(4.5)}$$

The wavelength of the photon emitted during this recombination is not fully quantified since the kinetic energy of the electron is not quantified. This is a free-bound transition as the wavelength of the photon is only limited by the electronic level structure of the atom.

4.2.4 Dielectronic recombination

The dielectronic recombination follows the reaction:

$$\mathrm{A}^+ + e^- \rightarrow A(m) + h\nu$$

(4.6)

It is a recombination between ion and electron. After recombination, the atom has two electrons in an excited state and the atom can be desexcited either by reionization or by emitting photon.

4.3 Base of emission spetroscopy

Emission spectroscopy is based on the analysis of the light energy emitted by atoms, ions or molecules to evaluate different plasma parameters. Usually, measured quantities as atom states populations are not common observables and are difficult to interpret. Models have to be used to link quantities to more classical parameters such as temperature, electron densities etc. For thermal plasma, the most common model is based on the local thermal equilibrium hypothesis.

4.3.1 Local Thermal Equilibrium

In order to have plasma in total thermodynamic equilibrium, it first has to be isothermal. Moreover, all the light emitted by the gas must be reabsorbed. When those conditions are checked, the medium can be totally described with the pressure and the temperature only. Unfortunately, such kind of plasma is rare in laboratory: one can easily notice that laboratory plasma do not reabsorb all the emitted light. It leads to an imbalance in radiative phenomena. In addition, they are subject to pressure and temperature gradients.

The local thermal equilibrium states that if the plasma is driven by collisional processes and contains small temperature gradients, total thermal equilibrium laws except the Planck law can be used to describe the arc column. In other words, energy transfer by collision must be much greater than the losses by radiations.

4.3.1.1 Criteria for the existence of Local Thermal Equilibrium

The problem of the definition of criteria for the existence of LTE is the subject of many works, because of its importance in electrical discharge.

The two most important studies conducted in this area are the work of Griem **[Grie-1]** and, especially of Drawin **[Draw-1, Draw-2].**

Griem offers a test for determining the validity of the assumption of LTE: LTE is realised when spontaneous transitions between the first excited level and fundamental level are ten time less important than the transitions by electrons collisions.

The minimum electron density to satisfy this condition is given by the relation :

$$N_e^{cr} = 9 \times 10^{11} (E_1 - E_0)^3 T_e^{1/2} \quad cm^{-3} \qquad \textbf{(4.7)}$$

The difference $(E_1 - E_0)$ between the first excited level and the fundamental being expressed in eV.

Using more accurate cross sections, Drawin **[Draw-1]** has refined the approach and has proposed the following relationship:

$$N_e \geq 6{,}5 \times 10^{16} \frac{g_{max}}{g_{min}} \left(\frac{E_{max-}E_{min}}{E_H}\right)^3 \left(\frac{kT_e}{E_H}\right)^{1/2} .\{\emptyset_1(\Delta U_{max})\ atom, \emptyset_2(\Delta U_{max})\ ion \quad \textbf{(4.8)}$$

Where: $\Delta U_{max} = \frac{E_{max-}E_{min}}{kT_e}$, $E_{max-}E_{min}$ is the larger energy gap between the excitation levels of the atom, g_{max} and g_{min} the statistical weights of the corresponding levels, $\emptyset_1$ and $\emptyset_2$ functions tabulated by authors, N_e expressed in cm^{-3}, and E_H the ionization potential of hydrogen.

For an argon plasma at atmospheric pressure and for a temperature about 10^4 K, electronic density N_e must be greater than or equal to $4{,}4 \times 10^{17}\ cm^{-3}$ for that LTE can be etablished **[Vac-1].**

Four typical temperature ranges are derived from these criteria and are suitable for deciding how far the hypothesis of LTE is justified **[Etem-1]**:

- In the fringes of the arc, temperature as low as 8000 K can still be measured under the assumption of LTE.
- In the axis of the plasma close to the anode of free-burning arc temperatures range around 12000 K.
- Close to the tip of the cathode of a high intensity arc temperatures are above 16000 K.
- In the immediate vicinity of the tip of the cathode temperatures are around 20000 K.

4.3.2 Thermal Equilibrium Laws

✓ **Maxwell law:** allows to determine the velocity distribution function of a population of particules at the temperature T, where dN the number of particules of given species at a velocity included between v and $v + dv$:

$$\frac{dN}{N} = \left(\frac{m}{2\pi kT}\right)^{3/2} exp\left(-\frac{1}{2}\frac{mv^2}{kT}\right) 4\pi v^2 dv \quad \textbf{(4.9)}$$

✓ **Blotzmann law:** gives the ratio of population between a high level (m) and a low level (n), of statical weight g_m and g_n, and whose excitation level are E_m and E_n:

$$\frac{N_m}{N_n} = \frac{g_m}{g_n} exp\left(-\frac{E_m - E_n}{kT}\right) \quad \textbf{(4.10)}$$

If we call N the total density of particules for given species, we obtain:

$$\frac{N_m}{N} = \frac{g_m}{U(T)} exp\left(-\frac{E_m}{kT}\right) \quad \textbf{(4.11)}$$

Where $U(T) = \sum_m g_m exp\left(-\frac{E_m}{kT}\right)$. U(T) is called partition function of species considered.

- ✓ **Saha law:** allows the determination of the degree of ionization of the plasma. It is written in the form:

$$\frac{N_e N_i}{N_0} = \frac{2U_i}{U_0} \cdot \frac{(2\pi m_e kT)^{3/2}}{h^3} exp\left(-\frac{E_i - \Delta E}{kT}\right) \quad \textbf{(4.12)}$$

Where: N_e, N_i and N_0 are the numerical densities of electrons, ions and neutral atoms, U_i and U_0 the partition functions of ion and atom, h the Planck constant, E_i the ionisation potential of considered species, and ΔE the lowering of ionisation potential caused by the presence of charged particules.

- ✓ **Planck law:**

In an enclosure with thermodynamic equilibrium, some particles are excited or ionized with absorption of radiation, others are dexcited or recombined with emission radiation. Whether $B_\lambda(T)$ is the power emitted per volume and solid angle unit, it depends only on temperature for a fixed value of λ:

$$B_\lambda(T) = \frac{2hc^2}{\lambda^5} \frac{1}{exp\left(-\frac{hc}{\lambda kT}\right) - 1} \quad \textbf{(4.13)}$$

It is the law of blackbody radiation.

- ✓ **Dalton law:**

The total pressure of gaz is given by the expression:

$$P = \sum_k N_k \, kT \quad \textbf{(4.14)}$$

Where N_k is the density of specie k.

✓ **Electric neutrality law:**

The plasma is electrically neutral, i.e the charge densities of opposite sign are equal:

$$N_e = \sum_k Z_k N_k \quad \textbf{(4.15)}$$

Where: N_e is the electron density, and Z_k the charge density of specie k.

4.3.3 Spectral line radiation in plasma:

The spectrum of the electromagntic radiation emitted by a plasma can be generally separated into two components (Figure 4.1):

- The first is called continuous spectrum: it corresponds to radiation emitted by electrons from collisions with heavy species or during recombination.
- The second is called spectrum line or discontinuous spectrum. It corresponds to photons that are emitted by an atom, ion or molecule when they are deexcited.

The wavelength of these lines is related to the energy of the considered transitions. Spectral line emitted by an atom or ion is not infinitely thin, usually, it is subject to broadening. It depends on the physical conditions of the emitting particle **[Chap-1]** and can have several causes which will be explained below.

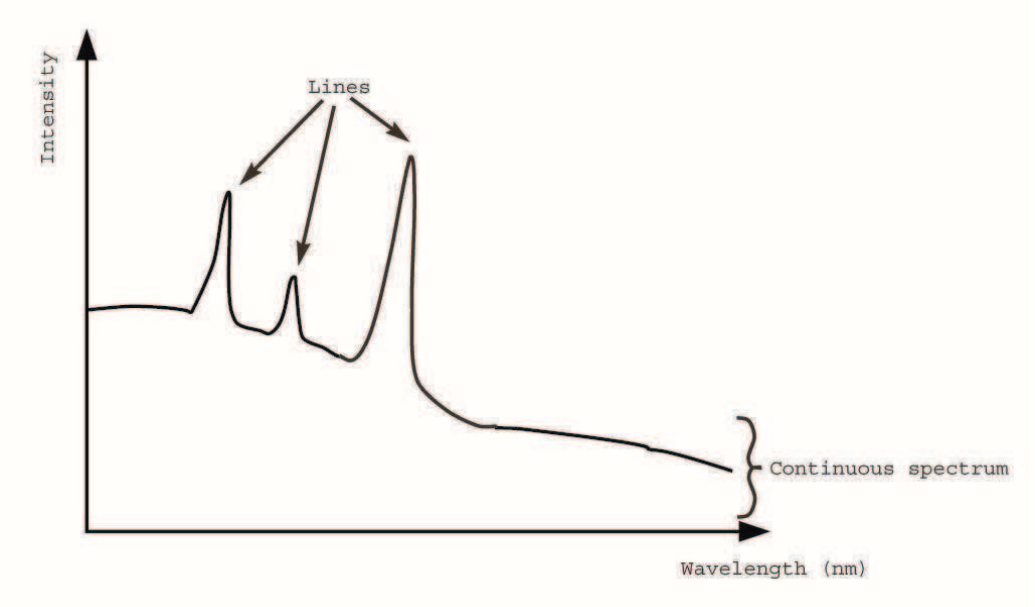

Figure 4. 1: Spectral lines on / the continuous spectrum of radiation.

4.3.3.1 Broadening of spectral lines

Spectral lines emitted by ions (atoms) in a plasma are not strictly monochromatic.
Rather, they are broadened and have finite width. They may even be shifted from the original positions. In this section, we look at different broadening mechanisms of spectral lines.

- ✓ **Natural Broadening of spectral line**

There is first the natural broadeningt which is due to the fact that a lifetime of transition is not infinite. It is a consequence of uncertainty relation of Heisenberg:

$$\delta t \delta \nu \approx 1 \tag{4.16}$$

- ✓ **Doppler broadening of spectral lines**

The Doppler broadening is the result of the frequency shift of electromagnetic waves emitted by particles in motion. For a particle moving with a velocity v in the direction of observation, the frequency of the electromagnetic wave perceived by the observer will be shifted from the emission frequency when the particle is at rest ν_0, according to the relation:

$$\frac{v}{c} = \frac{\Delta \nu}{\nu_0} \tag{4.17}$$

Where c is the light celerity.
By considering that the particule velocity follows the relation (maxwell law), the profile of Doppler broadening is:

$$I(v) = I(v_0) exp^{-c\frac{v-v_0}{v_0\left(\frac{2kT}{m}\right)^{1/2}}} \tag{4.18}$$

Where m is the mass of emitter particle.
Profile due to Doppler broadening is Gaussian. For thermal plasmas, this source of broadening is often negligible.

- ✓ **Stark broadening of spectral lines**

It is produced by charged particles surrounding the emitter. The electric field produced by particles passing close to a particle in the process of deexcitation perturb its electronic levels. It is usual to split the problem into two distinct parts. Ions are not very mobile

during the lifetime of the transition, and we consider the electric field to be constant: it is the quasi-static approximation. At the opposite, electrons have a high mobility. Their effect on the electronic levels is taken into account with the impact theory.

In thermal plasma, the Stark broadening is often preponderant. The lorentzian line profile induced by this effect is usually studied to measure electron density.

4.3.3.2 Spectroscopic methods

From the light emitted by the plasma, by applying the LTE assumption and the laws described previously, it is possible to measure various plasma parameters such as temperature and electron density.

- ✓ **Mesure from the energy of a line** :

It has been chosen to present three of the most famous method to exploit atomic emission line spectra:

- The absolute intensity of a line;
- The Fowler-Mline method;
- The Boltzmann diagram.

They are described in detail in **[Vac-1]**. In this section we present a brief description.

- ✓ **The absolute intensity of a line**

It is possible to calculate the density of emitted level if we know the energy emitted by a line :

$$N_n = J.\frac{4\pi\lambda_{nm}}{A_{nm}hc} \quad \textbf{(4.19)}$$

Where :

A_{nm} : probability of transition;

N_n : density of atom in energy state n;

h : Planck constant.

When the local thermodynamic equilibrium is achieved, the population N_n of different energy level is governed by the Boltzmann law. Once the population of the state n is obtained experimentally, the equation (4.11) allows to calculate the plasma temperature. This method has several limits, first the transitions probabilities must be known precisely to ensure good

value of temperature. This is not always possible since data may be available in literature with large uncertainty. The second limit is an experimental one, the spectrum must be calibrated with the help of a ribbon tungsten lamp spectrum to measure absolute intensity.

✓ **The Fowler-Milne method**

The emission coefficient of a spectral line ε_{nm} as function of temperature in LTE condition is given by:

$$\varepsilon_{nm} = \frac{h\lambda_{nm}}{4\pi c} g_n A_{nm} \frac{N(T,P)}{U(T)} exp\left(-\frac{E_n}{kT}\right) \quad \textbf{(4.20)}$$

Where N(T,P) is the density of particles at temperature T and pressure P and U(T) is the partition function.

When carrying our interest on the evolution of equation (4.20) with the temperature, we can see that *U(T)* and $exp\left(-\frac{E_n}{kT}\right)$ increase with temperature. For atoms, N(T) decreases with temperature due to ionization, while for the ions, N first increases and then reaches a maximum before decrease. ε_{nm} reaches a maximum for a temperature called "maximum emission temperature". The maximum can be used to relate emission coefficient to plasma temperature if the maximum emission is reached in the plasma column. Indeed, for a cylindrical plasma column, it can be stated that:

$$\frac{E(r)}{E_{max}} = \frac{N(T)U(T_{max})}{N(T_{max})U(T)} \frac{e^{\frac{-E_n}{kT}}}{e^{\frac{-E_n}{kT_{max}}}} \quad \textbf{(4.21)}$$

The main advantages of this method are its simplicity and its reliability. First, as it can be performed with only one line profile, there is no need of spectrum calibration. All the work can be done with relative intensity spectra if the same recording parameters are used. Moreover, there is no need of transition probabilities to calculate the temperature profile.

The normalized coefficient emission as a function of the temperature can be calculated with the help of partition function and plasma composition. Data were computed for numerous argons ions and atoms lines, some are available on figures 4.2 and 4.3.

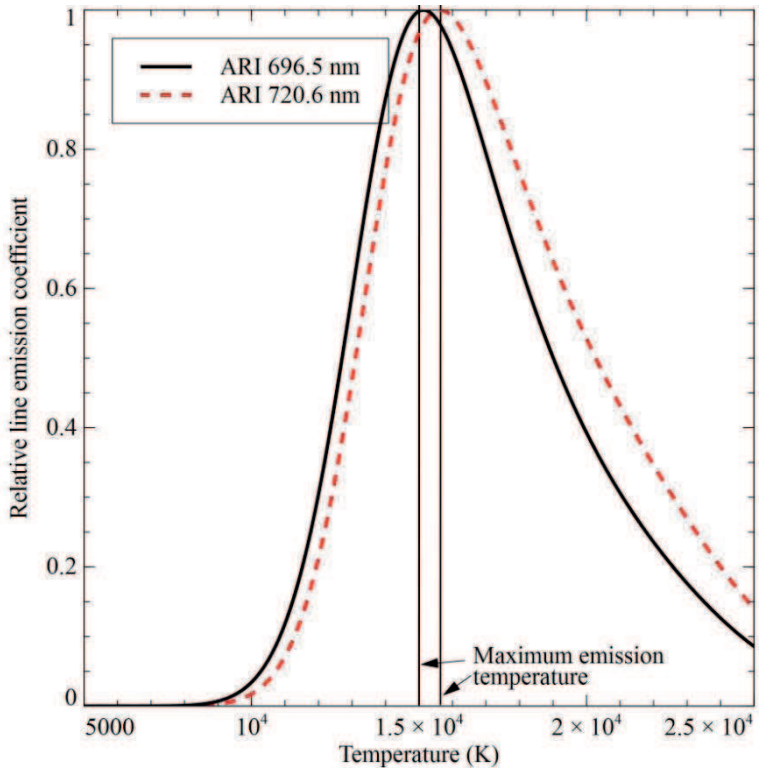

Figure 4. 2: Relative emission coefficient for two lines of neutral argon as a function of the temperature.

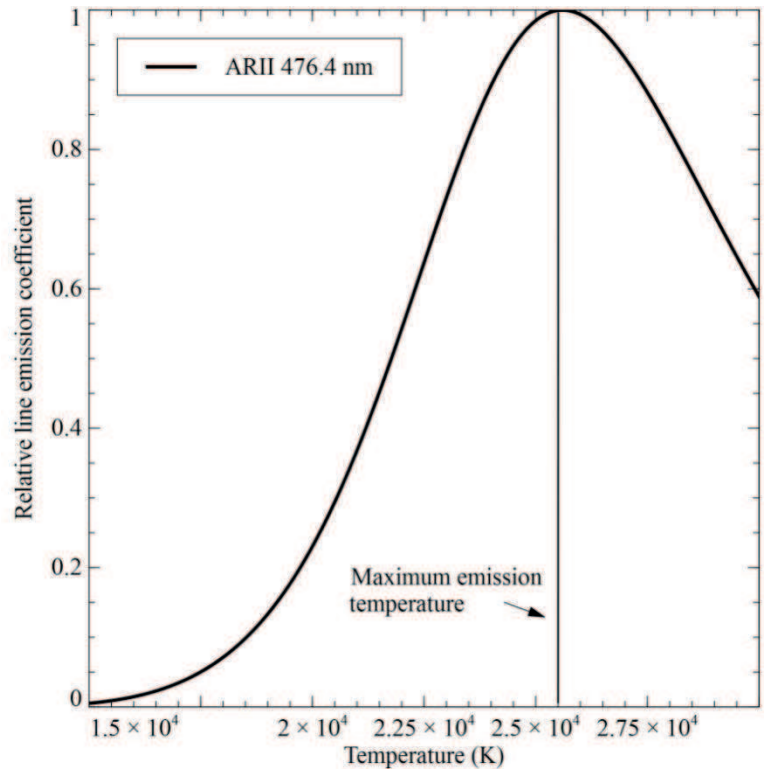

Figure 4. 3: Relative emission coefficient of the Ar^+ line at 476.4 nm as a function of the temperature.

✓ **The Boltzmann diagram**

We have seen previously, that when a gas is in thermodynamic equilibrium, the population of its levels was governed by Boltzmann law. For any level m, we have:

$$n_m = g_m \frac{n(T)}{U(T)} exp\left(-\frac{E_m}{kT}\right) \quad \textbf{(4.22)}$$

We can relate the intensity of a line to the population of different levels using the emission coefficient:

$$\varepsilon = \frac{h\nu}{4\pi} A_{mn} n_m \quad \textbf{(4.23)}$$

With A_{mn} the probability of transition between level m and n, n_m the atom density at level m, h the planck constant, and ν the frequency of the line.

To obtain the temperature of the plasma, we must measure the population of several levels, then we find the temperature T graphically with the slope of the function.

$$ln\left(\frac{n_m}{g_n}\right) = -\frac{E_m}{kT} + ln\left(\frac{n(T)}{U(T)}\right) \quad \textbf{(4.24)}$$

The above equation can be transformed by taking in account the line intensity :

$$ln\left(\frac{\varepsilon\lambda 4\pi}{A_{nm} hc g_n}\right) = -\frac{E_m}{kT} + ln\left(\frac{n(T)}{U(T)}\right) \quad \textbf{(4.25)}$$

Of course, as we are interested by the temperature, we can work in relative intensity and neglect the constants:

$$ln\left(\frac{\varepsilon_{relatif}{}^{\lambda}}{A_{nm} g_n}\right) = -\frac{E_m}{kT} + B \quad \textbf{(4.26)}$$

The plot of this equation gives two crucial informations. The exploitation of graphic allows to ensure that population levels follows a Boltzmann law if we obtain a straight line. In this case, the plasma is in LTE, while considering $T_{excitation} = T_{electron} = T_{heavy\text{-}species}$.

The slop of this line give us the access to excitation temperature. This method is of prime interest in thermal plasma diagnostic since it allows to check the hypothesis of LTE or partial

LTE. Indeed, in this case the spectrum calibration is not needed since relative intensity can be used to construc the boltzmann plot. Finally, this method is based on transition probabilies that can be a source of error since some data are known with 50 % of uncertainty.

✓ **Abel inversion**

Abel inversion is widely used in many context and, in laser-plasma studies it leads to a 2D electrons density map reconstruction from phase-shift maps recorded using interferometry **[Nom-1, Gizz-1].** Abel inversion is an indispensable tool that provides a physical quantity function of the radius r from measurements performed on several cord **[Fauch-1].** Several methods of Abel inversion existed in literature **[Jaf-1, Mer-1, Sem-1].** Our own method is based on spline smoothing who was firstly used by Glasser and al **[Glas-1]**.

Whether I(y) the total intensity measured on considered cord MM1 figure 4.4, and J(R) the local emissivity of plasma. If R is the radius of plasma with cylindrical symmetry, we have:

$$I(y) = 2\int_y^R J(r)\frac{r}{\sqrt{r^2-y^2}}dr \qquad \textbf{(4.27)}$$

Knowing I(y) for several values of y between 0 and R, we can deduce J(r) using Abel inversion:

$$J(r) = -\frac{1}{\pi}\int_r^R \frac{dI(y)}{dy}\frac{1}{\sqrt{y^2-r^2}}dy \qquad \textbf{(4.28)}$$

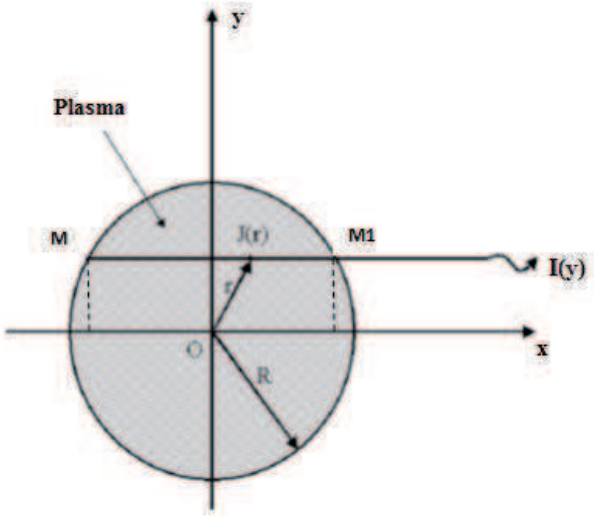

Figure 4. 4: Abel inversion scheme.

4.3.4 Experimental setup

4.3.4.1 The TIG device

The TIG device we used is composed of a “SAF-Air liquide” torch and a 12 cm water cooled copper anode. The torch contains a 3.2 mm diameter water cooled cathode surrounded by an alumina cup (figure 4.5). The plamagene gas injection is placed all around the cathode, this cup allows sheathing the plasma to keep the atmosphere of plasma free from air. The simulation was performed without the gas sheathing. As a consequence, we were forced to feed the torch with low argon flow (1 sL/min) to make the comparison possible. The DC power supply used is a NERTABLOC TH 260 from the “Air liquide” company with a LC filter to limit the amplitude of 100 Hz current intensity ripples. A typical voltage measurement between the arc electrodes is available on figure 4.6 to proove the quality of the power supply.

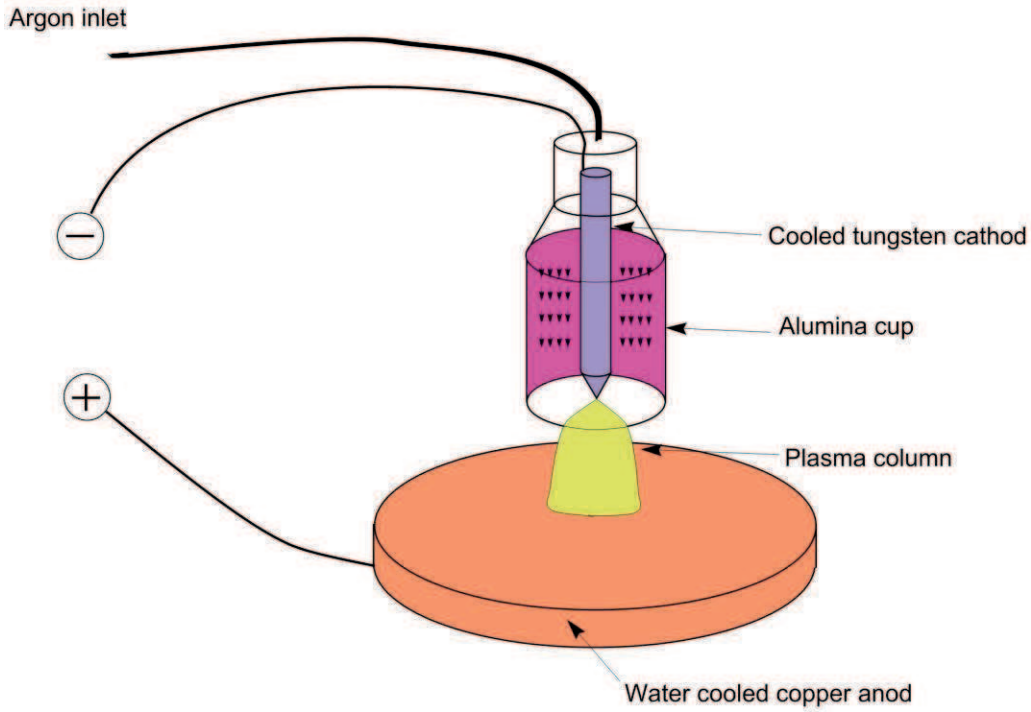

Figure 4. 5: Scheme of the TIG device.

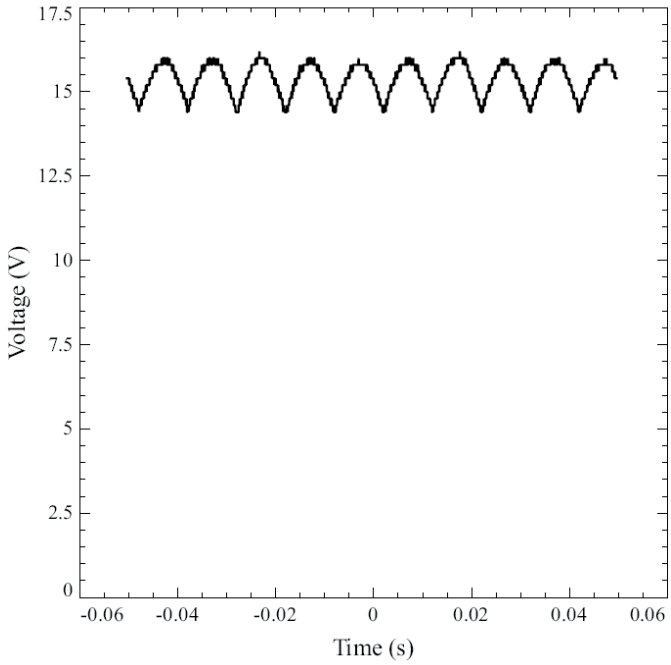

Figure 4. 6: Voltage between TIG electrodes.

4.3.4.2 General scheme

The experimental setup is shown in figure 4.7. This device allows to measure the experimental data needed for temperature calculation.

The monochromator used in this study is Chromex (SureSpectrum 500 is) with a focal length of 0.5 m. The adjustment width of the slit of the spectrometer is performed by a computer. A CCD camera of the Princeton Instruments brand (PIXIS 256) is positioned at the exit slit of the monochromator. The acquisition of images is controlled through WinSpec software. The CCD matrix of the camera is cooled by air. It is composed of 256 lines and 1024 columns, each pixel measuring 26 $\mu m \times 26\ \mu m$.

Two mirrors are used to form a periscop. It allows to turn the column image at the spectrocope entrance slit of a 90° angle in order to record data on a complete diameter. A lens of SiO_2 (transparent in the UV) with a diameter of 50 mm and a focal length of 200 mm allows to focus the beams from the plasma column on the entrance slit of the monochromator. A diaphragm is positioned before the lens in order to work in Gauss conditions. The spectroscopic device requires precise alignment of the optical elements which therefore cannot be moved easily. For this reason, we have mounted the TIG on a robot of the brand Charlyrobot to ensure its displacement. Thus, even if optical elements are static the whole plasma column beetwen the anode and the cathode can be probed. The torch is

positioned along the vertical axis. The image of the plasma on the entrance slit of the monochromator is realized out with a magnification of 0.38 (reduction). This magnification allows to form the image of a full plasma diameter on the CDD array of the camera. This technique is used by Alvarez et al **[Alv-1].** It allows a faster acquisition than existing technique because the complete diagnostic plasma on the diameter is made with a single camera acquisition.

The robot which provide the movement of the TIG device is interfaced with a computer (Amstrad PC 3286) of 640 kb of memory base. A program in Quick Basic allows the robot to move along the vertical axis.

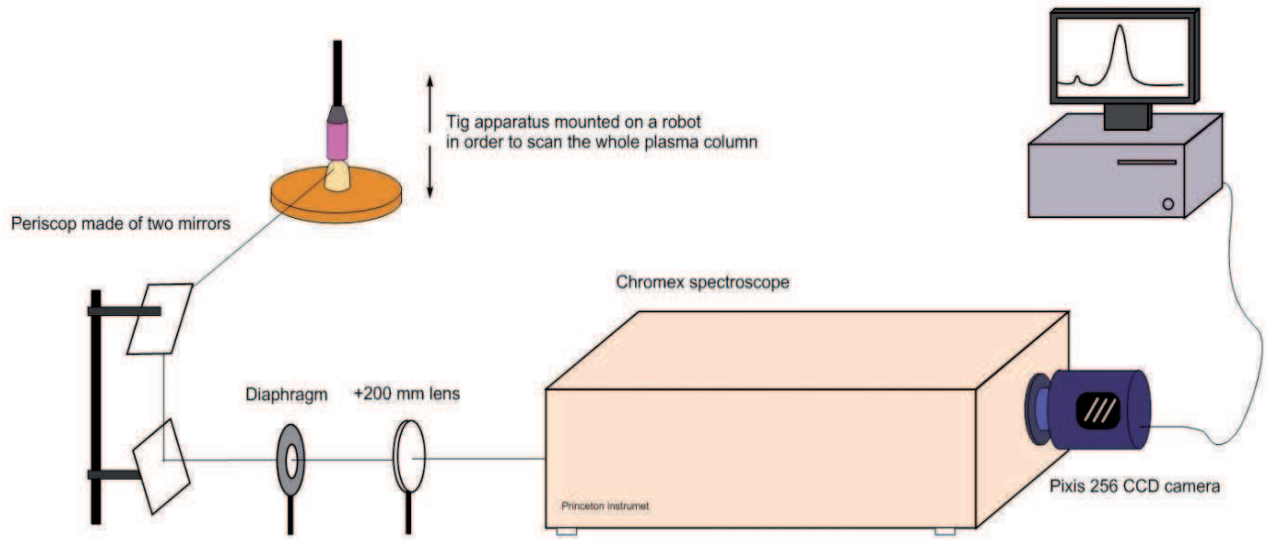

Figure 4. 7: Diagram of the optical emission spectroscopy.

4.3.5 Method for measuring the temperature of the plasma

4.3.5.1 Why Fowler Milne method?

The advantage mentioned just after justify our choise of Fowler Milne method.This method does not require knowledge of transition probabilities or the measure of absolute emission factors. We just have to know the temperature T_{max} corresponding to a maximum emission factors.

To measure the temperature, we use tables giving temperature as function of the intensity of the normalized line relative to the intensity at T_{max}.

Murphy **[Murp-1]** confirms that the Fowler-Milne is a very precise method. Even, if n or U depend strongly on the number of electronic transitions considered in the calculation of

partition function, the ratio n/U depends very little on it. This leads to a measure of temperature with low uncertainty.

4.3.5.2 Argon lines

We are interested in the intensity of 696.5 nm emission line of argon I for several reasons. First this line is very intense, it allows to improve the signal/noise ratio. Then, this line was the subject of many studies, so we can access easily to Stark broadenig and other database and we are sure that self-absorption is negligible **[Had-1].**

Using Fowler-Milne method, we measure temperature in argon gas, with two different value of current: 100 and 200 A. The inter-electrodes distance was set to 10 mm and the argon flow to 1 $sL.min^{-1}$.

We swept the column from the top to bottom by recording 2D spectra for every 0.5 mm (figure 4.8). The slit of the spectroscope has a width of 0.05 mm. The spatial resolution according to z abscissa is 0.05mm, while the resolution according to y depends of the size of the CCD's pixels and the magnification of the optical system which is 0.38.

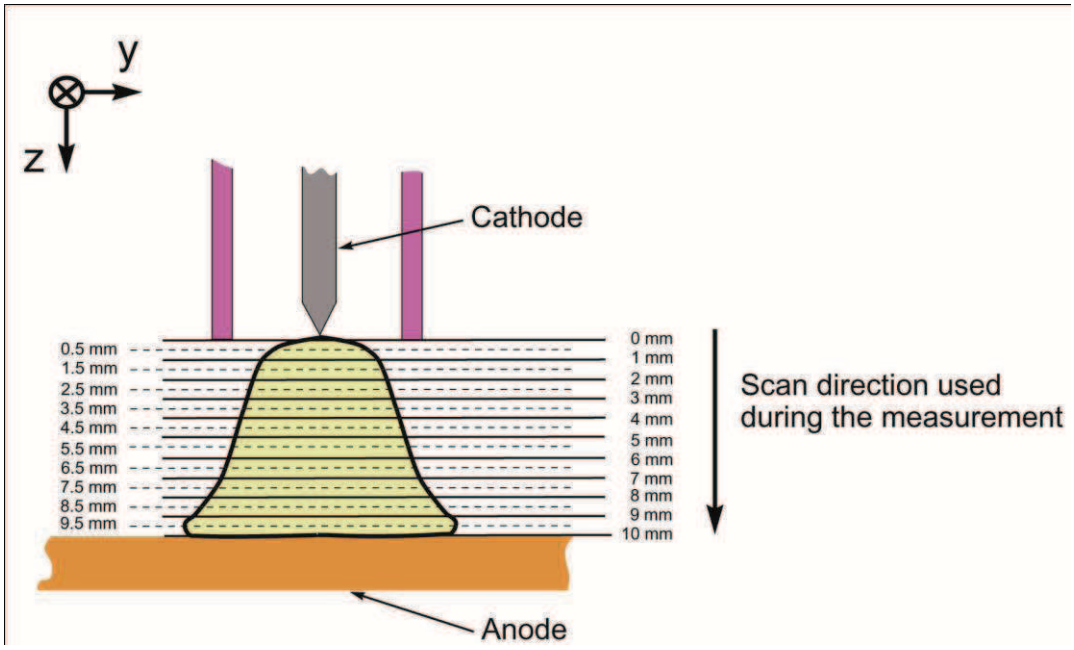

Figure 4. 8: Illustrative scheme for taking measurements.

4.3.6 Results and Discussion

Intensity profiles were recorded all over the plasma column and the Abel inversion was performed to get the emission coefficient. Some of them are available for an arc with a current of 100 A (figure 4.9). The maximum intensity can be found by looking for a hole or a

plate at the centre of the emission coefficient profile. Areas at the maximum emission temperature can be easily found since they are characterized by the most intense ε.

✓ **Cathodic region**

The analysis of emission coefficient profile as a function of z position shows that the maximum emission intensity cannot be determined properly at the vicinity of the cathode. Even if profiles let appear holes around r=0, the maximum intensity change drastically as z varies between 0 and 2 mm.

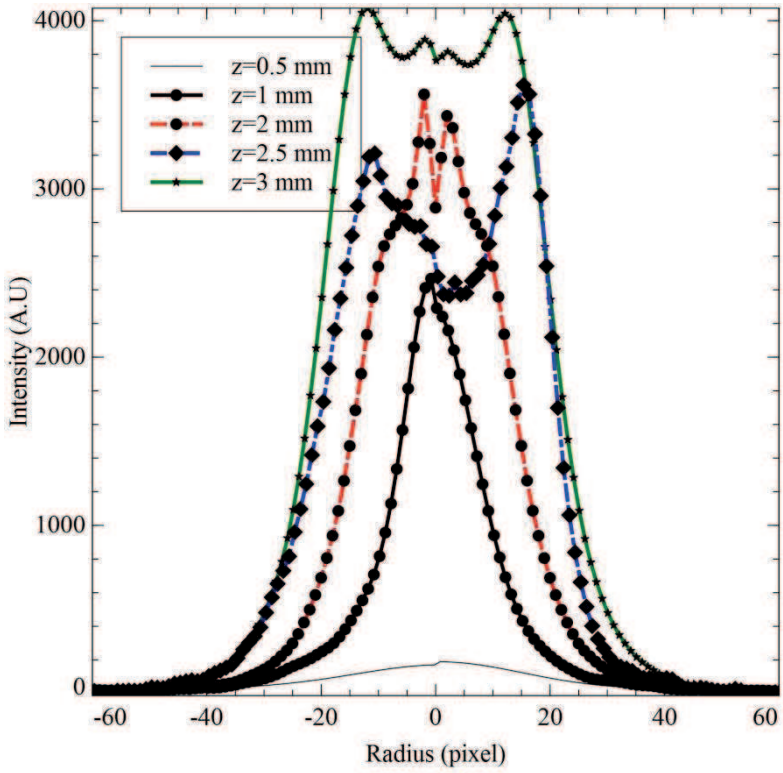

Figure 4. 9: Emission coefficient profile in the vicinity of the cathode.

This phenomenon is characteristic of a lack of light emitter compared to atmospheric pressure plasma at LTE. Two hypotheses were made by researchers to explain this phenomenon. Pellerin & al **[Pell-1]** stated that the lack of emitter was due to a drastic lowering of pressure at the cathode tip. Their hypothesis was supported by the analysis of typical thermalisation times. They found that for a 200 A free-burning arc, the length of LTE establishment is about 0.3 mm. At the contrary Pokrzywka **[Pok-1]** explains this situation by LTE departure since numerical simulation of plasma gives only small pressure variation around the cathode-tip.

To prove this hypothesis, we have chosen to compute emission coefficient as a function of the temperature for different pressure values to see if the pressure drop at the cathode-tip can be evaluated (fig. 4.10). By considering LTE and pressure drop, the analysis of profile at 0.5 mm from the cathode tip gives a pressure lower than 0,8 atm. It is obvious that such a low pressure cannot be reached in a free-burning arc. The only remaining hypothesis is a lower population on argon 4p levels than the one computed while considering LTE. This assumption has been proven with the help of collisional radiative models.

The determination of plasma temperature around the cathode-tip become quite difficult with the available scientific components at laboratory since the law which link states populations to temperature is found to be inadequate.

During the last fifty years, this change of maximum intensity around the cathode-tip was not always considered by researchers during their use of the Fowler Milne method. It may has lead to numerous errors in free-burning arc temperature maps **[Pok-1]**.

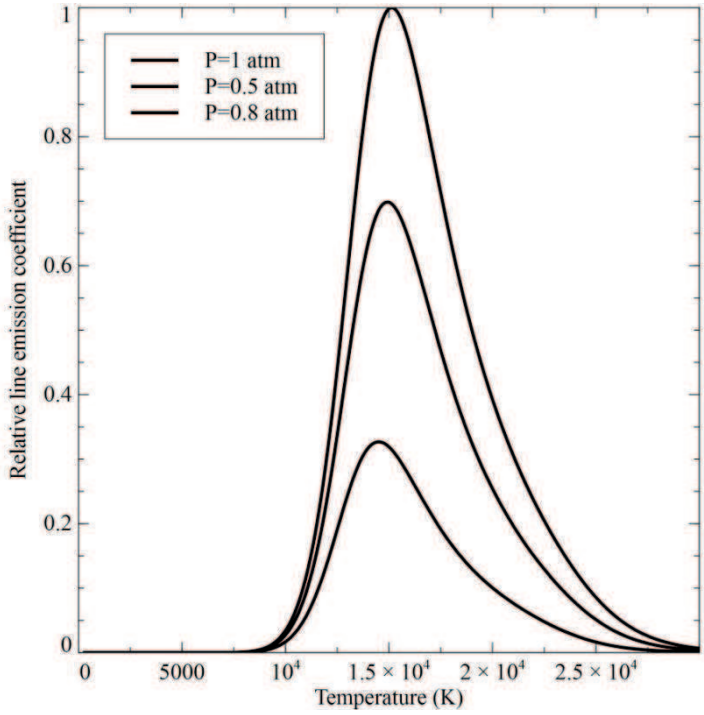

Figure 4. 10 : Emission coefficient as a function of the temperature for different pressure values.

✓ **Anodic region**

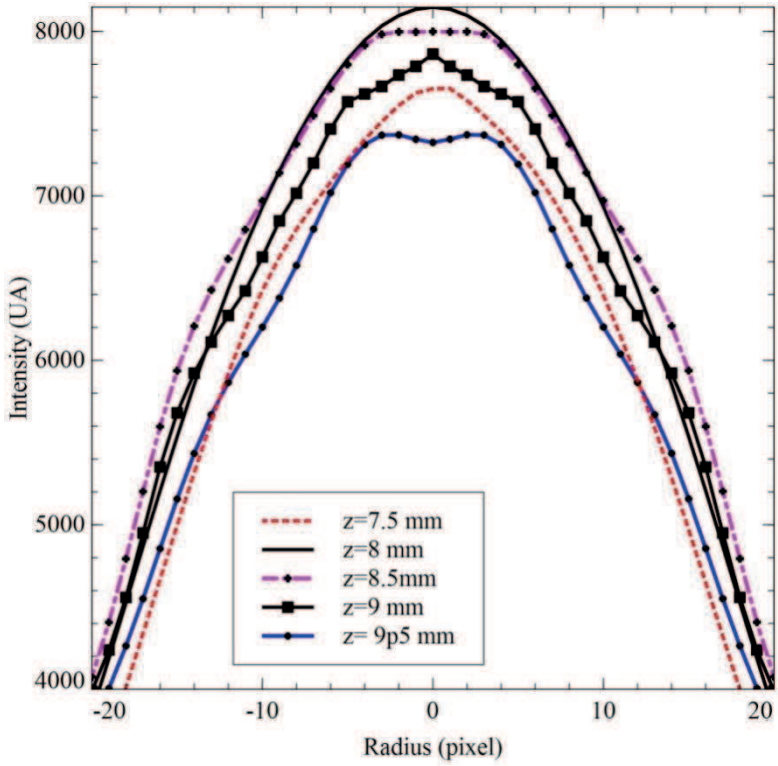

Figure 4. 11: Emission coefficient profiles at the vicinity of the anode for a 100 A current intensity free burning arc.

At 2 mm below the cathode-tip, the maximum intensity becomes stabilized, and temperature can be computed with the help of figure 4.2 data. By analyzing emission coefficient profile for ordinate higher than 2 mm it appears that ε decrease with the increase of z. It means that plasma temperature lowers with the increase of z. However, the profiles obtained in the vicinity of the anode show irregularities: a surplus of light is visible at z = 8 mm while there is a lack of light at the anode level. One possible explanation is a mirage effect that bends light rays skimming the anode. Obviously, the anode surface, heated by the plasma, has a temperature of a few hundred of Celsius degrees. As a consequence, the surrounding air is heated and a refractive index gradient in the –z direction is established near the electrode (figure 4.12). It is known that light rays are deflected in the direction of the refractive index gradient. Finally, this bends upward the light rays coming from the vicinity of the anode. This effect prevents the computation of temperature near the anode.

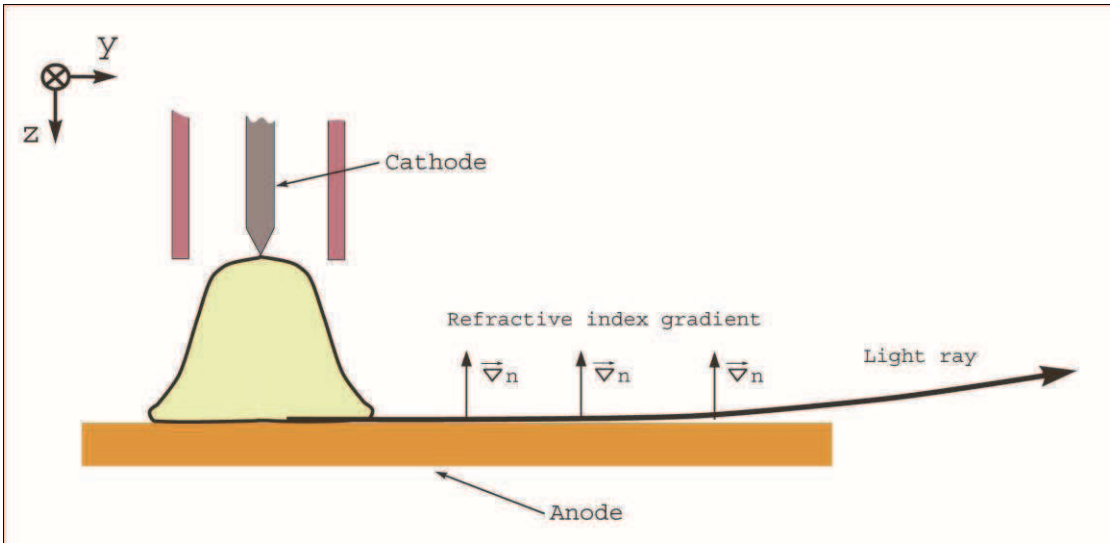

Figure 4. 12: Illustration of the mirage effect that perturbs measurement at the vicinity of the anode. Refractive index gradient are in the –z direction since refractive index is proportional to gas particle density.

✓ **Temperature map of a free-burning arc**

Due to the phenomena at the electrodes described before, the area where the Fowler-Milne method is applicable is limited. To produce temperature map of free-burning arc, the maximum intensity must be found and all the emission coefficient profile must be normalized on it. We wrote a software that scans each profile and use data from figure 4.2 to match relative emission coefficient to a temperature. Produced results are shown on figures 4.13 and 4.14.

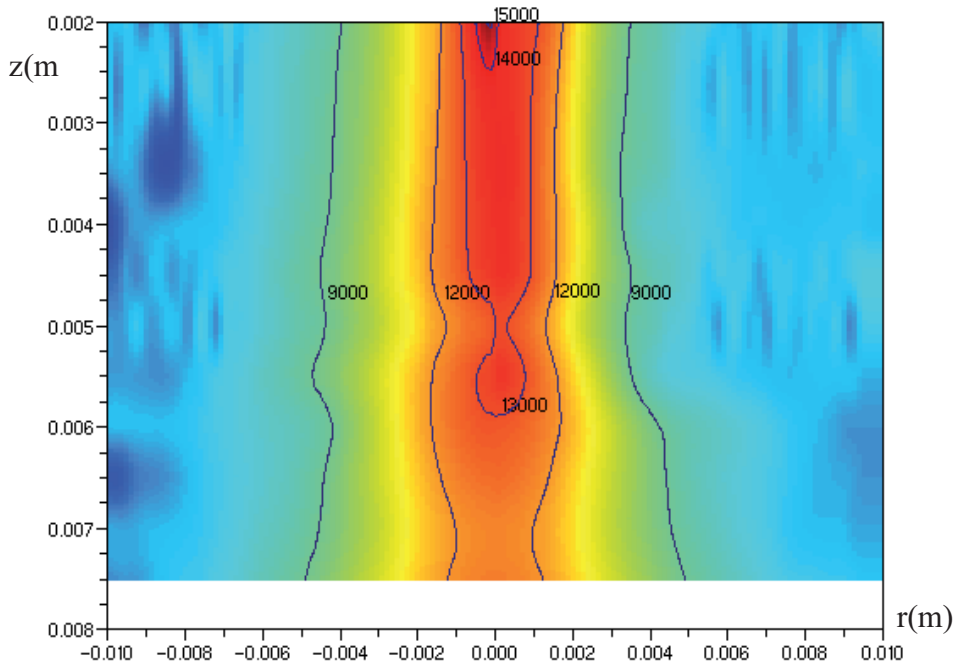

Figure 4. 13: Temperature map of a 100 A current intensity free burning arc.

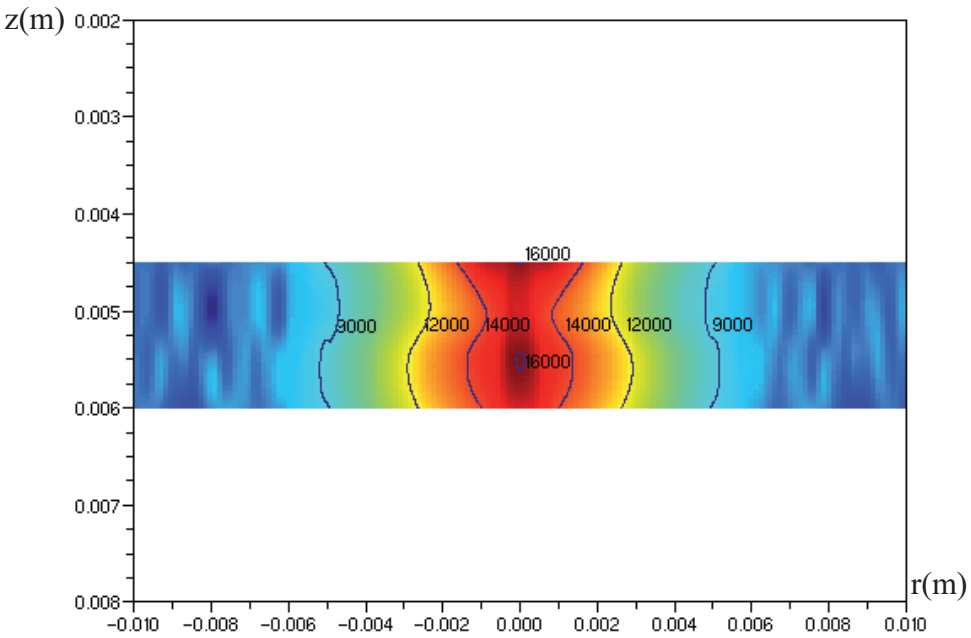

Figure 4. 14: Temperature map of a 200 A current intensity free burning arc.

4.3.6.1 Comparison of temperature maps

✓ **Temperature map of a 100 A current intensity free-burning arc**

The evolution along the axis of experimental temperature compared with that found by the model and those of experiment of Etemadi **[Etema-1]** is available on figure 4.15. It can be seen from this figure that the evolution of temperature given by the model and the experience is substantially the same.

From 3.5 mm to 7 mm the agreement is very good between the temperature of our experiment and that of Etemadi experiment. The calculated temperature is in agreement with our experimental temperature, with $\pm$ 1500 K difference. For the area near the cathode from 1 mm to 3 mm, the gap between the temperatures is more important about $\pm$ 3000 K. In this area close to the cathode, the model tends to overestimate slightly the temperature, we unfortunately have no experimental values very near to the cathode.

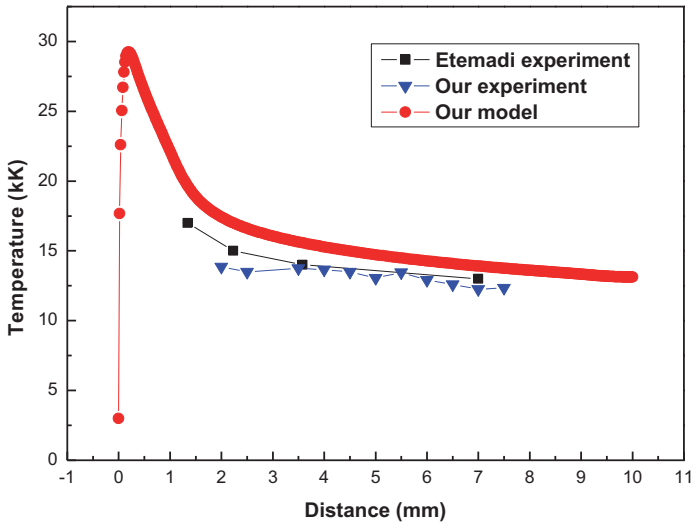

Figure 4. 15: Evolution of the temperature along the axis-comparison Model/Experience.

In order to have a view of the entire radial evolution of the temperature, we present two comparison, model/experiment and experiment/experiment.

✓ **Radial temperature Experiment/Model**

The experimental temperature field is shown on the left of figure (4.16). It is compared with the temperature field obtained by the model in argon at 100 A.

If the axial evolution of the temperature seems well predicted by the model, we can remark, from z = 2 mm to z =7.5 mm, that the 12000 K temperature iso-contour of the model have a radius of about 3.9 mm , while this iso-contour of temperature is located at radius of 1.5 mm in experiment results. The expansion of plasma in the model is more important than that of experiment. This may be explained by the gas sheathing of the free-burning arc which constricts the plasma and raise the column temperature.

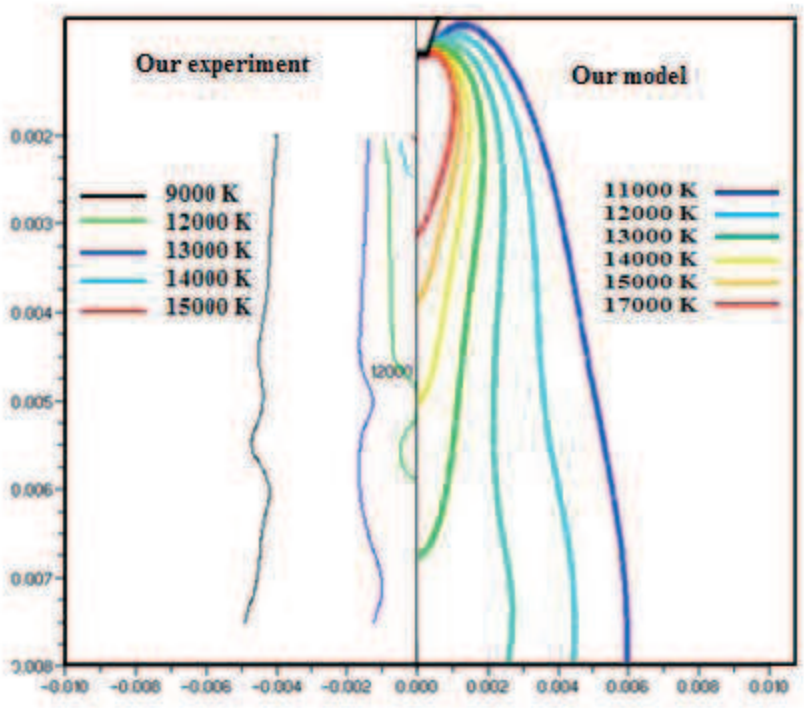

Figure 4. 16: Measured and calculated isotherms of free-burning argon arc, (I= 100 A, inter-electrodes distance =10mm).

✓ **Radial temperature Experiment/Experiment**

The experimental temperature field of Etemadi **[Etema-1]** is shown on the left of figure (4.17). Data were obtained by using neutral and ionic argon lines and the Fowler-Milne method. It is compared with the temperature field obtained by our experiment in argon at 100 A.

We observe radial spreading of the isotherms towards the anode, the highest temperature is observed in the cathode region, it is about 17000 K in Etemadi results at z = 1 mm and 15000 K at z = 2mm.

In the plasma column, it can be seen that the iso-contour of temperature of 13000 K and 12000 K of both measurements are almost the same.

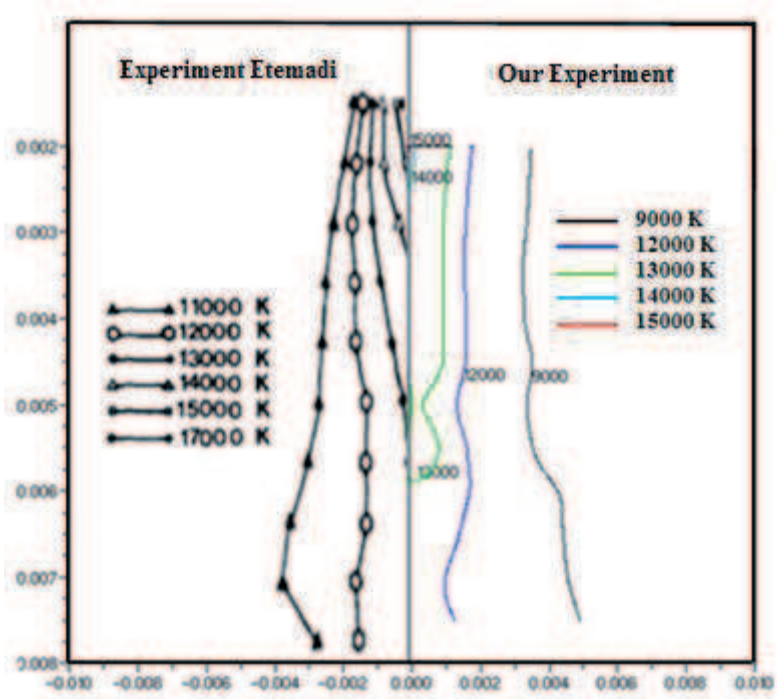

Figure 4. 17: Measurement isotherms of free-burning argon arc, (I= 100 A, Z =10mm).

- ✓ **Temperature map of 200 A current intensity free-burning arc**

The experiments temperature field of Etemadi **[Etema-1]** is shown on the left of figure (4.18). It's compared with the temperature field obtained by our experiment in argon at 200A.

Our temperature field is quite limited since only a two millimeters height slice at the center of the plasma column was probed successfully. However, results are in agreement with values obtained by Etemadi. The 14000 and 12000 K iso-contours are located at r = 1.5 mm and 3 mm respectively on our experiments result as those on Etemadi temperature map.

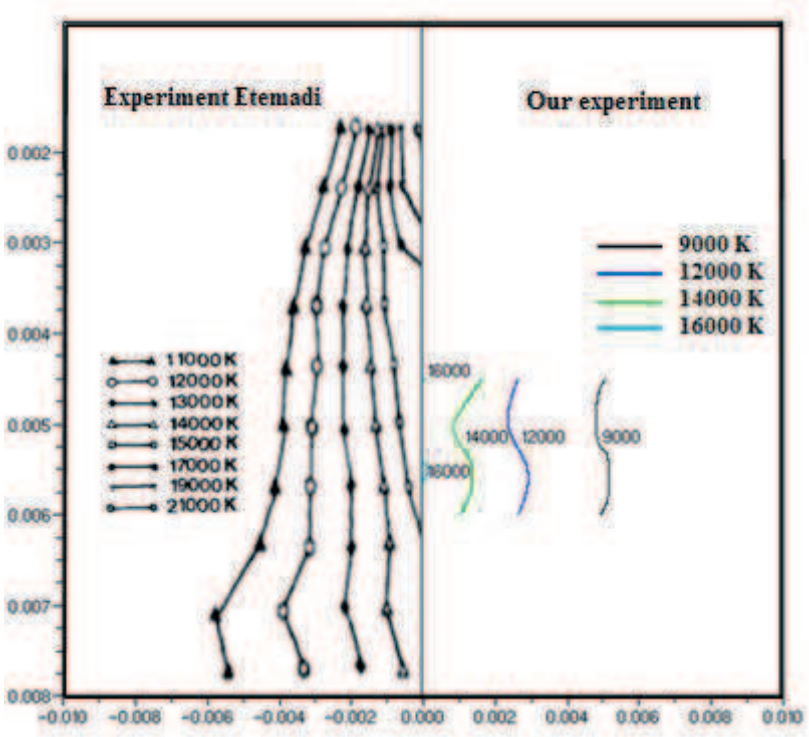

Figure 4. 18: Measurement isotherms of free burning argon arc, (I= 200 A, Z =10mm).

4.4 Conclusion

It is shown that LTE models are not adequate to describe the plasma column at the vicinity of the cathode. Our model is limited by the lack of electrode-plasma interaction and by the fluid description of the plasma. However, the model seems to be valid around the column center as it is checked by simulation/experimental results comparisons. Uncertainty about the model validity remains at the vicinity of the anode since a mirage effect prevents experimental measurements, and also because (as mentioned in chapter 2) of the simplification of the model on the enthalpy of electron. To limit mirage effect, one may works with smaller and better cooled anode. To conclude, it is shown that Fowler-Milne method is not adapted to probe in non-equilibrium area. It has to be coupled to Stark broadening studies at the cathode and to refractive index based methods for cold areas.

Bibliography

[Chap-1] Chapelle. J. « L'arc électrique et ses applications » : Etude physique de l'arc électrique – Tome 1. CNRS édition, (1984).

[Draw-1] Drawin,. H., W.: "Spectroscopic Measurement of High Temperatues, High Pressure". High temperature, Vol. 2, (1970).

[Draw-2] Drawin., H., W.: "Thermodynamic Properties of the Equilibrium and Nonequilibrium State of Plasma Conditions", Vol, 1, ed, Venugopalan M., Wiley – Interscience, (1971).

[Etema-1] Etemadi., K, "Investigation of High-Current Arcs by Computer-Controlled Plasma Spectroscopy ".PP 5. Thesis of University of Minnesota, (1982).

[Fauch-1] Fauchais. P and JF. Coudert. "Mesures de température dans les plasmas thermiques" . Rev Gén Therm, 35 :324–337, (1996).

[Fowl-1] Fowler, R., H and E. A. Milne. "The intensities of absorption lines in stellar spectra and the temperatures and pressures in the reversing layers of stars". Monthly Notices of the Royal Astronomical Society, 83:403-424, (1923).

[Jaf-1] Jaffe S.M., Larjo J. Henberg R., "Abel inversion using the fast Fourier transform", X^{th} International Symposium on Plasma Chemistry-Bochum, 1-21 pp 1-6, (1991).

[Had-1] Haddad G.N. and Farmer J.D. "Temperature determination in a free-burning arc : I. experimental techniques and results in argon". Journal of physics D, 17 :1189–1196, (1984).

[Hsu-1] Hsu K.C., Etemadi K., Pfender E., "Study of the free-burning high intensity argon arc". Journal of applied physics 54, p129, (1983).

[Grie-1] Griem, H, R.: Plasma Spectroscopy. McGraw-Hill, (1964).

[Gizz-1] Gizzi. L . A et al., Phys. Rev. E 49 (1994) 5628 (Erratum : Phys. Rev. E 50, 4266, (1994).

[Glas-1] Glasser J., Chapelle J., Boethner J.C., "Abel inversion applied to plasma spectroscopy: a new interactive method", Applied Optics 17, p3750-3753, (1978).

[Mer-1] Mermet J.M., Robin J.P., "Etude de l'inversion d'Abel en vue de la mesure de la répartition de la température dans un plasma inductif ", rev. Int. Htes. Temp. Et réfract. (10), pp 133-139, (1973).

[Murp-1] Murphy A. B., "Modified fowler-milne method for the spectroscopic measurement of temperature and composition of multielement thermal plasmas". Review of scientific instruments 65, p3423, (1994).

[Nom-1] Nomarski. M. G, Journal de la Physique et le Radium 16, 95, (1955).

[Pell-1] Pellerin S., Pokrzywka B., Musiol K, Chapelle J., "Diagnostic et étude de la zone cathodique d'un arc électrique". Journal de physique III 5, p2029-2042, (1995).

[Pok-1] Pokrzywka B., Musiol K., Pellerin S., "Etude de la zone cathodique d'un arc électrique". Compte rendu de l'académie des sciences 327, p391-398, (1999).

[Sem-1] Sember V, "Application of numerical methods for computation of the Abel integral equation for spectroscopic data", Acta Phys slov (41), pp 284-292, (1991).

[Vac-1] Vacquié. S., "l'arc électrique", Book . CNRS Editions, Eyrolles, Paris, (2000).

Chapter 4: Experimental study

CONCLUSION GENERALE

CONCLUSION

L'étude bibliographique des travaux réalisée sur les arcs électriques a orienté nos travaux de recherche vers la modélisation bidimensionnelle d'un arc libre intervenant dans des applications industrielles telles que le soudage, le découpage... Le plasma thermique crée par un arc électrique est considéré comme un fluide neutre et conducteur. A partir de là, on a défini sur une particule fluide un certain nombre de propriétés physiques : pression, masse volumique, température, etc... Les équations de conservations ont pu être alors appliquées. La conductivité du fluide nous a imposé de coupler aux équations de conservation les équations de l'électromagnétisme. L'ensemble de ce système ainsi formé, appelé équations de la magnétohydrodynamique, a été introduit en supposant le plasma en équilibre thermodynamique local et à pression atmosphérique. Par hypothèse, le milieu de l'écoulement a été considéré comme continu, laminaire et en régime stationnaire.

Pour résoudre numériquement ce système d'équations aux dérivées partielles deux méthodes s'offraient à nous : la méthode des éléments finis et la méthode des volumes finis. La méthode des volumes finis dont le principe est fondé sur les équations de conservation nous a semblé la plus adéquate pour notre modèle, pour cela, nous avons utilisé le logiciel commercial Fluent 12.0, dont la technique de résolution numérique est fondé sur l'algorithme de Patankar. Pour pouvoir utiliser la partie solveur du logiciel commercial Fluent 12.0, nous avons résolu notre modèle en utilisant les routines UDF Users-Defined-Function. Cette adaptation a été difficile, car ce logiciel est à l'origine, consacré au traitement des écoulements de combustion. Il nous a donc fallu adapter les routines pour prendre en compte les équations de l'électromagnétisme, les termes sources des équations différentielles, les propriétés thermodynamiques et les coefficients de transports du gaz.

Nous avons choisi, pour valider notre modèle et notre code calcul, de modéliser un arc libre dans l'argon à 100 A. le modèle est à deux dimensions avec une symétrie cylindrique. Les résultats de la simulation numérique ont été comparés aux résultats théoriques et expérimentaux issus de la littérature. Une analyse détaillée des différentes grandeurs caractéristiques a permis de conclure quant à la validité de notre modèle dans la colonne du plasma, le model n'est pas valide dans les régions proche des électrodes. A partir de là, nous avons décidé d'approfondir notre étude sur ce type d'arc. Pour cela, nous avons analysé

l'influence, sur les grandeurs caractéristiques du plasma, de paramètres comme la nature de gaz et le courant électrique.

Pour compléter l'étude théorique, nous avons développé dans le quatrième chapitre une étude expérimentale. Les mesures à proximité de la cathode sont inexploitables à cause d'un fort déséquilibre thermique du plasma, tandis que les mesures à proximité de l'anode sont perturbées par un effet mirage dû à l'échauffement de l'air entourant l'électrode.

Les résultats expérimentaux sont comparés aux résultats issus de notre modèle, et sont en bon accord avec les résultats du modèle, ce qui signifie que le modèle à l'ETL est validé dans la colonne de plasma.

La comparaison modèle-modèle présente une différence dans les zones proches des électrodes. Cette différence est principalement due aux choix des conditions limites imposés sur la cathode et à l'anode. La comparaison expérience-modèle a conduit à des différences sur l'évolution radiale de la température. Ces différences sont probablement dues à des écarts à l'équilibre thermodynamique.

Ce travail a été une étape vers le développement d'un modèle d'arc adapté aux régimes transitoires (arcs en extinction), de plus petites dimensions et en milieux réactif. Les résultats de cette étude ont montré l'importance de certaines conditions aux limites et des écarts à l'ETL que l'on trouve dans ce type d'arc. Ces points sont d'autant plus sensibles que les dimensions de l'arc sont petites et que le régime n'est plus stationnaire. Les futurs travaux vont donc s'orienter vers la prise en compte des écarts à l'équilibre thermodynamique local, à l'aide d'un modèle à deux températures. Un effort particulier sera fait sur le traitement des interactions arc-électrodes afin de s'affranchir autant que possible de conditions aux limites difficiles à fixer. Enfin sur le plan expérimental, il pourrait être intéressant de mettre en place de nouveaux moyens de diagnostic afin d'obtenir d'autres informations sur le plasma comme la vitesse de l'écoulement, cette dernière étant particulièrement sensible aux variations de courant.

Kheira HAMEURLAINE

Contribution à l'étude d'un arc électrique de faible puissance

Résumé

L'étude présentée ici entre dans la problématique générale des arcs électriques intervenant dans des applications industrielles telles que le soudage, le découpage, le traitement des déchets... Ce travail constitue une première phase de modélisation de cette étude générale. Le plasma est décrit par un ensemble d'équations de conservation de fluide et de l'électromagnétisme, complétés par des propriétés thermodynamiques et des coefficients de transport appropriés, en formant un système d'équations non linéaires fortement couplées. Ces équations sont écrites en supposant l'équilibre thermodynamique local, une symétrie cylindrique et un écoulement laminaire stationnaire. Ce système d'équations est résolu à l'aide du logiciel commercial FLUENT de type CFD fondé sur l'approche des volumes finis. Pour pouvoir utiliser la partie solveur nous avons résolu notre modèle en utilisant les routines UDF Users-Defined-Function.

Dans une première partie, nous présentons la validation du modèle à deux dimensions et à 100 A dans l'argon par des résultats de la littérature. Cette comparaison laisse apparaître un accord satisfaisant sur les profils de température dans la colonne de plasma et des différences dans les zones proches des électrodes dues aux conditions aux limites. Dans une deuxième partie, nous présentons une étude expérimentale, à l'issue de laquelle on constate que les profils de température expérimentaux sont en accord avec ceux du modèle dans la zone de colonne positive.

Mots clés: Arc électrique, Modélisation numérique, Plasma thermique, Argon, Fluent.

Contribution to the study of a lower power electric arc

Abstract

The study presented here enters the general problem of electric arc involved in industrial applications such as welding, cutting, waste treatment... This work constitutes the first numerical phase of modeling of this general study. The plasma is described by a set of fluid conservation equations, electromagnetic equations complemented by suitable thermodynamic and transport properties, forming a strongly coupled non-linear system. These equations are written assuming local thermodynamic equilibrium, a cylindrical symmetry and steady laminar flow. This system of equations is solved using commercial software FLUENT CFD-type based on finite volume algorithm. To use the solver part we solved our model using UDF macro Users-Defined-Function. In the first part, we present the validation of the two dimensional model in and 100 A in argon with the literature results. A detailed analysis of various characteristic quantities is presented. This comparison reveals a good agreement of the temperature profiles in the column plasma and differences in electrode areas due to boundary conditions. In a second part, we present an experimental study, the experimental temperature profiles are consistent with the model in the column area which means that the model is validated in the column of plasma.

Keywords: Electric Arc, Numerical modeling, Thermal plasma, Argon, Fluent.

GREMI – UMR 7344 (CNRS –Université d'Orléans)

14 rue d'Issoudun, - BP 6744 Orléans Cedex 2